The Institute of Paper Chemistry

Appleton, Wisconsin

Doctor's Dissertation

An Investigation of the Mechanism of High-Intensity Paper Drying

Christopher P. Devlin

June, 1986
Reprint October, 1990

AN INVESTIGATION OF THE MECHANISM OF HIGH-INTENSITY PAPER DRYING

A thesis submitted by

Christopher P. Devlin

B.S. 1979, The Pennsylvania State University

M.S. 1981, Lawrence University

in partial fulfillment of the requirements
of The Institute of Paper Chemistry
for the degree of Doctor of Philosophy
from Lawrence University
Appleton, Wisconsin

June, 1986

TABLE OF CONTENTS

SUMMARY

High-intensity paper drying can produce drying rates which are over an order of magnitude higher than those normally produced by conventional drying. High-intensity drying also causes a significant amount of moisture to exit the sheet as liquid, and produces higher sheet densities than both conventional wet-pressing and drying. The high-intensity drying process combines phenomena common to wet pressing and conventional drying, and to neither. However, it is the intensity of these phenomena, driven by high dryer surface temperatures and applied mechanical pressures, that leads to new and novel drying mechanisms. It is the purpose of this thesis to identify these high-intensity drying mechanisms based on experimental data.

For purposes of description, the high-intensity drying process is divided into three successive periods: Compression and Heat-Up Period, Liquid Dewatering Period, and Evaporation Period. While this division is not always based on strict demarcation points between the drying mechanisms, clarity requires that some division of the process be made.

In the Compression and Heat-Up Period, the compression process may be described as one of mechanical compression of an unsaturated sheet. However, heat transfer to the sheet modifies the compression process. The intense drying conditions cause a large amount of heat transfer in a short period of time. This results in a rapid generation of vapor at, and convective vapor transport away from, the hot surface. The vapor flow, acting in concert with the flow resistance of the sheet, pressurizes the areas where evaporation is occurring. This allows the temperature to exceed 212°F. As evaporation begins in areas away from the hot surface, the sheet can be considered to be divided into two zones: a vapor pressurized zone and an unsaturated zone. As the vapor pressurized zone

expands, an evaporation-convection-condensation mechanism transfers heat and redistributes moisture in the zone. As the compression process brings the sheet near the saturation point, no vapor or liquid has left the sheet. The sheet becomes saturated with liquid and a small amount of vapor, and further compression initiates liquid dewatering.

In the Liquid Dewatering Period, a significant amount of moisture leaves the sheet in liquid form. The amount of liquid dewatering is several times higher than what could be achieved by wet-pressing alone. In this investigation, the amount of liquid dewatering was found to be relatively independent of the dryer surface temperature and applied pressure. Liquid dewatering occurs by two mechanisms: volume reduction and vapor displacement. The volume reduction mechanism is similar to what occurs in wet pressing, and only produces a small amount of liquid dewatering. Vapor displacement of liquid in the network pores is the mechanism that causes the large increase in liquid dewatering in high-intensity drying over what can be achieved by wet pressing. Vapor displacement begins when the pressure drop in the sheet after saturation allows liquid near the hot surface to superheat, and a small amount flashes into vapor. The vapor begins to displace liquid in the network pores as it attempts to exit the sheet. As the vapor makes its way toward the cold surface, the sheet becomes divided into a vapor pressurized zone and a liquid pressurized zone. The large amount of liquid dewatering from this mechanism is both because of, and made possible by, the liquid in the network pores in the liquid pressurized zone which seals the sheet from the atmosphere. An important result of this sealing mechanism is that while a considerable amount of heat has been transferred to the sheet up to the end of liquid dewatering, only a small fraction has left the sheet with the liquid; the rest remains stored in the sheet.

While liquid dewatering is responsible for a significant part of the moisture removal in high-intensity drying, the majority of the initial moisture still leaves the sheet as vapor. In the Evaporation Period, a vigorous evaporation process begins. The evaporation process can be divided into two parts: pressurized flash drying, followed by progressive drying out of the sheet. Pressurized flash drying begins when liquid dewatering ends. Once vapor is able to exit the sheet, the vapor phase pressure begins to decline, allowing the liquid to flash evaporate using the stored energy and heat transferred into the sheet from the hot surface. Very quickly, a quasi-steady state is established in which the vapor phase pressure effects a balance between the evaporation rate and the vapor flow rate out of the sheet. Rough estimates show that the combination of liquid dewatering and pressurized flash drying removes over half of the initial moisture in the sheet.

High-intensity drying also produces sheet densities which are considerably higher than those achieved by conventional drying. The additional sheet densification occurs during pressurized flash drying and is a result of the applied load and considerably augmented by thermal softening. Thermal softening is enhanced because the fibrous structure is pressurized by vapor, allowing moisture and fiber wall material to reach elevated temperatures.

Later in the Evaporation Period, the drying rate becomes heat transfer limited as the stored energy is depleted, and the sheet begins to dry out progressively from the hot surface to the cold surface. The sheet again can be considered to be divided into zones, namely, a zone of fibers and vapor, and an evaporation zone. This progressive sheet drying is essentially a high temperature conventional drying process but occurs more quickly because of convection driven heat transfer and mass flow processes. At this time, the evaporation rate depends on

the heat transfer rate, and evaporation occurs at a pressure just high enough for the vapor to overcome the flow resistance and exit the sheet.

Lastly, it can be concluded from the results of this investigation that, with few exceptions, the overall high-intensity drying mechanism does not change significantly with the drying conditions employed. Only the rates of change of the individual mechanisms, and hence the overall drying rate, are increased by employing increasingly intense drying conditions.

INTRODUCTION

High-intensity paper drying uses higher dryer surface temperatures and applied mechanical pressures than conventional (cylinder) drying to produce higher drying rates than conventional drying. Results from a study by Ahrens, et al.,[1] given in Fig. 1, show that as the sheet temperature approaches 100°C (212°F) the drying rate increases dramatically.

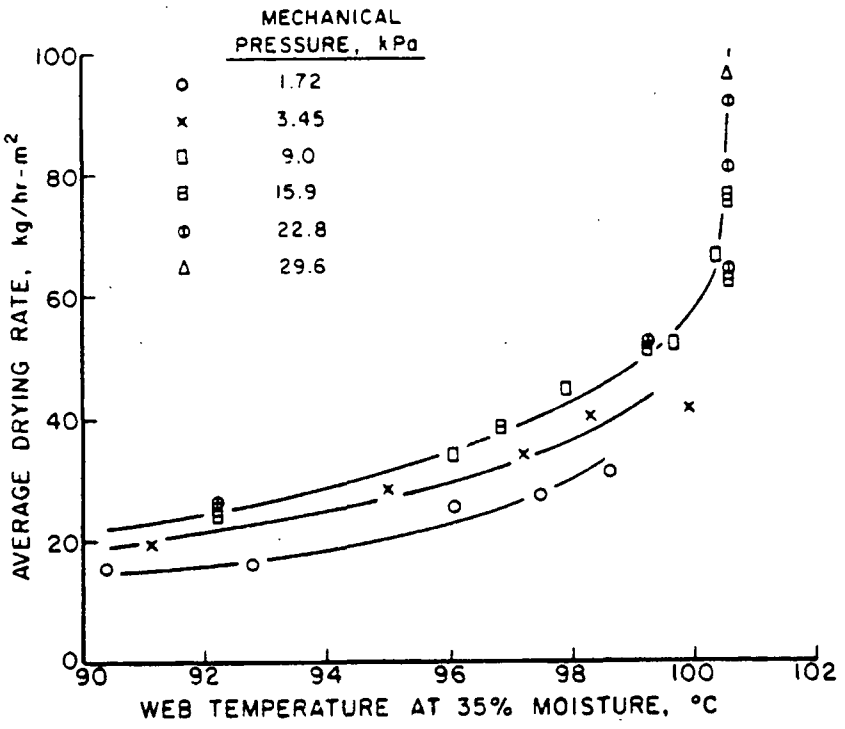

Figure 1. Correlation of average drying rate with a typical web temperature for unbleached southern softwood kraft handsheets, 42 lb/1000 ft^2 basis weight 60% initial moisture content.[1]

The increase in drying rate was attributed to higher heat transfer rates than occur in conventional drying, and a convective movement of vapor out of the sheet.[1,2] This is in contrast to the slower, diffusive vapor flow found in

conventional drying. Based on these characteristics, high-intensity drying has at least three advantages over conventional drying:

1. Higher drying rates make possible the design of smaller dryer sections, reducing capital costs.
2. Higher drying rates make possible higher production rates.
3. A convective movement of vapor could push out or drag along liquid water as it exits the sheet. This would leave less water to be evaporated and reduce operating costs.

THESIS OBJECTIVE

To date, most research on high-intensity drying has concentrated on quantifying drying rates for various combinations of dryer surface temperatures, applied mechanical pressures, furnishes, basis weights, and initial moisture contents. The objective of this thesis is to identify the dewatering and densification mechanisms that occur during the high-intensity drying process.

BACKGROUND

Published literature on mechanisms in high-intensity drying is scant and generally emphasizes convective vapor and liquid transport. A mathematical model of the process has also been written. However, an experimentally supported description of the mechanisms and their interrelationships is lacking, giving rise to this investigation.

VAPOR CONVECTION AND LIQUID DEWATERING

Holm, et al.[3] first suggested that a convective vapor transport mechanism could be operative in conventional drying based on results of a computer simulation. Ahrens, et al.[1] reported on a laboratory study in which drying temperatures and pressures up to 460°F and 4.3 psi were used in various combinations. They observed a dramatic increase in drying rate as the sheet temperature approached 212°F. This was attributed to a change from a diffusive to a convective vapor removal mechanism. They used the term "high-intensity" drying to distinguish between vapor removal via convection from removal by diffusion. Impulse drying is a form of high-intensity drying in which the wet sheet is heated and pressed simultaneously for short periods (e.g., 5-35 milliseconds) in a heated press nip. In an impulse drying study, Arenander and Wahren[4] concluded that vapor convection was responsible for the high drying rates they observed. They also postulated that, depending on the initial sheet moisture content, the high degree of sheet compression augmented by the vapor phase pressure gradient could cause liquid in the network pores to be pushed out of the sheet instead of evaporated.

The best direct evidence for the existence of vapor convection was provided by Ahrens[5] in a high-intensity drying study, and Burton[6] in an impulse drying

study. For vapor convection to exist, a pressure gradient must be present. Ahrens and Burton measured vapor phase pressures at the hot side of the sheet during their experiments. The pressure data are shown in Fig. 2 and 3. Both noted that the magnitude of the vapor phase pressure peak increased with higher hot surface temperatures and applied pressures.

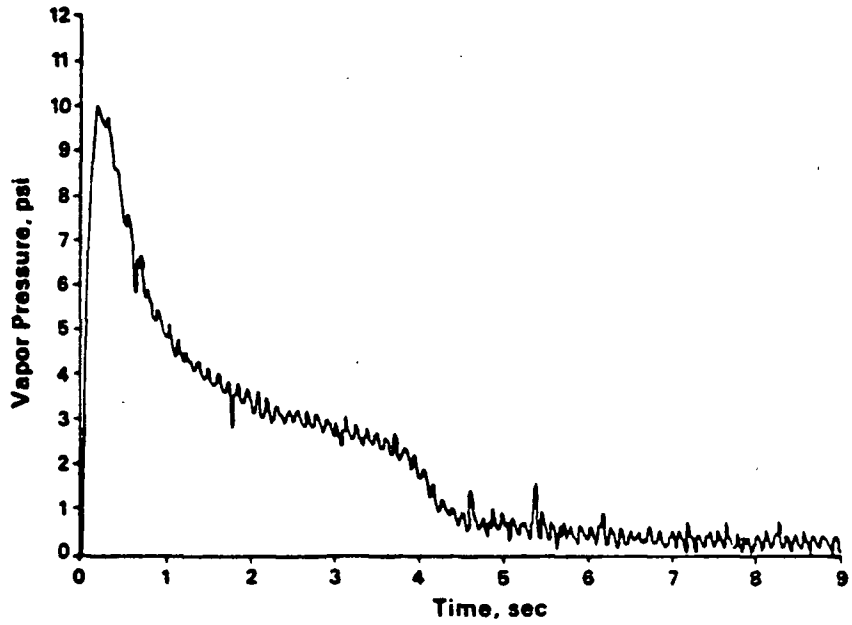

Figure 2. Vapor phase pressure at hot surface for an unbleached softwood kraft handsheet, 42 lb/1000 ft^2 basis weight, 60% initial MC, 300°F surface temperature and 46.5 psi applied pressure.[5] (Note: pressure given is gage pressure.)

POUNDER'S MATHEMATICAL MODEL

Pounder's[7] mathematical model is the only complete model of high-intensity drying to date. The model was developed from a highly simplified model by Ahrens.[8] Pounder's model introduces such details as liquid convection from sheet compression, vapor convection, higher than normal boiling point temperatures in the sheet due to higher applied pressures, and various hygroscopic

effects present in a water-fiber system. The model divides the sheet into different zones that contain various amounts of fiber, liquid water, and water vapor during three distinct drying periods assumed for the high-intensity drying process. Equations for liquid and vapor convection are used to describe moisture movement in the sheet. Equations for conduction and convection heat transfer are used to describe heat flow in the sheet. When compared to experimental drying data, the model qualitatively predicts high-intensity drying behavior under a variety of drying conditions. Quantitatively, the model accurately predicts drying rates, but overestimates the amount of liquid dewatering that occurs in high-intensity drying. For this reason the model is not used for experimental data comparison in this thesis.

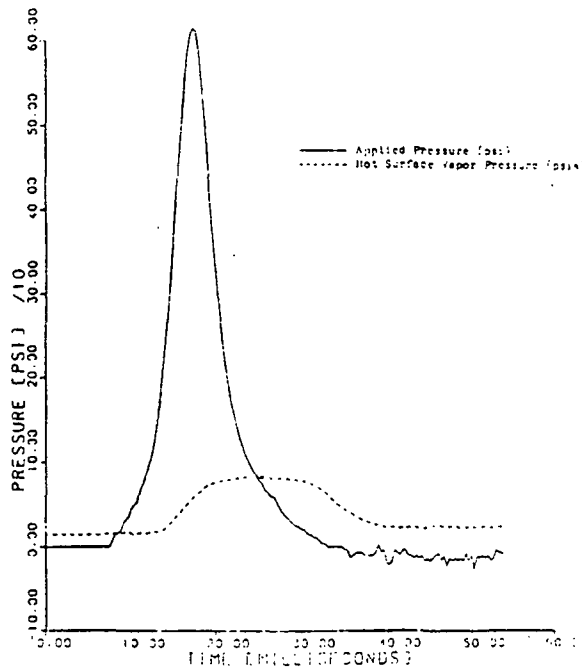

Figure 3. Vapor phase pressure at hot surface plotted with applied pressure for impulse dried, unbleached softwood kraft handsheet, 34 lb/1000 ft^2 basis weight, 66% initial MC, 600°F surface temperature and 600 psi peak applied pressure.[6]

EXPERIMENTAL

EXPERIMENTAL STUDIES

The experimental program for this thesis consists of a series of separate studies, each directed to a specific aspect of the high-intensity drying process. The studies can generally be divided into those that investigate water transport and those that investigate heat transfer in high-intensity drying. It is difficult to isolate and study a specific transport mechanism because of the simultaneous occurrence of heat transfer and mass flow in drying. For this reason it is not the goal of each study to give complete information on a specific transport mechanism. Only after analyzing all of the experimental data can the contributions of the various transport mechanisms be evaluated by drawing evidence from each of the studies. This point will become more clear later in the thesis. Details on the specific procedures for each of the studies are given in Appendix I. Only a brief outline of each of the studies is presented here.

The water transport studies begin with the Drying Rate Study to determine the overall time scale of events in high-intensity drying. The Liquid Dewatering Study investigates how much water leaves the sheet as liquid during drying. The Liquid Movement Study gives qualitative evidence on the redistribution of liquid in the sheet during drying.

The heat transfer studies focus on resolving which transport processes are responsible for heat transfer in high-intensity drying. The Heat Flux Study investigates heat flow to the sheet during drying. In the Internal Sheet Temperature Study, the temperature is measured at different points through the

sheet thickness during drying. The Caliper Study shows the changes in sheet caliper under high-intensity drying conditions.

Previous studies have taken drying rate and heat flux data for only certain sheet basis weights, initial moisture contents, dryer surface temperatures, and at much lower applied pressures. The majority of the studies in this thesis yield information on variables that have never before been measured.

DRYING CONDITIONS

The drying conditions used in the experimental studies are listed below.

1. 300°F/400 psi (150°C/2760 kPa)
2. 300°F/700 psi (150°C/4825 kPa)
3. 525°F/400 psi (275°C/2760 kPa)
4. 525°F/700 psi (275°C/4825 kPa)

The temperature is the initial hot surface temperature, and the pressure is the final applied mechanical pressure on the sheet. These conditions are similar in temperature, but at least two orders of magnitude higher in applied pressure than the conditions used in the high-intensity drying study by Ahrens, et al.,[1] shown in Fig. 4.

PULP PREPARATION

A run-of-the-mill unbleached, southern softwood, kraft pulp was used in this investigation. The pulp was obtained in wet lap form. It was thoroughly washed, and beaten at 2.2% consistency to 625 ml CSF in a Valley beater. The pulp was then centrifuged, fluffed, and stored in sealed bags at 40°F at 30% consistency.

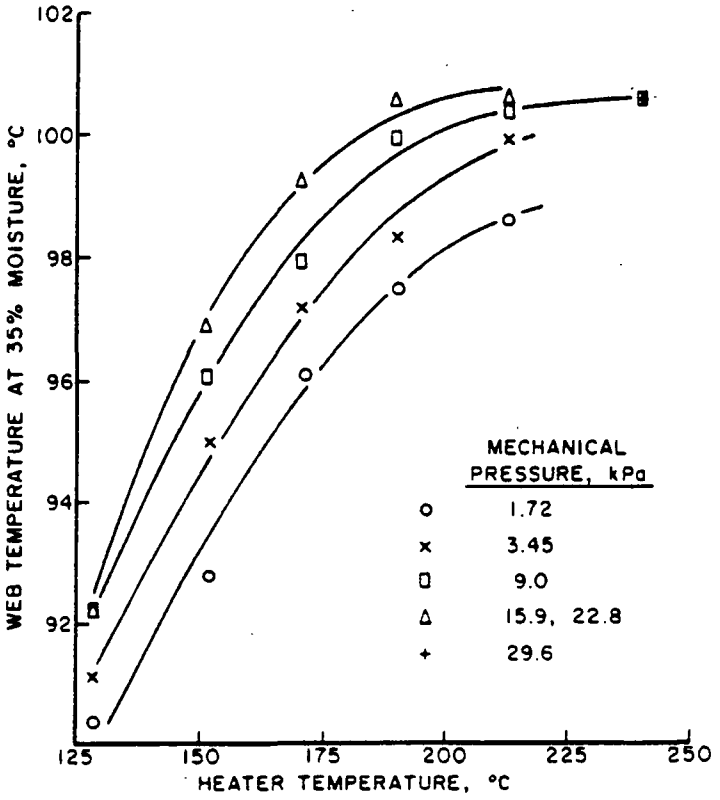

Figure 4. Effect of heater temperature and applied pressure on web temperature (measured at time when web is at 35% moisture content).[1]

HANDSHEET FORMATION

All handsheets were made on a constant-rate filtration apparatus. This apparatus is discussed in detail elsewhere.[9] The apparatus permits the formation of a handsheet from a dilute slurry at a constant rate under conditions of controlled fiber dispersion. In this work the slurry consistency was always 0.012%. The target basis weight of the handsheets was always 42 lb/1000 ft^2. After forming, the sheets were pressed to a moisture content of approximately 57% and stored in sealed plastic bags at 40°F for no more than 48 hours before being dried.

EXPERIMENTAL APPARATUS

Figure 5 shows a diagram of the drying apparatus used in this thesis. The drying apparatus consists of five systems: pressure, heating, moisture removal, and temperature and caliper measurement. Each of these is discussed below. In addition, at the end of this section is a list of the manufacturers and model numbers of the equipment.

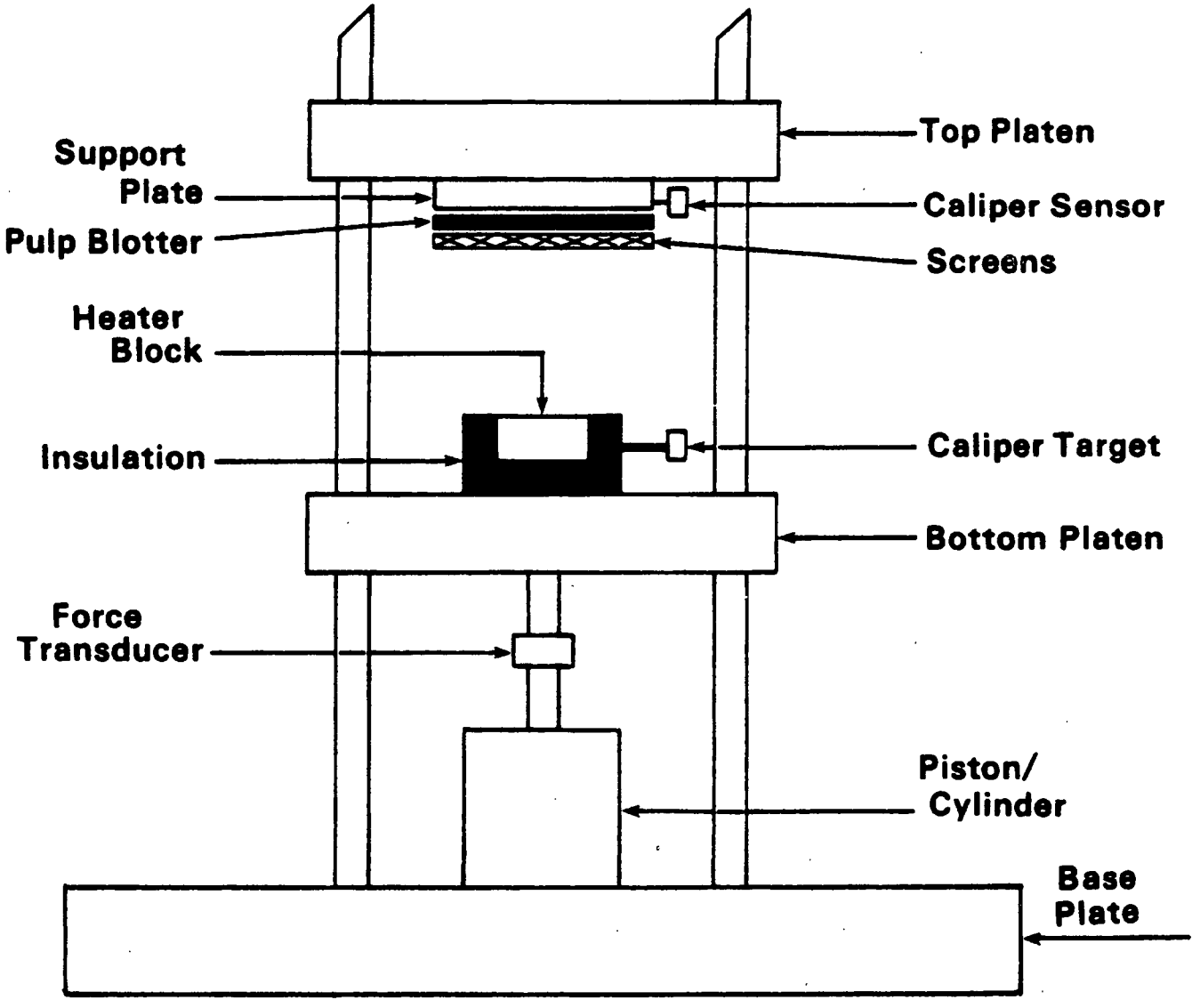

Figure 5. Diagram of drying apparatus.

Pressure System

The basic structure of the apparatus is a four threaded column, flat-bed press. During a drying run, a hydraulically loaded piston moves the bottom platen upward to contact the stationary top platen. The time of contact is regulated by a digital timer that controls the length of time hydraulic fluid flows to the piston. The timer can cause press engagement for time spans of 0.01 second to 99.9 seconds. The press is powered by a closed system, hydraulic power unit connected to the piston. The piston has a 5 inch bore and 3/4 inch stroke. The hydraulic power unit has a pumping capacity of 5 GPM and is driven by a 5 hp motor. The unit can produce pressures of 250 psi to 1250 psi on a 5.5 inch diameter web.

A quartz, piezoelectric force transducer is located between the piston and bottom platen to measure the force exerted on the sheet during drying. Figure 6 shows recordings of the applied pressure during four drying runs. There is a small amount of pressure overshoot in each case before the pressure reaches its setpoint. The pressure also appears to be decreasing with time after the overshoot. This is not an actual pressure decrease, but a result of the force transducer slowly discharging and producing a weaker signal.

Heating System

Thermal energy for drying is supplied by a 6 inch diameter, 2 inch thick Electrolytic Tough Pitch copper block. The drying surface of the block is coated with 0.0001 inch of a hard chrome alloy to prevent oxidation of the copper. The block is heated with two 1-kW electric cartridge heaters located 1/2 inch below the surface of the block. Calcium silicate insulation, with a thickness of 2 inches, provides insulation for the block. A Type T surface thermocouple is

located in the center of the block. The thermocouple is threaded in from the back side of the block through a 1/16 inch hole.

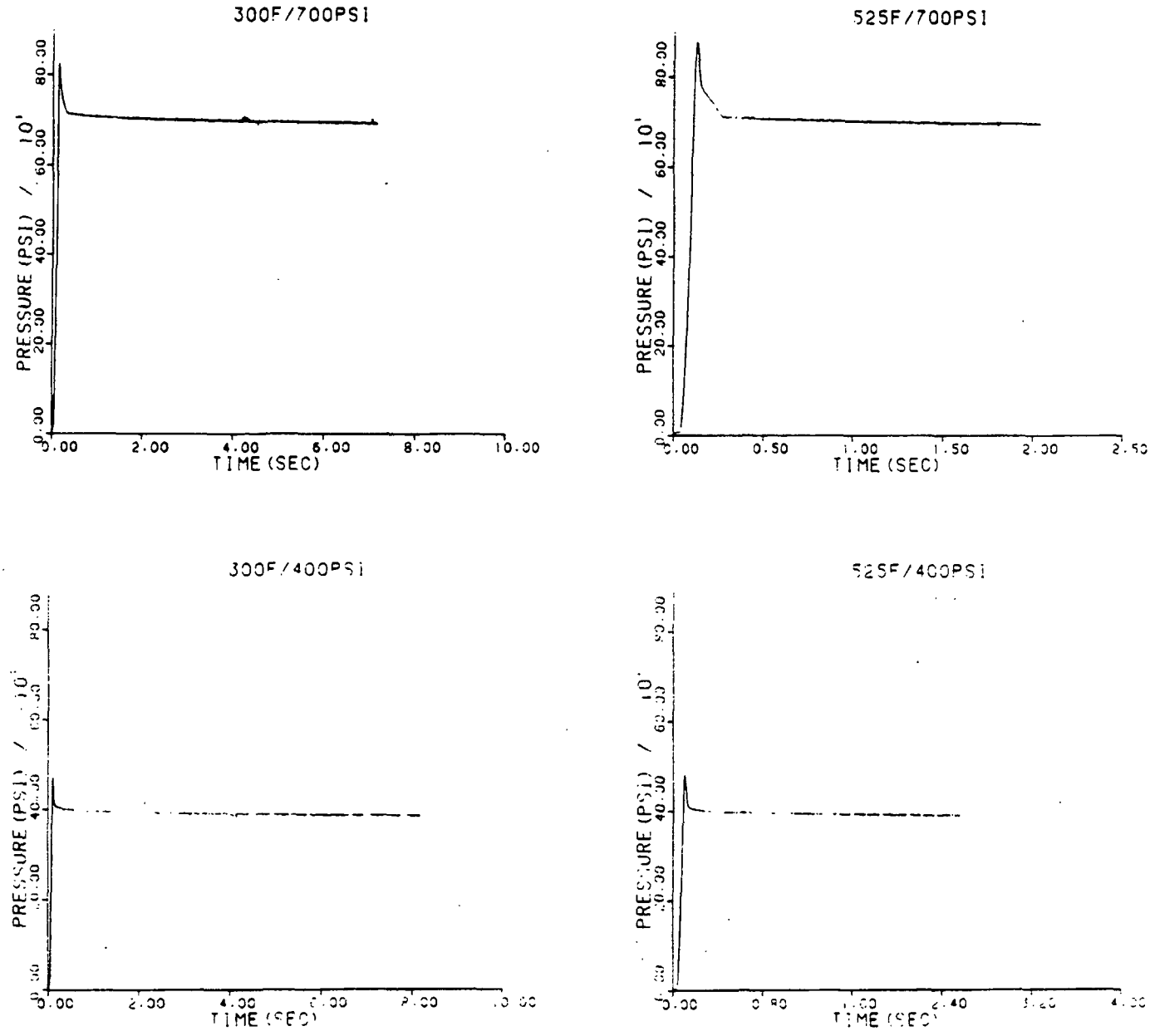

Figure 6. Applied pressure data.

Moisture Removal System

The top platen is held stationary by lock nuts on the columns which are tightened against the top and bottom of the platen. On the bottom side of the platen is a support plate. The purpose of the plate is to provide a rigid surface for the copper block and sheet to contact. The plate is made of hardened tool steel and is 8 inches in diameter and 3/4 inch thick. The top side of the plate has a 350 W tubular heater imbedded in it for heating the plate during caliper runs. The bottom side of the support plate has radial grooves machined into it to facilitate vapor removal from the compression zone. Two screens of 20 and 48 mesh, and a pulp blotter located between the screens and support plate, also aid in vapor and liquid removal. When caliper data are taken the pulp blotter is removed, and the support plate is electrically heated to 215°F to facilitate moisture removal from the compression zone.

Temperature Measurement System

The temperature measurement system consists of the thermocouples, ice-point reference junctions, and a single-ended, multiple input amplifier. The voltages of the surface thermocouple and in-sheet thermocouples are fed to a reference junction (32°F), and amplified by a factor of 100.

Caliper Measurement System

The caliper system does not contact the sheet but is mounted onto the copper block (target) and support plate (sensor). In reference to the sheet, the caliper measurement is relative to the distance between the sensor and target. The system works on the impedance variation caused by eddy currents induced by the sensor in the aluminum target. The system was calibrated by placing metal shims of known thickness in the compression zone, engaging the press, and adjusting

the target until the correct caliper was read by the system. The measurement range of the system is 0-0.180 inch.

LIST OF EQUIPMENT

Description	Manufacturer	Model Number
Laboratory Press	Fred S. Carver, Inc.	2697-S
Hydraulic Cylinder	Hydro-Line Mfg. Co.	N2R
Hydraulic Power Unit	Hydro Systems Co.	PVB6RSY20CMC
Digital Programable Timer	Automatic Timing and Controls Co.	353A351A30PX
Force Transducer System	PCB Piezotronics, Inc.	204A
Electric Cartridge Heaters	Chromalox Industrial Heating Products	CIR-5050
Calcium Silicate Insulation	Johns-Manville	Marinite^{R} XL
Surface Thermocouple (Type T)	Medtherm Corp.	TCS-061-T-1.625-CN-GGS6-B2-AB
Tubular Heater	Chromalox Industrial Heating Producsts	TSSM-20
Fine Gage Thermocouples (0.002 inch Diameter - Type T)	Omega Engineering, Inc.	COCO-002
Ice-Point Reference Junction Amplifier	Omega Engineering, Inc.	Omni-Amp II B
Displacement Measuring System	Kaman Sciences Corp.	KD-2310-45/851552-K010

DATA ACQUISITION

The analog signals from the thermocouples, force transducer and caliper system were fed into a Tracor-Northern model 1500 Digital Signal Analyzer for digitization and storage. The data were subsequently put on magnetic tape and

transferred to the Institute's Burroughs computer. In this way the entire history of a drying run was preserved and could be retrieved at any time. Appendix VIII lists the names of data storage files for the different drying conditions used in this thesis.

RESULTS

DRYING RATE STUDY

Table 1 shows the average overall drying rates and times for the four drying conditions. Figure 7 gives the sheet weight loss data, reported as relative moisture removed (RMR)[1], versus time. Appendix III gives the sheet weight data from which the RMR values were computed. The average initial moisture content of the handsheets was 56.7%, with a standard deviation of ± 0.8% in all runs. The average basis weight was 41.4 lb/1000 ft^2, with a standard deviation of ± 0.9 lb/1000 ft^2 in all runs.

Table 1. Drying rate data.

Drying Condition, °F/psi	Average Overall Drying Rate,[a] lb/hr/ft^2	Average Overall Drying Time,[a] seconds
300/400	37	5.0
300/700	46	4.0
525/400	147	1.25
525/700	184	1.0

[a]To 0.95 RMR.

In all cases the drying rates are significantly higher than those typical of conventional drying.[10] For the 300°F cases, the drying rates are approximately 7 to 10 times higher than those for conventional drying.[1] The increase in drying rates for these conditions is largely caused by the much higher applied pressure because a hot surface temperature of 300°F is not uncommon in conventional

1. $RMR = \frac{\text{initial sheet weight - sheet weight at time t}}{\text{initial sheet weight - o.d. sheet weight}}$

drying. The drying rates for the 525°F cases are over an order of magnitude higher than those found in conventional drying. For these cases, the much higher hot surface temperature has a dramatic effect on drying rate, in addition to the effect of the applied pressure.

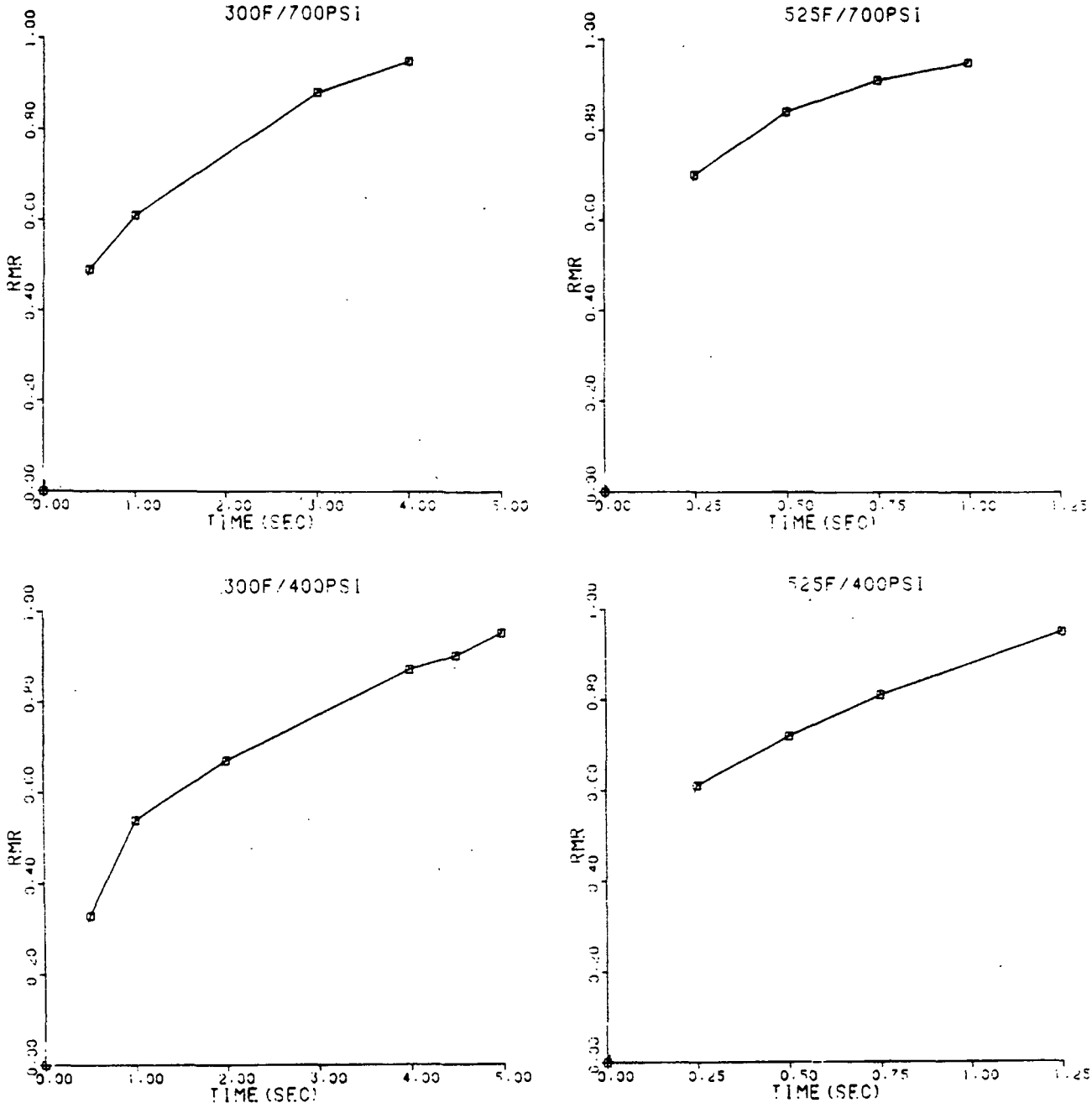

Figure 7. Relative moisture removal data.

Since the RMR values in Fig. 7 were determined gravimetrically, they are probably greater than the true values because of evaporation during the time taken to extract the sheet from the compression zone and weigh it.

LIQUID DEWATERING STUDY

The liquid dewatering results were obtained by using the lithium loss technique.[11] For comparison to liquid dewatering in high-intensity drying, a room temperature wet-pressing study was also done. For this study, the heater block of the drying apparatus was left at room temperature and the applied load was maintained on the sheet for the time indicated.

Table 2 shows the final percentages of liquid dewatering during drying and wet pressing. The percentage of liquid dewatering is defined as the percentage of the initial moisture which exits the sheet as liquid. Appendix IV gives the amounts of lithium from which the liquid dewatering values were computed. Also given are the data from which the wet-pressing results were calculated.

Table 2. Liquid dewatering data from lithium loss measurements.

Drying Condition, °F/psi	Average Liquid Dewatering, %
300/400	28
300/700	34
525/400	30
525/700	27

Wet-Pressing Data

Pressing Condition, sec/psi	Average Liquid Dewatering, %
0.5/400	3
0.5/700	5
1.0/400	3
1.0/700	9

Figure 8 shows how much moisture left the sheet as liquid (LMR) and vapor (VMR) during drying, in addition to the amount of RMR with time. The LMR data are the values of the amount of liquid dewatering at the time specified. The VMR data were computed as the difference between the RMR and LMR measured data. All three quantities are based on the initial amount of moisture in the sheet.

The experimental data plotted in Fig. 8 show that for all drying conditions approximately 71% of the initial moisture leaves the sheet as vapor, and 29% exits as liquid. For the 300°F cases, liquid dewatering is over 0.75 sec from the start of drying. In the 525°F cases, liquid dewatering is over before 0.25 sec from the start of drying. For the 525°F cases, liquid dewatering took place so quickly that only the final amounts could be measured. The data given in Table 2 for wet pressing under similar conditions shows that at 700 psi, liquid dewatering continues for at least 1 sec, and 9% of the initial liquid is pressed out of the sheet. At 400 psi, liquid dewatering is over before 0.5 sec from the start of pressing, and only 3% of the initial liquid is pressed out of the sheet.

LIQUID MOVEMENT STUDY

For this study, chlorine, as lithium chloride, was added to the handsheet stock slurry. When a sheet is dried the chlorine moves only with the liquid and not with the vapor. Thus, when a sheet is dried to dryness the chlorine distribution through the thickness of a sheet is indicative of the local cumulative evaporation in the sheet, and, hence, net liquid movement. The chlorine distributions were determined using Scanning Electron Microscope/Energy Dispersive Spectroscopy.[12-13] The data are only semiquantitative in that the absolute amount of chlorine in the sheet is not measured; only the relative occurrence of chlorine in a section of the sheet is measured.

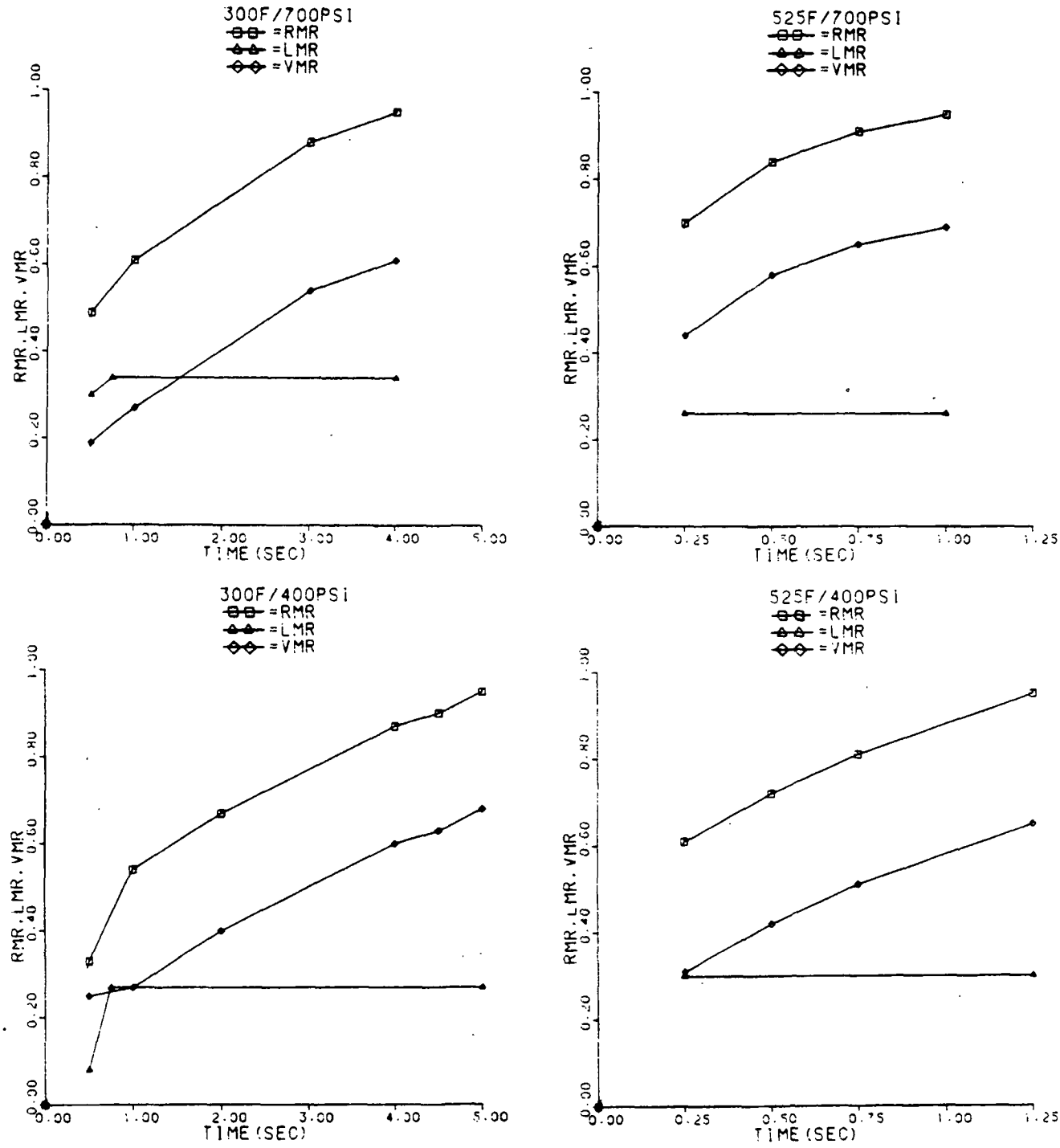

Figure 8. Amounts of moisture removal in liquid and vapor form.

Figure 9 shows the final chlorine distributions for sheets dried at the four drying conditions. Also given is a distribution for a freeze-dried sheet intended to show the initial moisture distribution in the sheet before high-intensity drying. The high-intensity drying distributions are further defined as having hot surface and cold surface sides. The hot surface is that part of the sheet which is in contact with the heater block. The cold surface is that part of the sheet which contacts the screens, as shown by the arrangement depicted in Fig. 5. These designations are used throughout the remainder of this thesis.

All of the drying conditions induced significant amounts of liquid movement. To varying degrees, each condition has a U-shaped chlorine distribution. However, in light of subsequent interpretations of the other experimental data, a suitable reason for why the distributions take on this shape cannot be found. Thus, these data are presented here without further comment.

HEAT FLUX STUDY

Figure 10 shows representative hot surface temperature data plotted with the corresponding computed heat flux from the hot surface to the sheet for each drying condition. Table 3 shows the percentages of liquid dewatering computed from sheet energy balances, using the integrated heat flux and sheet weight data. For comparison the percentages of liquid dewatering from the lithium loss measurements are also given. Details on the calculations are given in Appendix V.

The most intense drying condition had the highest peak heat flux, and the least intense condition had the lowest peak heat flux. Also, the 525°F cases had higher peak heat fluxes than the 300°F cases. These higher heat transfer rates are consistent with the drying rates observed earlier. The results of the liquid dewatering calculations show that all drying conditions had similar amounts of liquid dewatering. These results are similar to those obtained by the lithium loss measurements.

Freeze-Dried

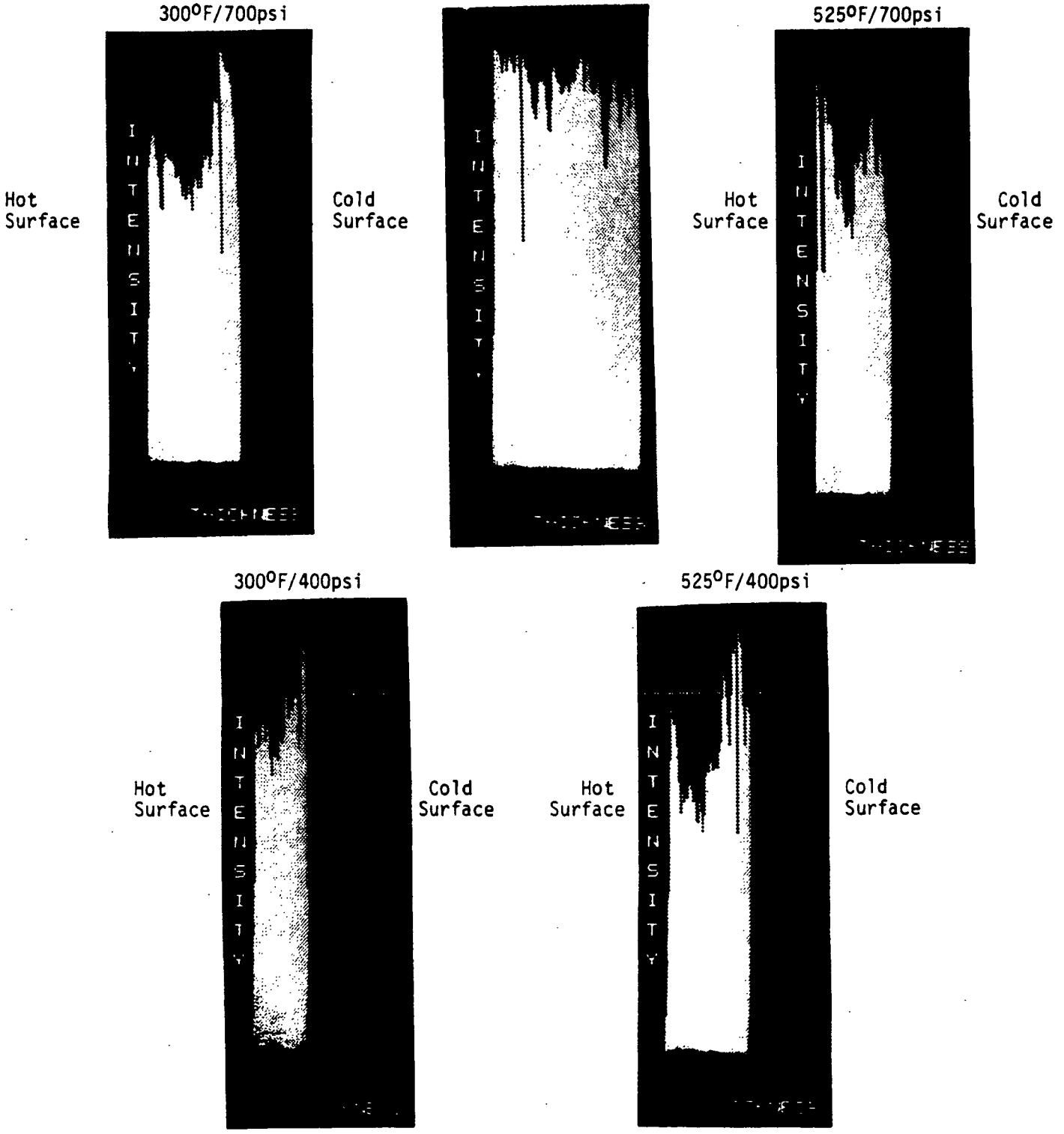

Figure 9. Chlorine distribution data.

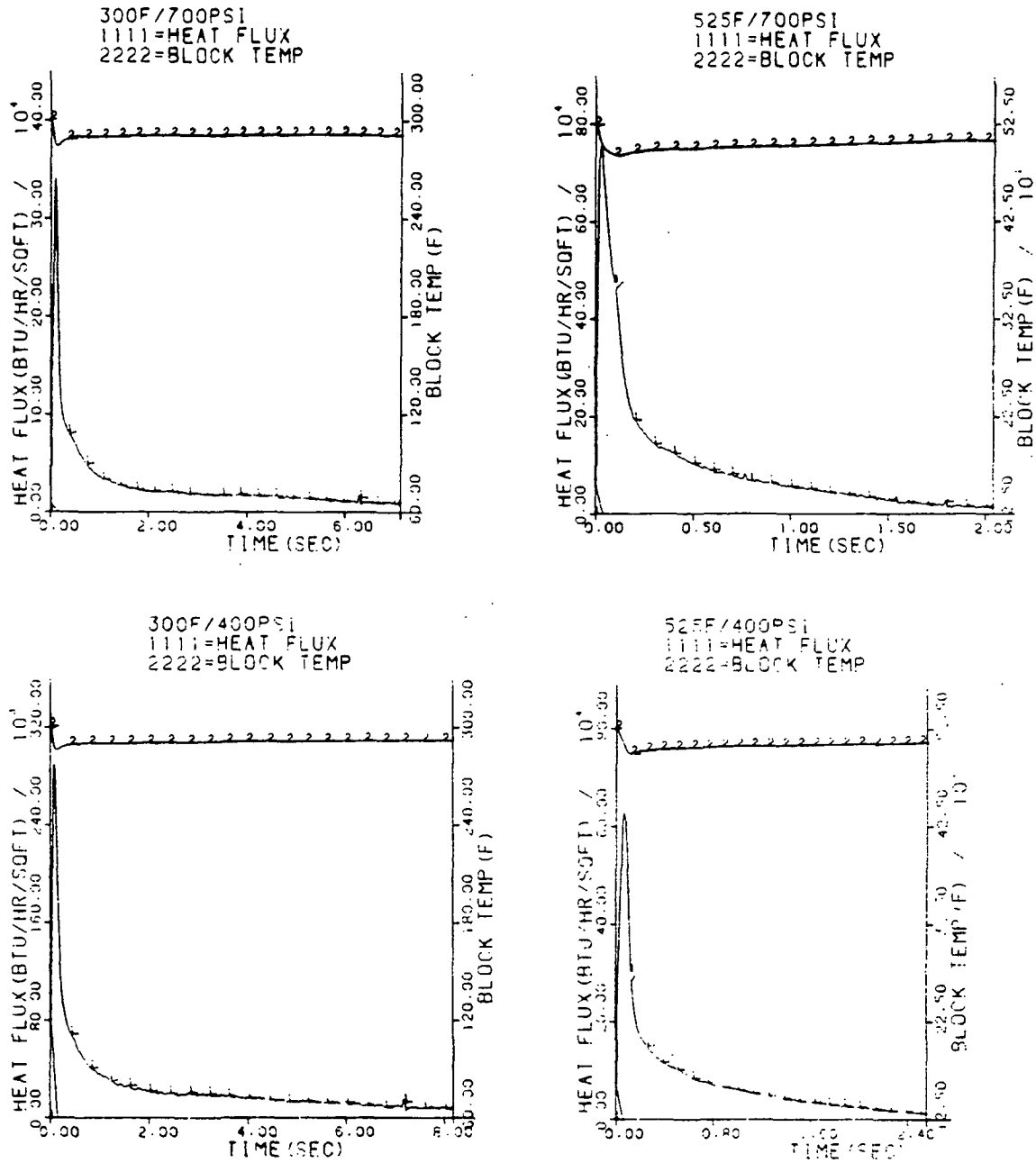

Figure 10. Surface temperature and heat flux data.

Table 3. Liquid dewatering data from heat transfer measurements.

Drying Condition, °F/psi	Average Liquid Dewatering (Heat Transfer), %	Average Liquid Dewatering (Lithium Loss), %
300/400	25	28
300/700	30	34
525/400	25	30
525/700	31	27

At the end of drying the values of the heat fluxes did not approach zero. This indicates that heat losses were occurring from the sheet to the surroundings. A study was done to find whether the losses were significant. The details on the study are found in Appendix VI. The results of the study show that heat losses were not significant to the 0.95 RMR point in drying and would not significantly affect the heat transfer measurements used in computing the liquid dewatering results. In addition, radiation heat transfer to the sheet from the hot surface is also not accounted for in this thesis. The calculation in Appendix VII shows that radiation heat transfer to the sheet is negligible in high-intensity drying. Several authors[14-16] have shown that radiation in porous media is also negligible for temperatures below 750°F and small particle sizes.

INTERNAL SHEET TEMPERATURE STUDY

Figure 11 shows representative hot surface temperature and internal sheet temperatures for each drying condition. The internal temperatures were recorded at equal basis weight fractions through the thickness of the sheet. Throughout this thesis the internal sheet temperatures are referred to using the following nomenclature. The temperature measured by the thermocouple 1/4 of the way through the sheet from the hot surface is referred to as the 1/4 basis weight temperature. The temperature measured by the thermocouple 1/2 of the way through the sheet is referred to as the 1/2 basis weight temperature. The temperature measured by the thermocouple 3/4 of the way through the sheet from the hot surface is referred to as 3/4 basis weight temperature.

The internal sheet temperatures have four distinct periods: an initial period where all of the temperatures rise rapidly, a period where the temperatures peak consecutively starting from the hot surface, a period where the temperatures

decline to a minimum point in the curves, and a final period where the temperatures rise as the end of drying is approached.

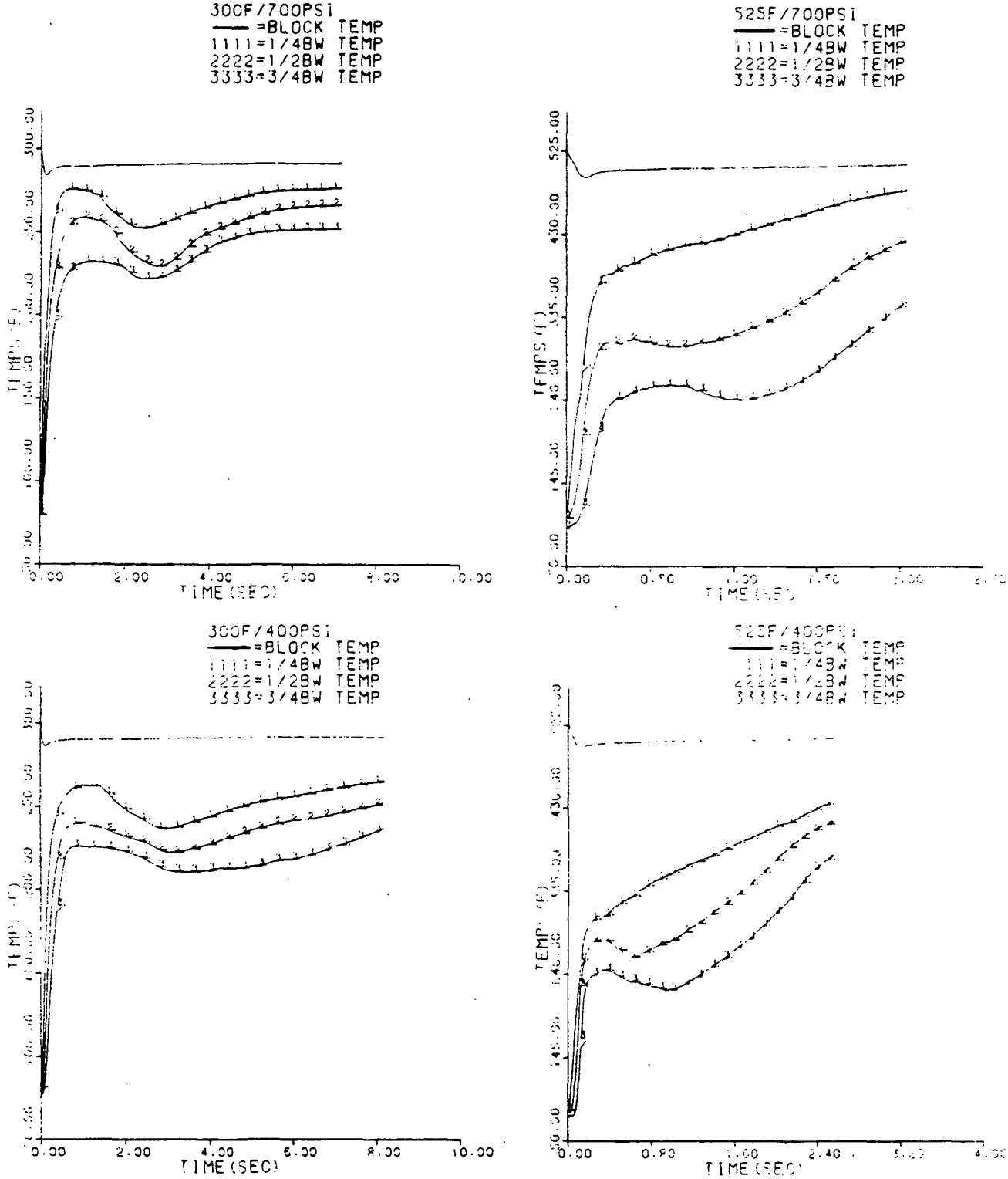

Figure 11. Internal sheet temperature data.

CALIPER STUDY

Figure 12 shows representative caliper data for each drying condition. The final calipers for all drying conditions differed little. The caliper curves have three distinct periods: A rapid sheet compression period, a long period where the caliper decreases significantly more slowly, and an even longer, final period where the caliper decreases more rapidly and then changes very slowly as the end of drying is approached.

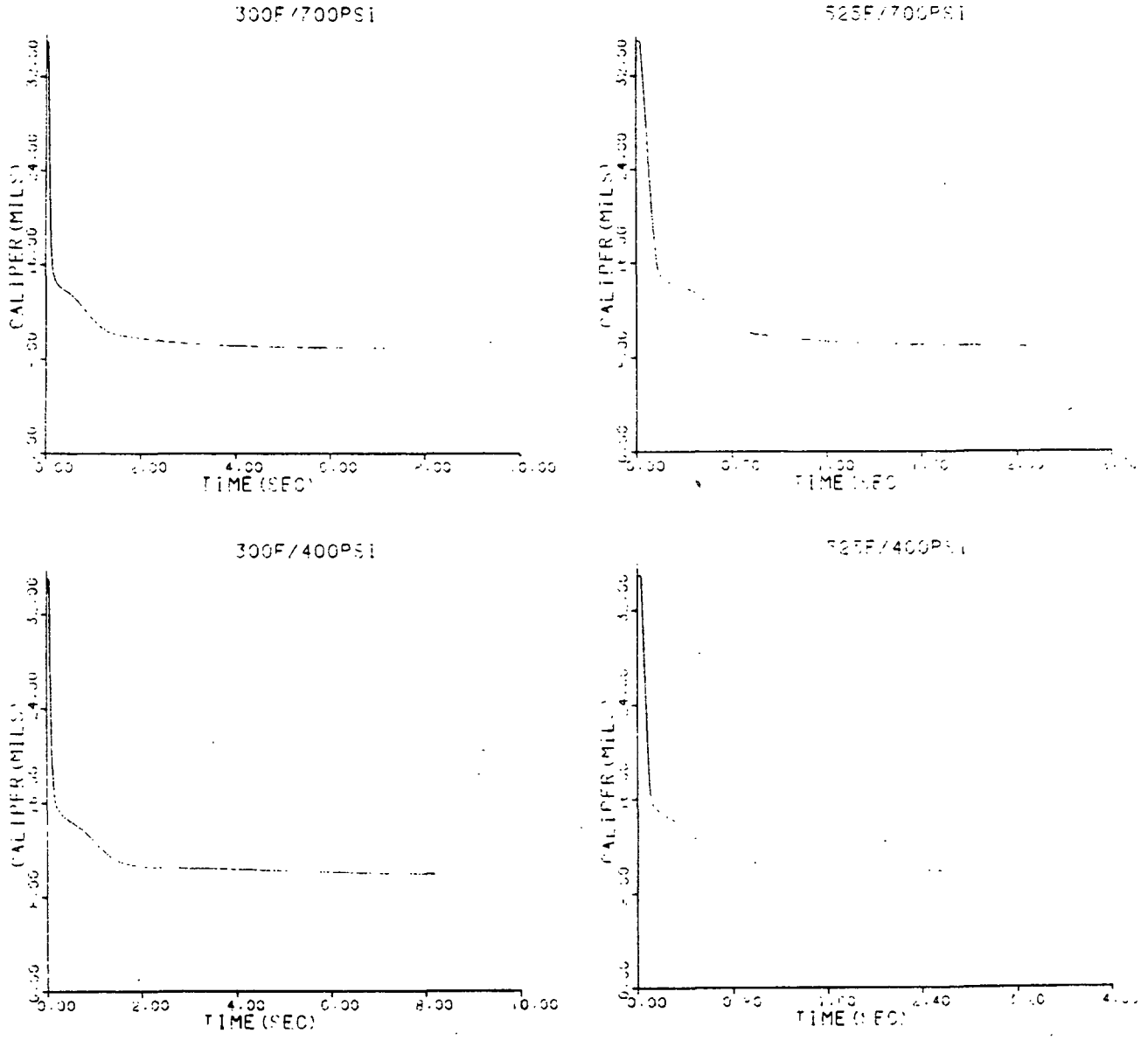

Figure 12. Caliper data.

MECHANISMS OF HIGH-INTENSITY DRYING

For any sheet consolidation process, dewatering and densification are the key measures of process performance. In high-intensity drying, drying rates can be an order of magnitude higher than those typical of conventional drying. High-intensity drying also causes a significant amount of moisture to exit the sheet as liquid, and produces higher sheet densities than both wet pressing and conventional drying.

High-intensity drying combines phenomena common to wet pressing and conventional drying, and to neither. However, it is the intensity of these phenomena which leads to new and novel drying mechanisms. It is the purpose of the following discussion to identify these mechanisms based on the experimental data. Quantitative modeling is not attempted here.

For purposes of description, the high-intensity drying process is divided into three successive periods: Compression and Heat-Up Period, Liquid Dewatering Period, and Evaporation Period. In Fig. 13, the vertical dashed lines are used to denote the time boundaries between the periods. Line A denotes the time boundary between the Compression and Heat-Up and the Liquid Dewatering Periods. Line B denotes the time boundary between the Liquid Dewatering and the Evaporation Period. Line C denotes the 0.95 RMR point for the particular drying condition. This notation is used in many of the figures that follow. The experimental data supporting boundaries A and B will be given later. It is recognized that these boundaries do not always represent strict demarcation points between the different dewatering and densification mechanisms which occur over the drying interval. However, clarity requires that some system of time boundaries be

employed. It is felt that these boundaries represent the most logical division of the data.

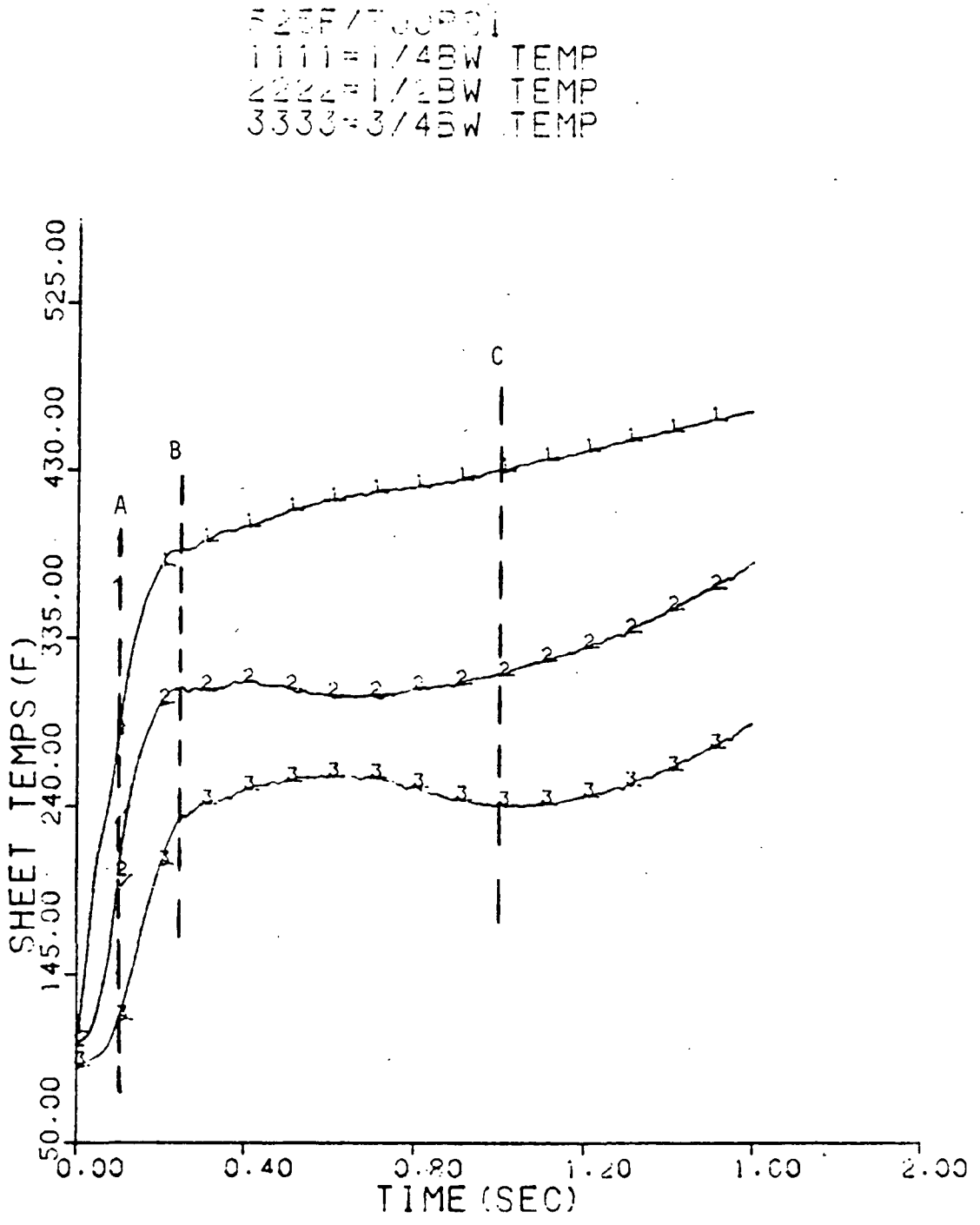

Figure 13. Sheet temperature data with vertical dashed lines denoting time boundaries between drying periods.

The mechanisms occurring in each of the periods are explained in terms of the physical processes which govern them, namely, sheet compression, heat transfer, and mass flow. Although each of the mechanisms is examined separately, several occur simultaneously, and the interrelationships among them are shown.

Many of the mechanisms discussed herein would not occur if not for the intense drying conditions compared to conventional drying. Although not explicitly stated in many places, these more intense conditions give rise to the new and novel mechanisms occurring in high-intensity drying, and should be kept in mind throughout the following discussion.

COMPRESSION AND HEAT-UP PERIOD

INITIAL SHEET COMPRESSION NEGLECTING THERMAL EFFECTS

High-intensity drying begins when the applied pressure brings the hot surface and sheet into contact. In this investigation, the response time of the hydraulic power unit is responsible for the relatively slow applied pressure rises shown in Fig. 14. This, in turn, is responsible for the relatively slow initial sheet compression rates shown in Fig. 15. The decline in sheet caliper causes the pore volume to decrease and air to be driven from the network. In addition, the data in Fig. 15 also show that sheet compression occurs at approximately the same rate for all drying conditions. These data are similar to caliper data recorded during the wet-pressing of unsaturated sheets shown in Fig. 16.[17] A calculation of the liquid saturation caliper for a typical sheet used in this investigation aids in explaining this similarity. The initial sheet moisture content and basis weight in this investigation averaged 56.7% and 41.4 lb/1000 ft^2, respectively. For these characteristics, the sheet will become saturated with liquid at a caliper of 0.0156 inch. The data in Fig. 17 show that this caliper is not achieved until later during compression. Hence, it appears that the initial compression process in high-intensity drying may be described as one of mechanical compression of an unsaturated sheet. However, simultaneously with compression, heat transfer to the sheet will modify the compression process, as discussed below.

EFFECTS OF HEAT TRANSFER TO THE SHEET DURING COMPRESSION

Initially, there is a large temperature difference between the hot surface and the sheet. The computed heat flux to the sheet from hot surface temperature

measurements is shown in Fig. 18. The magnitude of the heat flux is largely dependent on the intensity of the drying condition, as shown by the data.

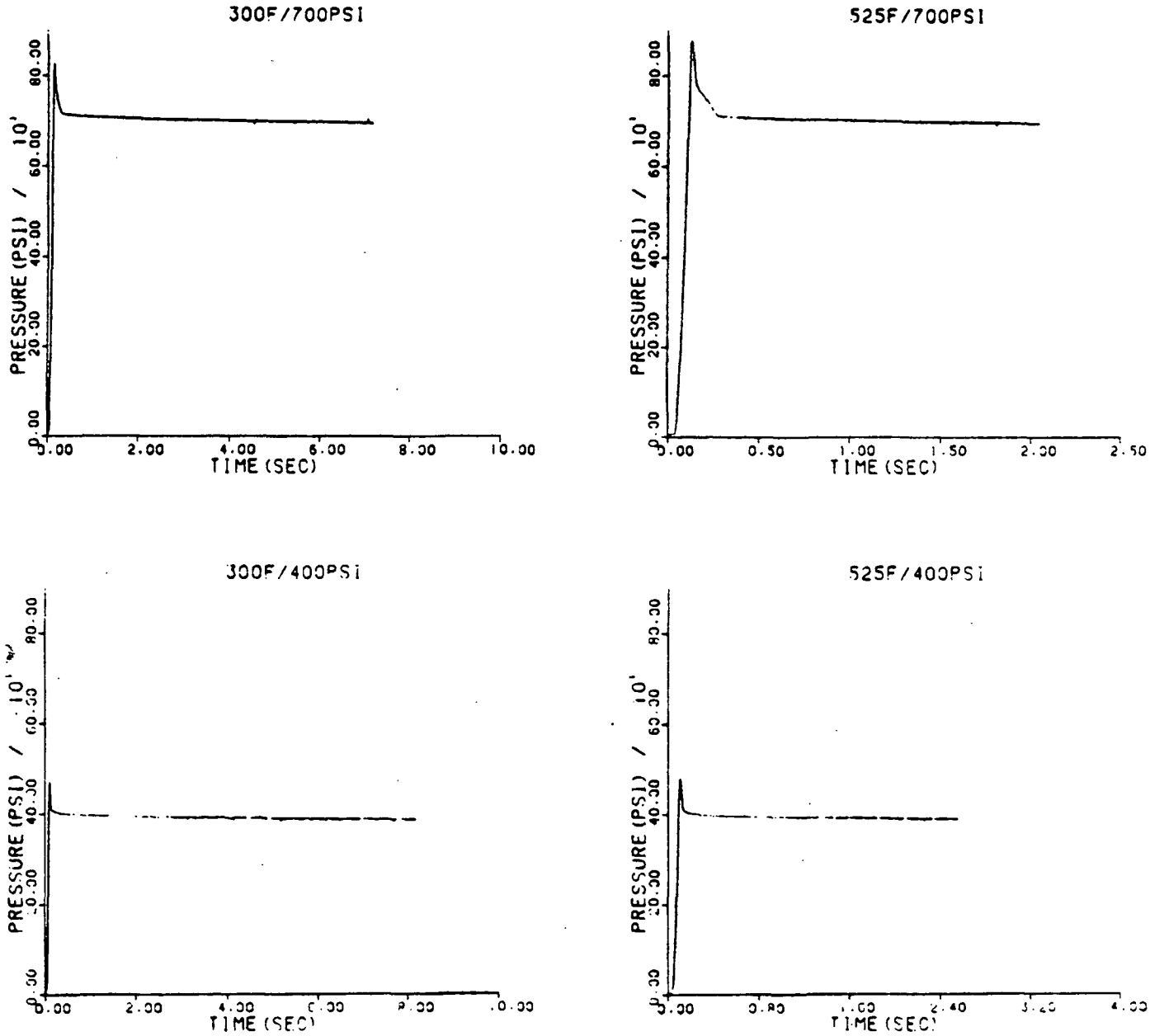

Figure 14. Applied pressure data showing relatively slow rise to set point.

Heat transfer to the sheet during compression causes the temperature to rise in the manner shown in Fig. 19. Later in the period, the data show that the temperature near the hot surface becomes greater than 212°F. Given the

conditions in the sheet at this time, there are only two ways this can happen: the sheet has dried out to the 1/4 basis weight point and the fibers are storing energy, or the water is being heated under pressure, allowing the temperature to rise.

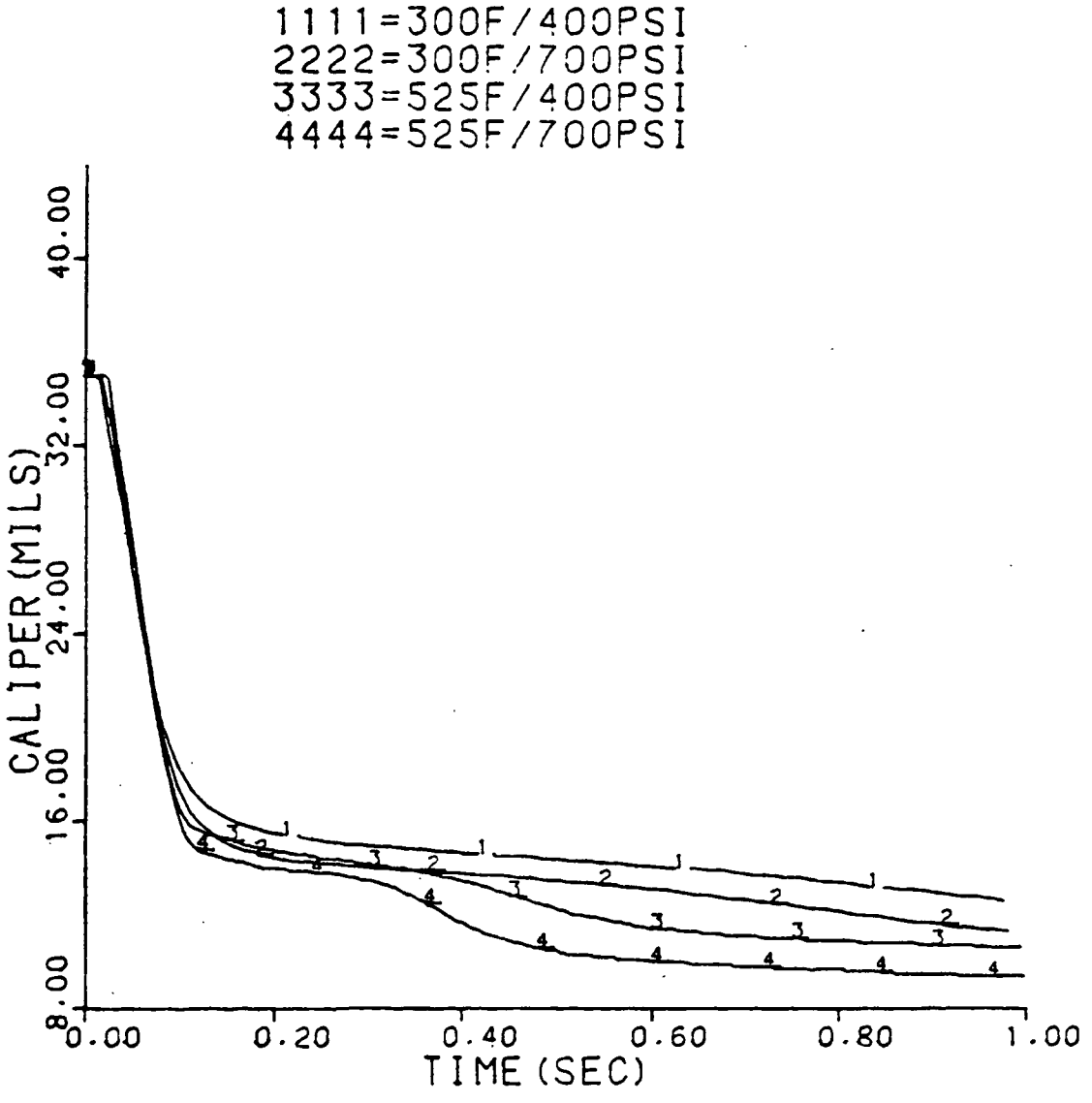

Figure 15. Caliper data showing relatively slow, but uniform initial sheet compression rates.

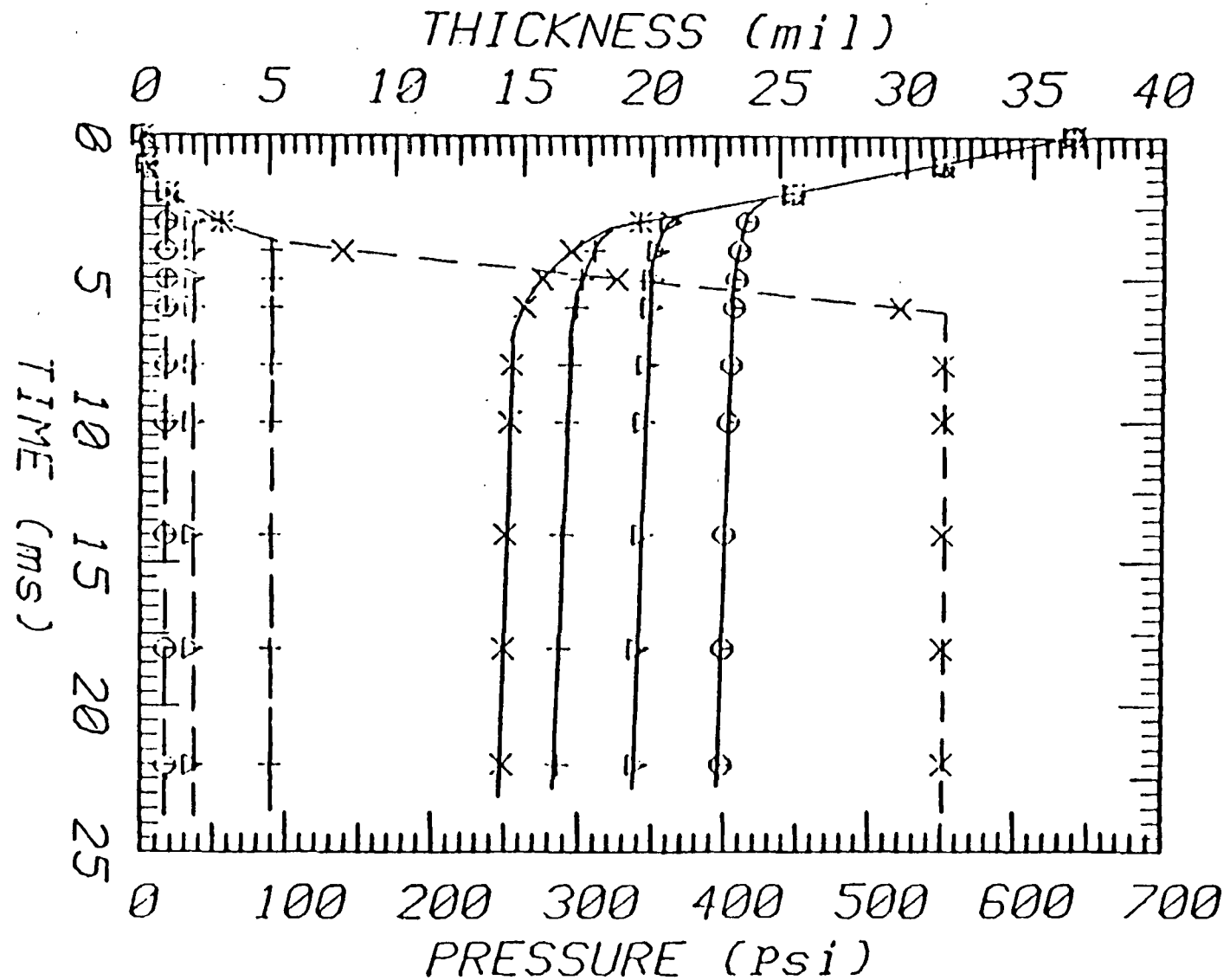

Figure 16. Corresponding caliper (solid lines) and applied pressure (dashed lines) data for wet pressing of unsaturated sheets, made from bleached, softwood kraft pulp, 291 mL CSF, 41 lb/1000 sq ft basis weight, and 50% initial moisture content.[17]

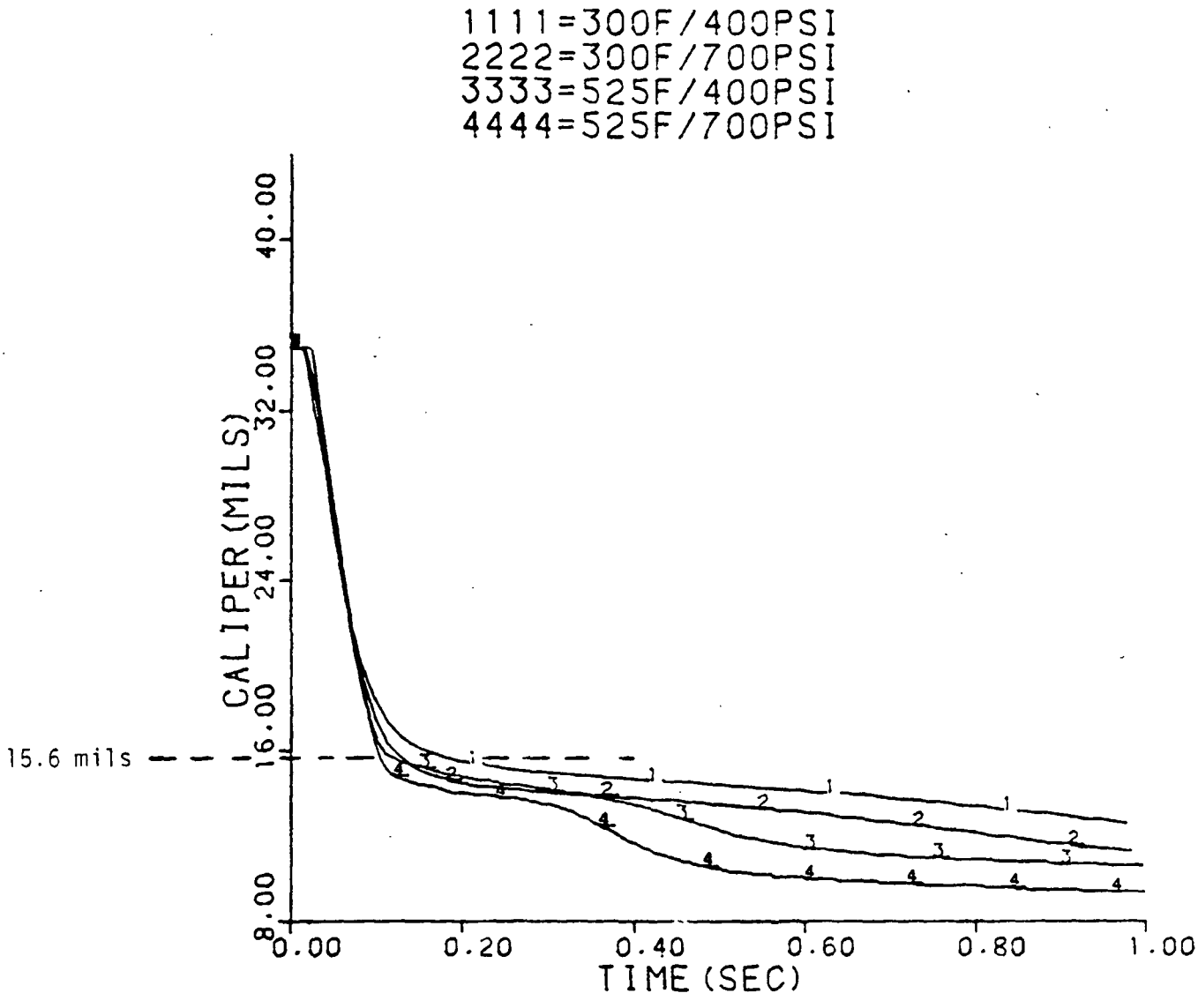

Figure 17. Caliper data showing that saturation caliper (15.6 mils) is not reached until later stages of compresssion.

Table 4 shows the cumulative amount of heat transferred to the sheet by the end of this period for each drying condition. The data were obtained by integrating the heat fluxes over time. The results of these integrations are plotted in Fig. 20. Table 4 also shows the amount of energy needed to raise the sheet temperature to 212°F, accompanied by the amount of energy to raise the

temperature to 212°F and evaporate all of the liquid initially in the sheet. Both of these later values were calculated based on the average amounts of liquid and fiber initially present in the sheet and an initial temperature of 80°F.

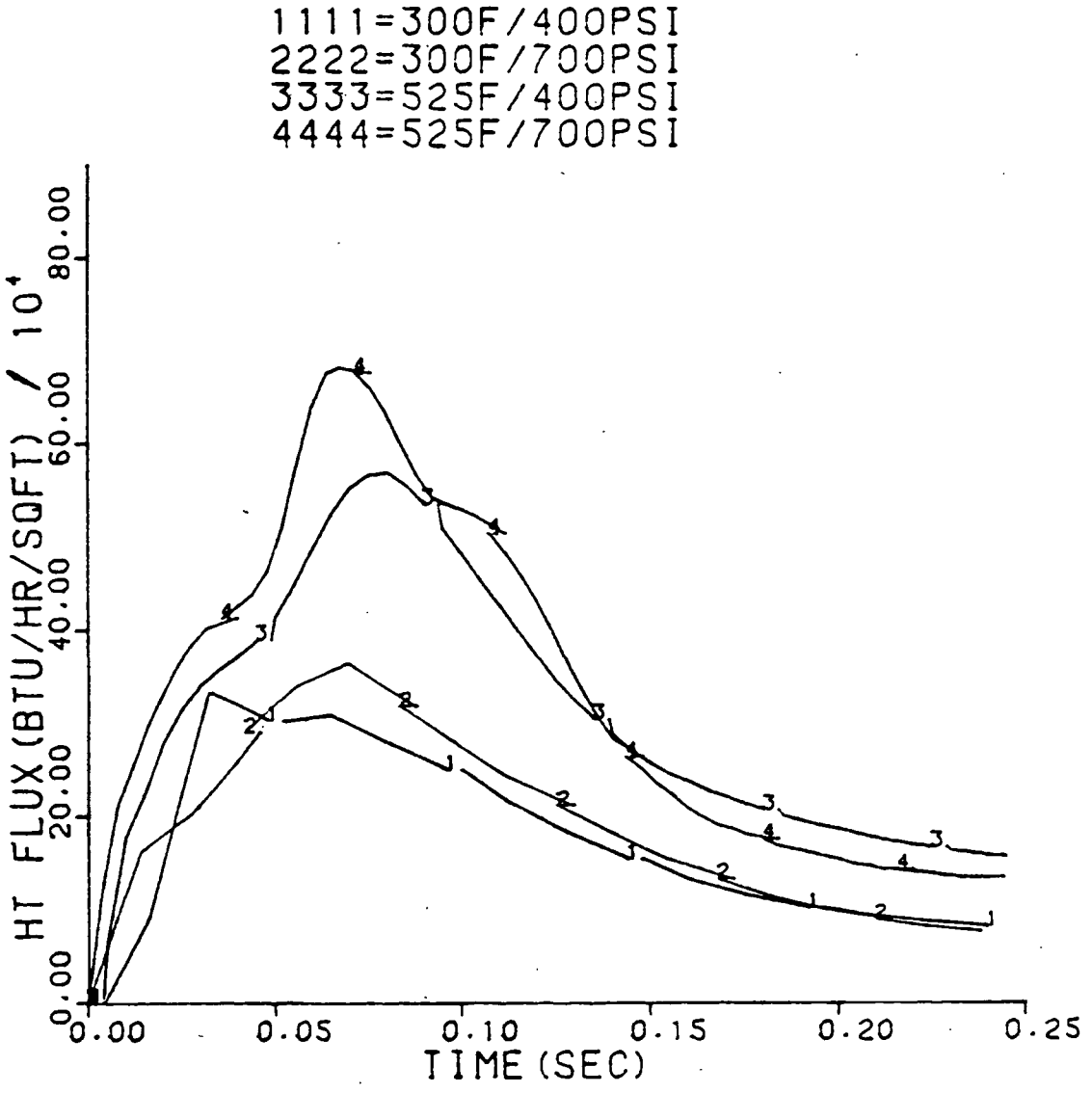

Figure 18. Heat flux data showing high heat transfer rates to the sheet during compression.

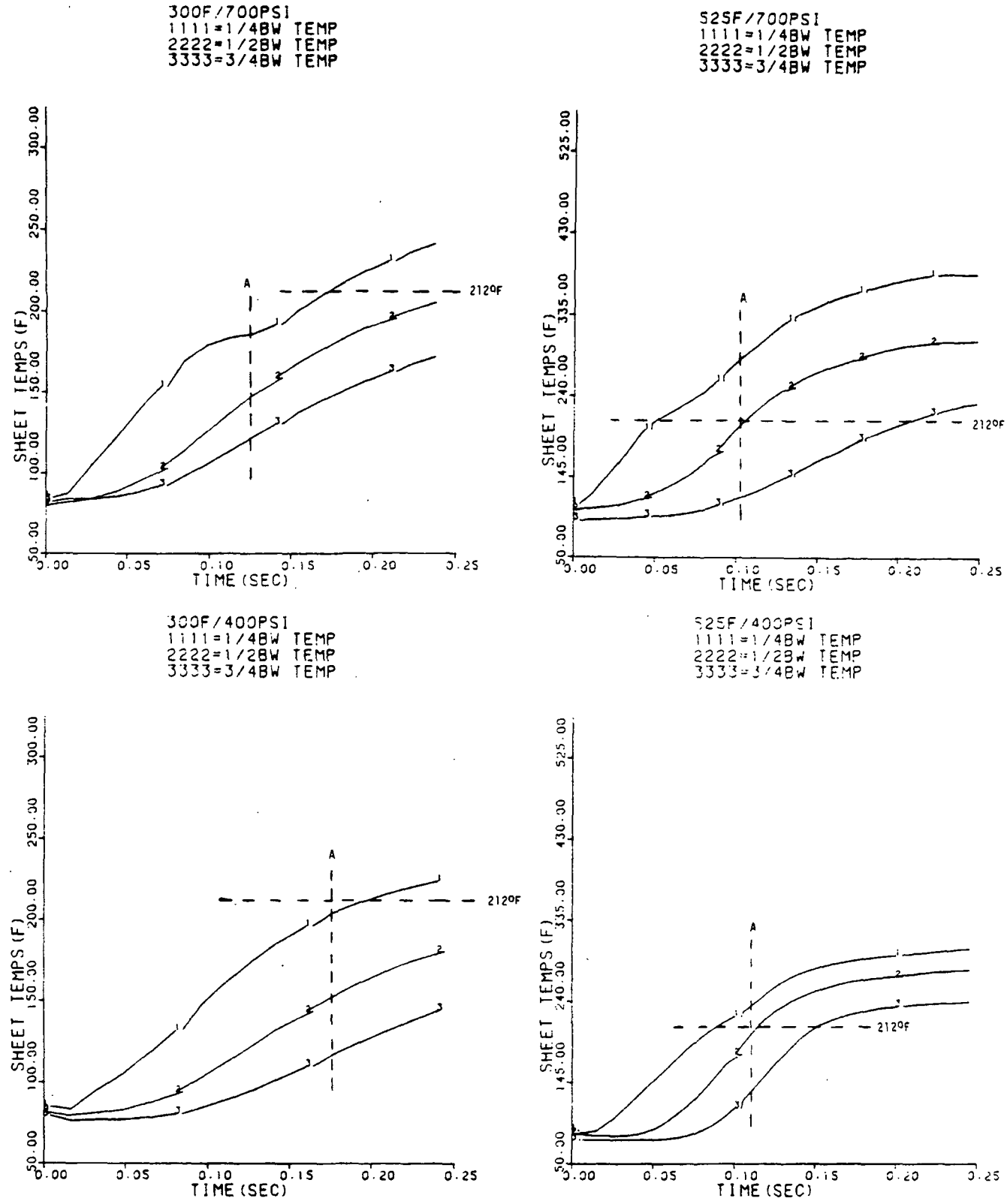

Figure 19. Sheet temperature rise during compression.

Table 4. Heat transfer data.

Drying Condition, °F/psi	Cumulative Heat Transfer,[a] Btu	Calculated Sensible Heat,[b] Btu	Calculated Total Heat,[c] Btu
300/400	1.74 (t=0.176 sec)		
300/700	1.55 (t=0.126 sec)		
525/400	2.25 (t=0.120 sec)	1.48	10.08
525/700	2.44 (t=0.104 sec)		

[a]From Fig. 20 (X 0.165 ft^2) at times listed.
[b]Sensible enthalpy change of liquid and fibers from 80 to 212°F, mass of initial liquid in sheet = 8.86×10^{-3} lb., mass of fiber in sheet = 6.77×10^{-3} lb.
[c]Sensible enthalpy change plus latent enthalpy change at 212°F, latent enthalpy change at 212°F = 970.3 Btu/lb.

Clearly, the heat input is only enough to cause a small amount of evaporation. Therefore, the areas where the temperature exceeds 212°F cannot be dried out, and part of the sheet must be pressurized.

Vapor or liquid flow, or both, acting in concert with the flow resistance of the sheet can be the only reason a part of the sheet becomes pressurized in this period. The flow resistance must be considerably greater than in conventional drying because of the reduction in sheet volume during compression. Liquid flow can be ruled out because the caliper data in Fig. 21 show that the temperature near the hot surface exceeds 212°F before the sheet is compressed to the saturation caliper of 0.0156 inch. This indicates that vapor is pressurizing a portion of the sheet. This, in turn, indicates that evaporation and vapor convection are occurring inside the sheet at this time.

There is no other direct evidence to show that evaporation and vapor convection are occurring inside the sheet. However, the heat flux data, plus vapor phase pressure data from other, similar investigations indicate that evaporation

and vapor convection are occurring at the hot surface during this period. The heat flux data shown in Fig. 22 peak at values which are typical of boiling heat transfer,[18] and suggest that a vigorous evaporation process is occurring at the hot surface. The vapor phase pressure data of Ahrens[5] and Burton[6] are shown in Fig. 23 and 24, respectively. These data indicate that evaporation and vapor convection were occurring at the hot surface early in drying during these experiments. Since these experiments were conducted under similar drying conditions as those used in this investigation, similar conclusions can be drawn about evaporation and vapor convection at the hot surface herein.

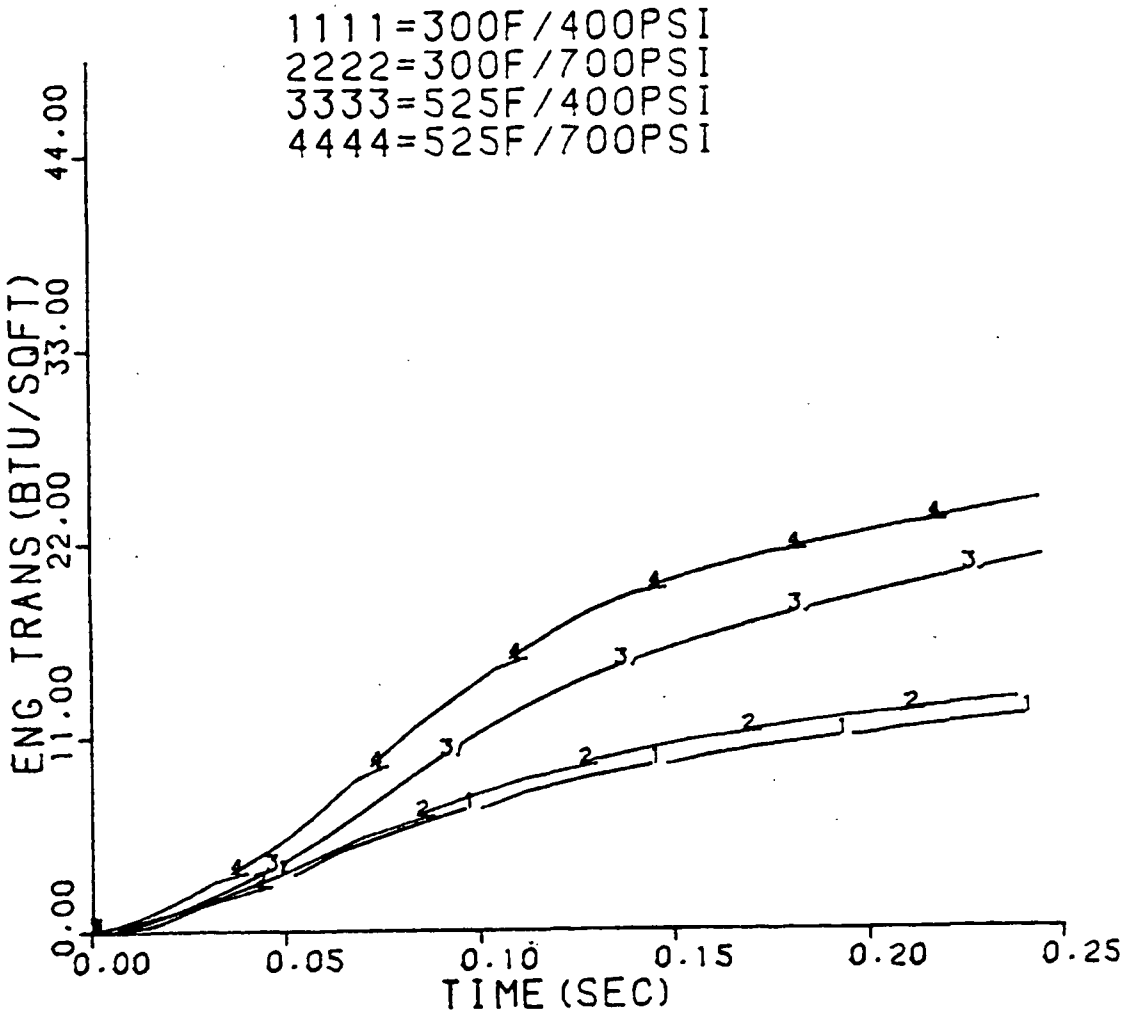

Figure 20. Cumulative amount of heat transferred to the sheet during compression.

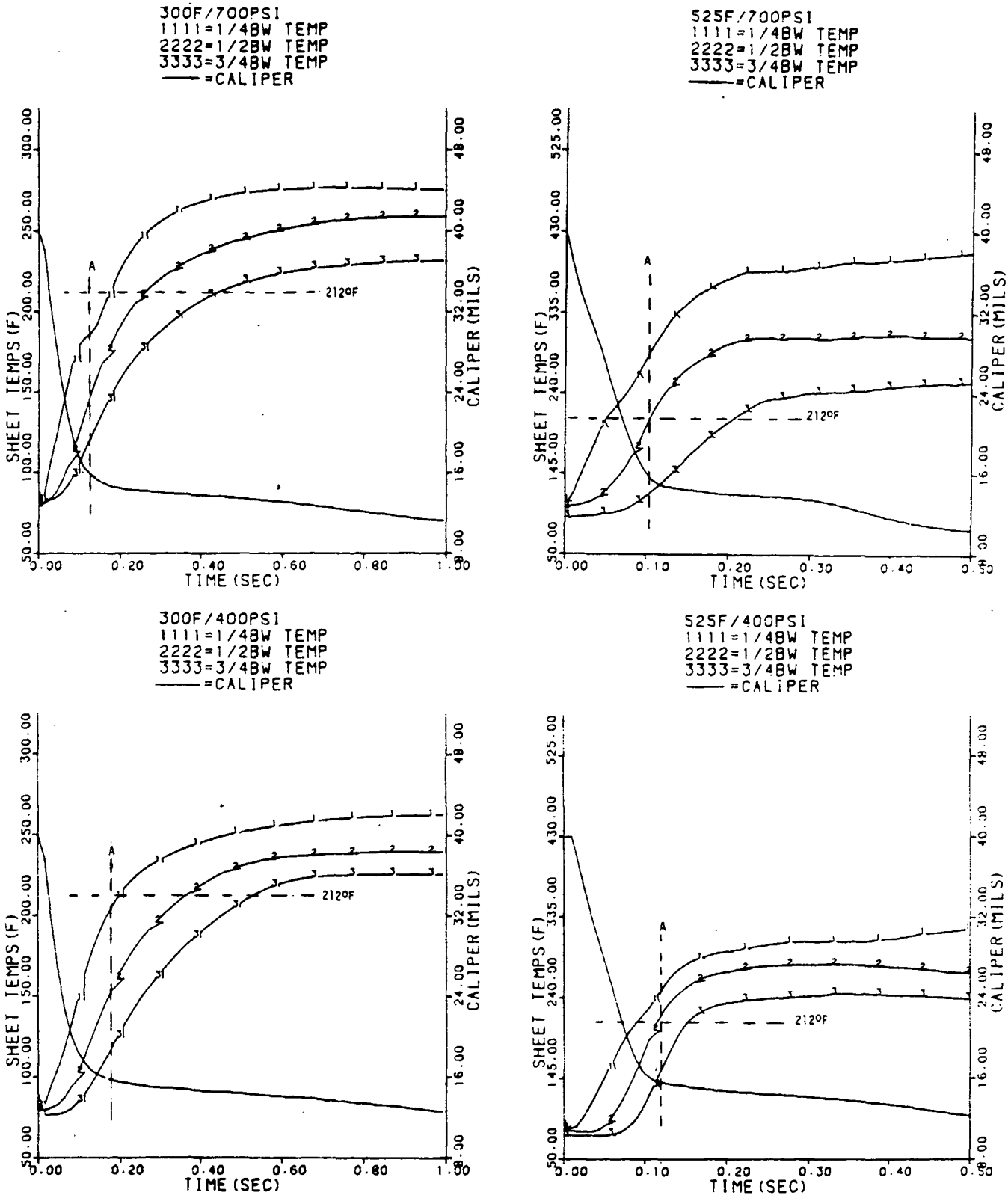

Figure 21. Sheet temperature and caliper data showing that the temperature near the hot surface exceeds 212°F before the saturation caliper (15.6 mils) is reached.

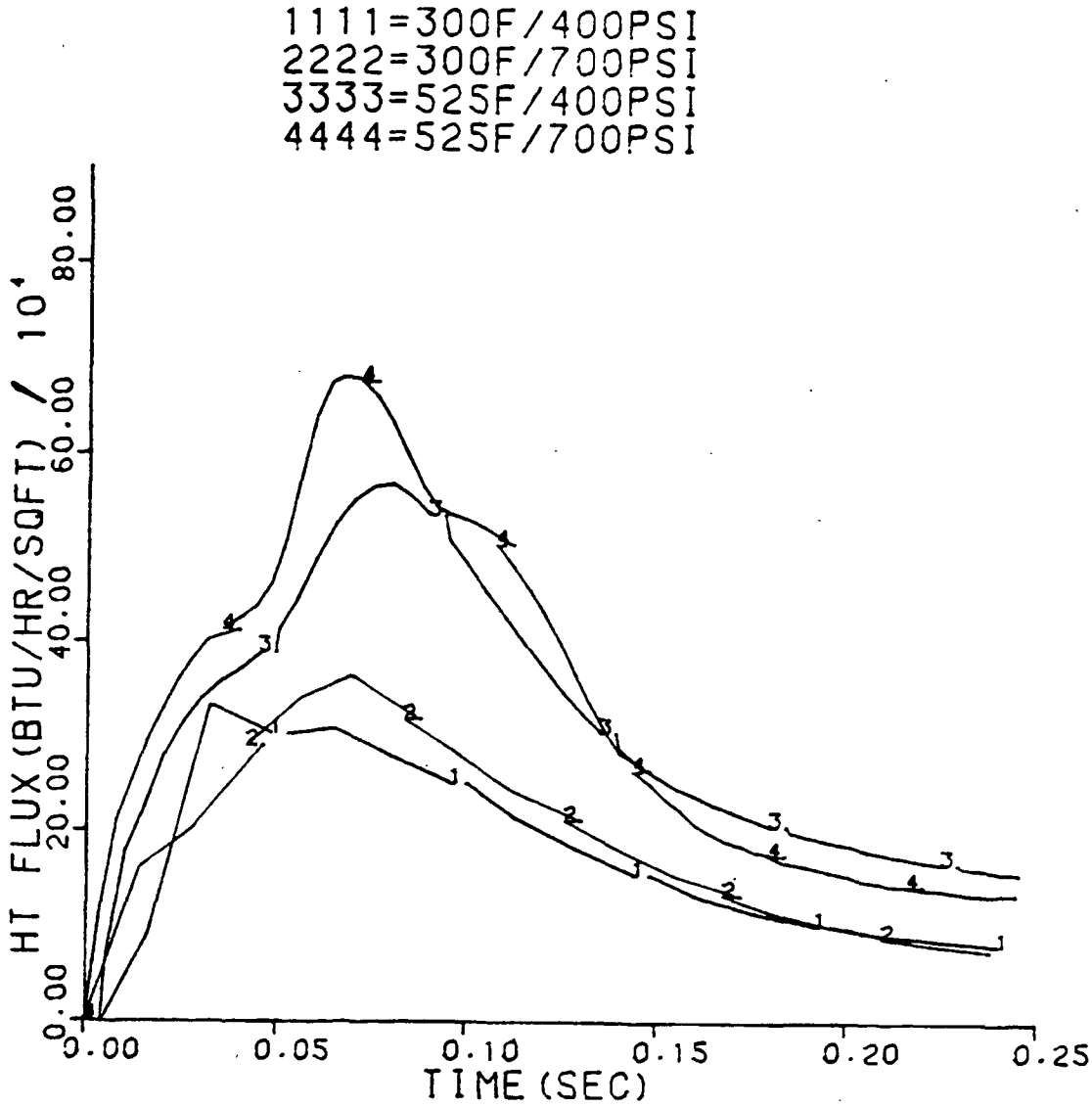

Figure 22. Heat flux data peak at values which are typical of boiling heat transfer.[18]

IN-SHEET HEAT TRANSFER AND MASS FLOW MECHANISMS DURING COMPRESSION

Given the above circumstances, evaporation must eventually begin away from the hot surface because the sheet is not saturated and heat is still being transferred into the sheet. As evaporation begins away from the hot surface, the sheet can be considered to be divided into two zones through its thickness: an expanding vapor pressurized zone (VPZ) where temperatures are 212°F or

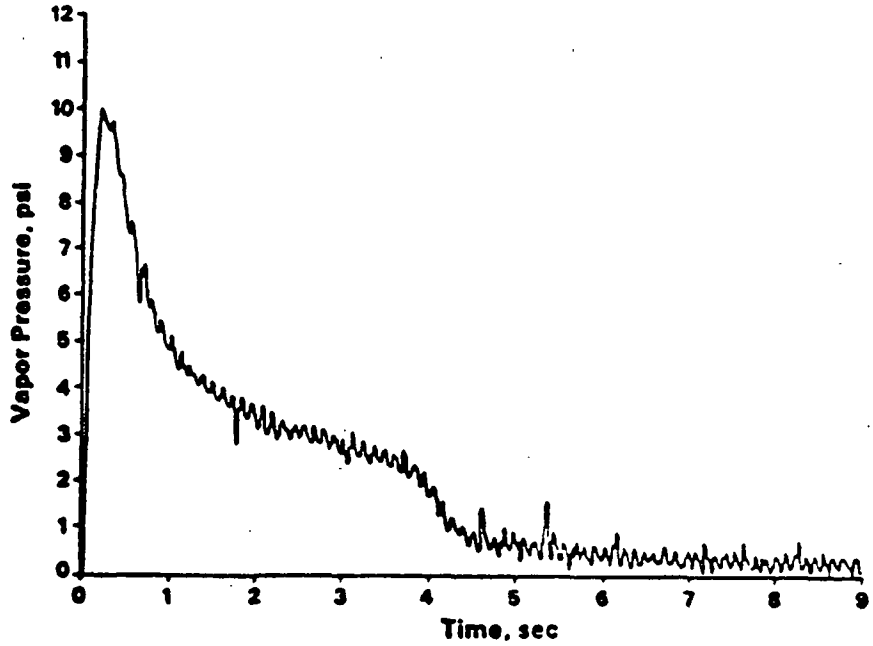

Figure 23. Vapor phase pressure at hot surface for an unbleached softwood kraft handsheet, 42 lb/1000 ft^2 basis weight, 60% initial MC, 300°F surface temperature and 46.5 psi applied pressure.[5] (Note: pressure given is gage pressure).

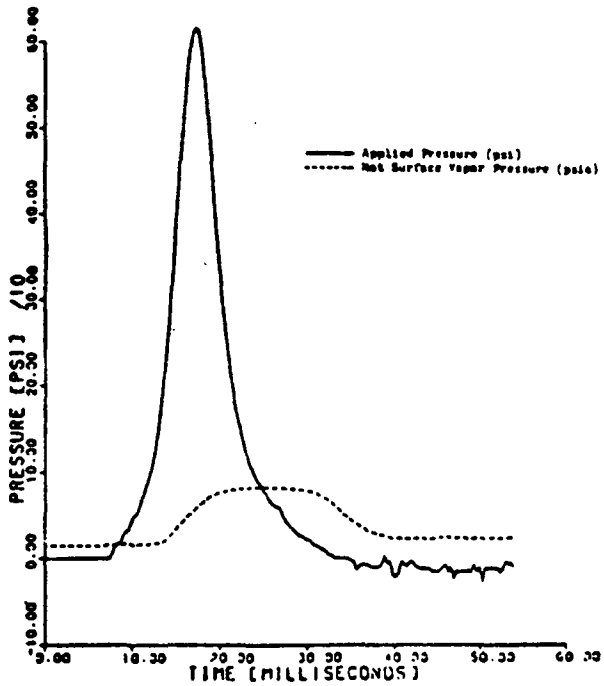

Figure 24. Vapor phase pressure at hot surface plotted with applied pressure for impulse dried, unbleached softwood kraft handsheet, 34 lb/1000 ft^2 basis weight, 66% initial MC, 600°F surface temperature and 600 psi peak applied pressure.[6]

greater, and a contracting unsaturated zone (USZ) where temperatures are lower than 212°F. In the VPZ, a vapor phase pressure gradient will develop because of differing evaporation rates caused by differing local heat transfer rates and the increasing flow resistance caused by sheet compression. This vapor phase pressure gradient has a significant influence on the events in this period, as discussed below.

As the VPZ begins to expand, evaporation will have already reduced the supply of liquid at the hot surface. A smaller amount of liquid near the hot surface will affect heat transfer to the sheet because evaporating liquid is a more efficient heat transfer medium than vapor or fiber. When vapor begins to occupy the pore spaces at the hot surface, the effective thermal conductivity of the area will decline and slow the rate of heat transfer into the sheet, even as compression is making the heat transfer distance shorter. In addition, the increasing sheet temperature will also slow the heat transfer rate by lowering the driving force. It is likely then, that the decline in the heat fluxes shown in Fig. 25, are caused by the decline in the effective thermal conductivity at the hot surface and the rising sheet temperatures.

Away from the hot surface, the vapor phase pressure will suppress evaporation and cause heat storage in the liquid and fibers as the VPZ moves progressively toward the cold surface. Heat storage will cause the temperatures in the VPZ to exceed 212°F. These elevated temperatures will also promote conduction heat transfer into the USZ. Also, it is possible that the vapor flow will displace or entrain liquid in the network pores, and by doing so, redistribute liquid and sensible heat into the USZ.

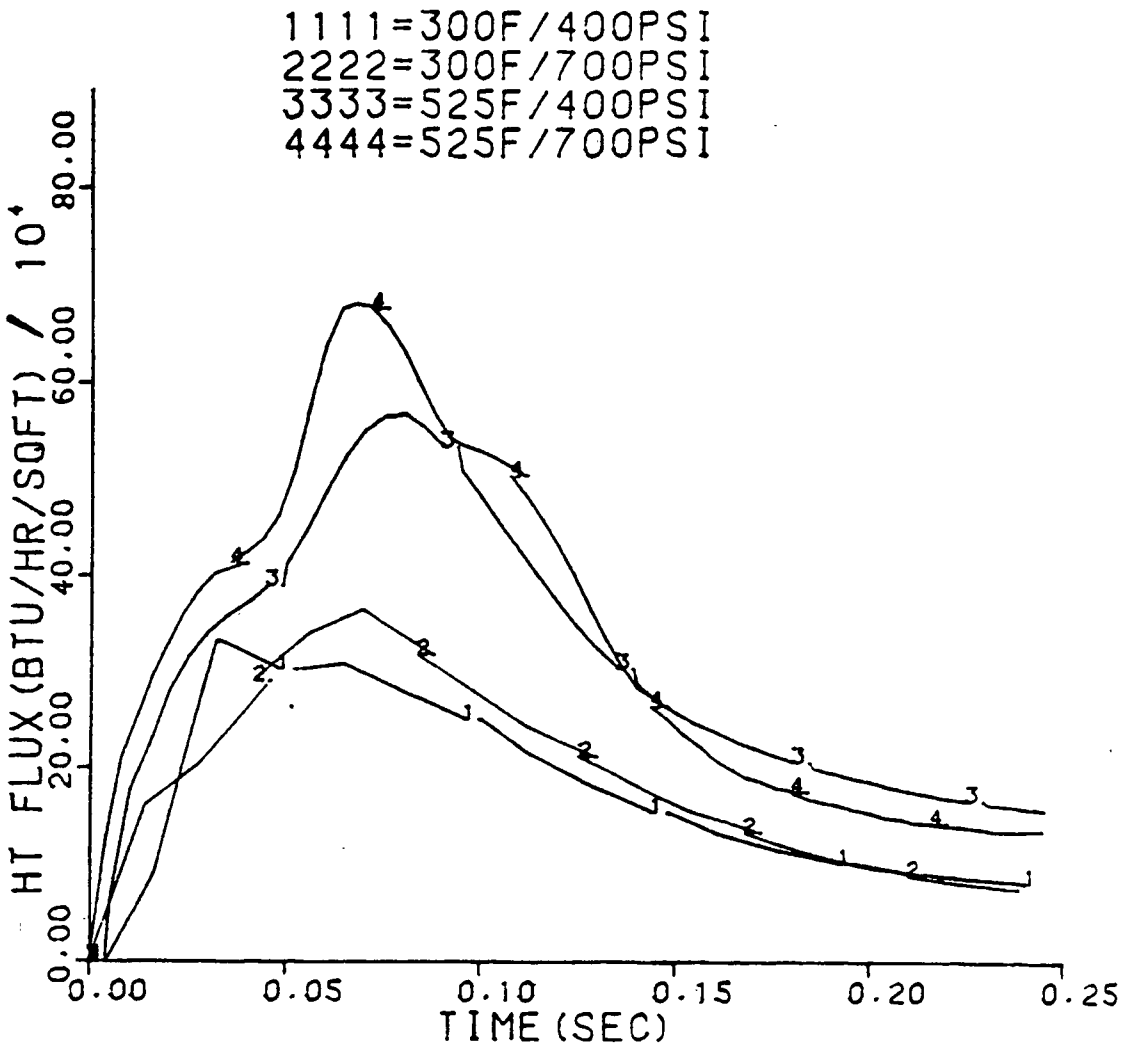

Figure 25. Heat flux data begin to decline during sheet compression.

However, the most important contribution of the vapor phase pressure gradient is to heat transfer and mass flow. Once evaporated, vapor will flow toward the cold surface through the network pores until it contacts cooler liquid and fiber, whence it will condense. This evaporation-convection-condensation (E-C-C) mechanism, plus heat conducted through the network, is the primary means by which heat is transferred to the evaporation sites in the VPZ. In fact, the temperature data in Fig. 26 show that the 3/4 basis weight temperature is below 212°F during all of this period, making it unlikely that any vapor will leave the sheet. In addition to transferring heat, vapor condensation will also increase the local

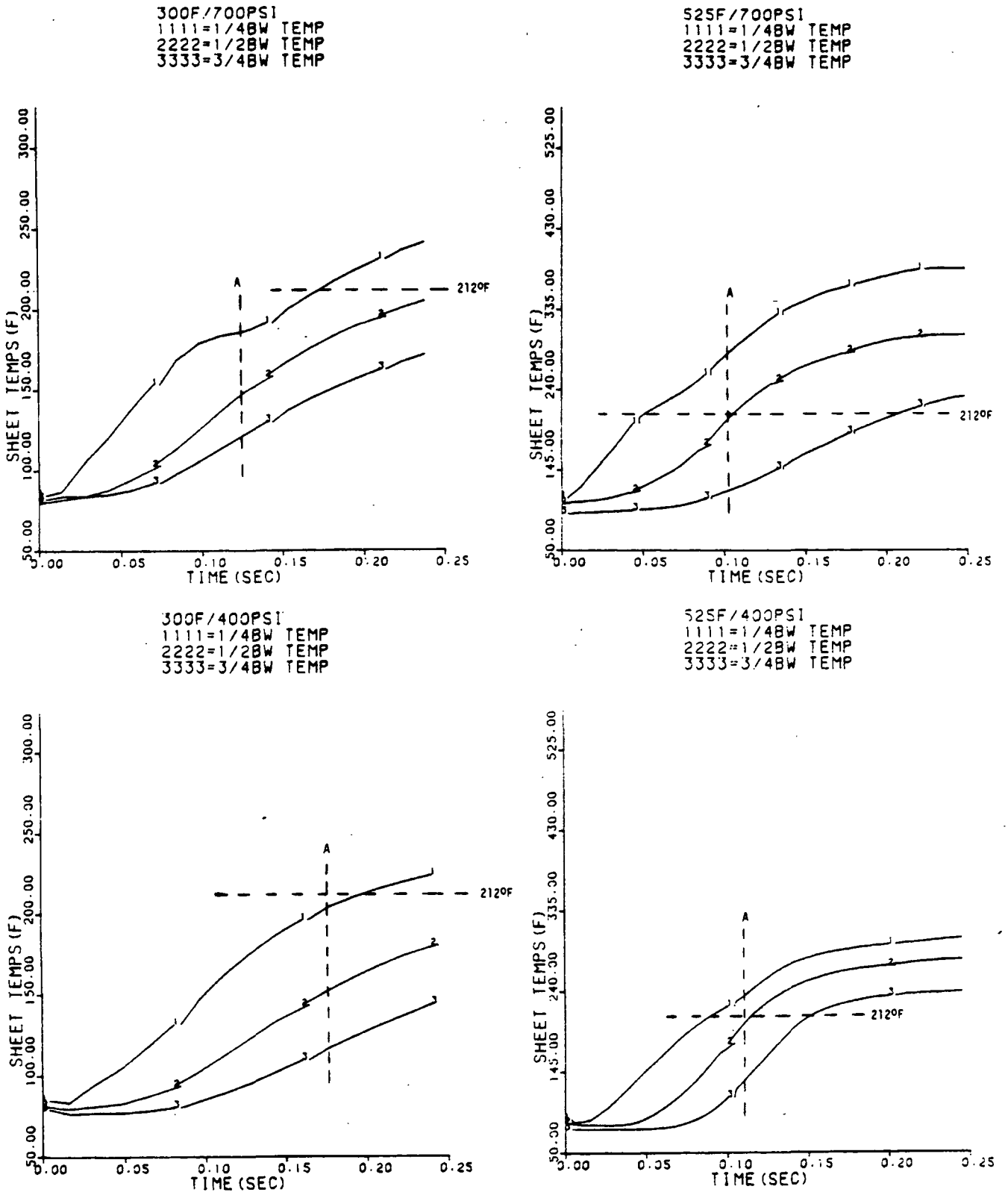

Figure 26. Sheet temperature data showing that the 3/4 basis weight temperature is below 212°F during compression.

saturation level and flow resistance. There are probably other effects from the vapor phase pressure gradient than those listed here. However, the above mechanisms are thought to be the most important and will become magnified in importance as compression continues.

CONDITIONS IN THE SHEET NEAR THE SATURATION POINT

All of the above events are occurring as the sheet caliper is still being rapidly reduced by the applied pressure. As the sheet approaches the saturation caliper, temperatures are above 212°F in over 1/2 of the sheet in the 525°F cases, and in about 1/4 of the sheet in the 300°F cases, as shown by the data in Fig. 27. This indicates that the VPZ now occupies a significant portion of the sheet thickness.

One effect of the elevated temperatures is thermal softening of the fibers, as it is well known that several of the constituent fiber polymers will begin to soften and flow under pressure at temperatures above approximately 175°F.[19-21] Fiber softening would explain why the 525°F cases, which have higher sheet temperatures than the 300°F cases, reach the saturation caliper earlier, as shown by the data in Fig. 28. In addition, the vapor phase pressures must also be higher in the 525°F cases. However, the vapor phase pressure does not seem to impede sheet densification to any significant degree because the data show that the 525°F cases reach the saturation caliper before the 300°F cases.

As previously noted, during the Compression and Heat-Up Period it is unlikely that any vapor leaves the sheet because the 3/4 basis weight temperature is below 212°F. In addition, any liquid movement out of the sheet is also unlikely because at temperatures below 212°F there can be no significant liquid pressure in the USZ until saturation is reached. This indicates that the volume available for vapor is growing smaller as the caliper is being reduced. Near saturation,

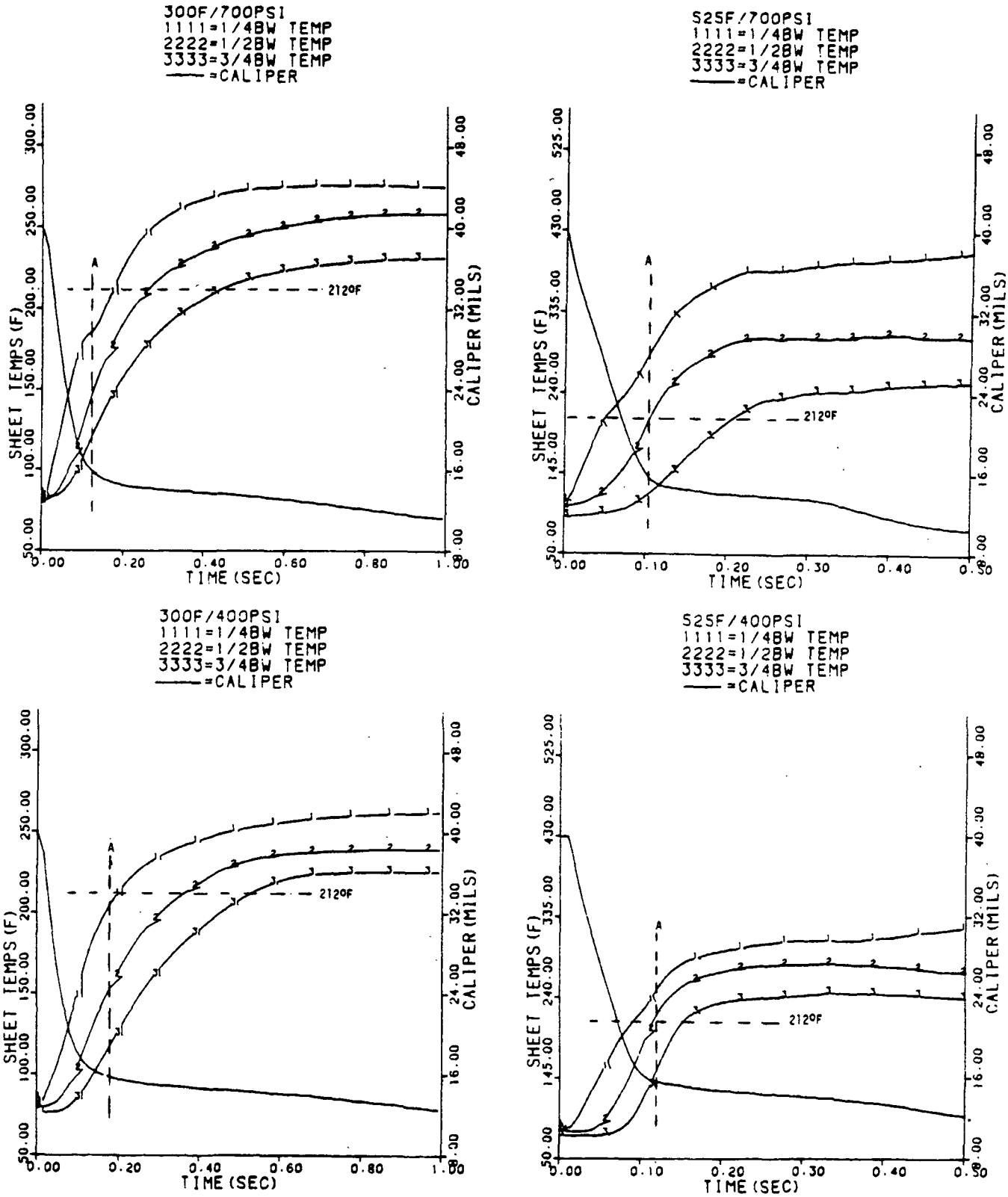

Figure 27. Sheet temperature and caliper data showing that the temperature near the hot surface exceeds 212°F as the saturation caliper (15.6 mils) is approached.

only a very small amount of vapor can remain in the VPZ, causing a considerable amount of energy storage in the liquid and fibers. This continues to allow the temperature and vapor phase pressure to rise in the VPZ. However, it is unlikely that all of the vapor is condensed and a completely liquid filled sheet exists at the saturation caliper in high-intensity drying. A liquid filled sheet would reinitiate the evaporation process at the hot surface. The heat flux data do not indicate this, as the heat fluxes decline rather smoothly as shown in Fig. 29. Thus, further compression will cause saturation followed by liquid dewatering. In this context, saturation is defined as an air-free sheet filled with liquid and a small amount of vapor.

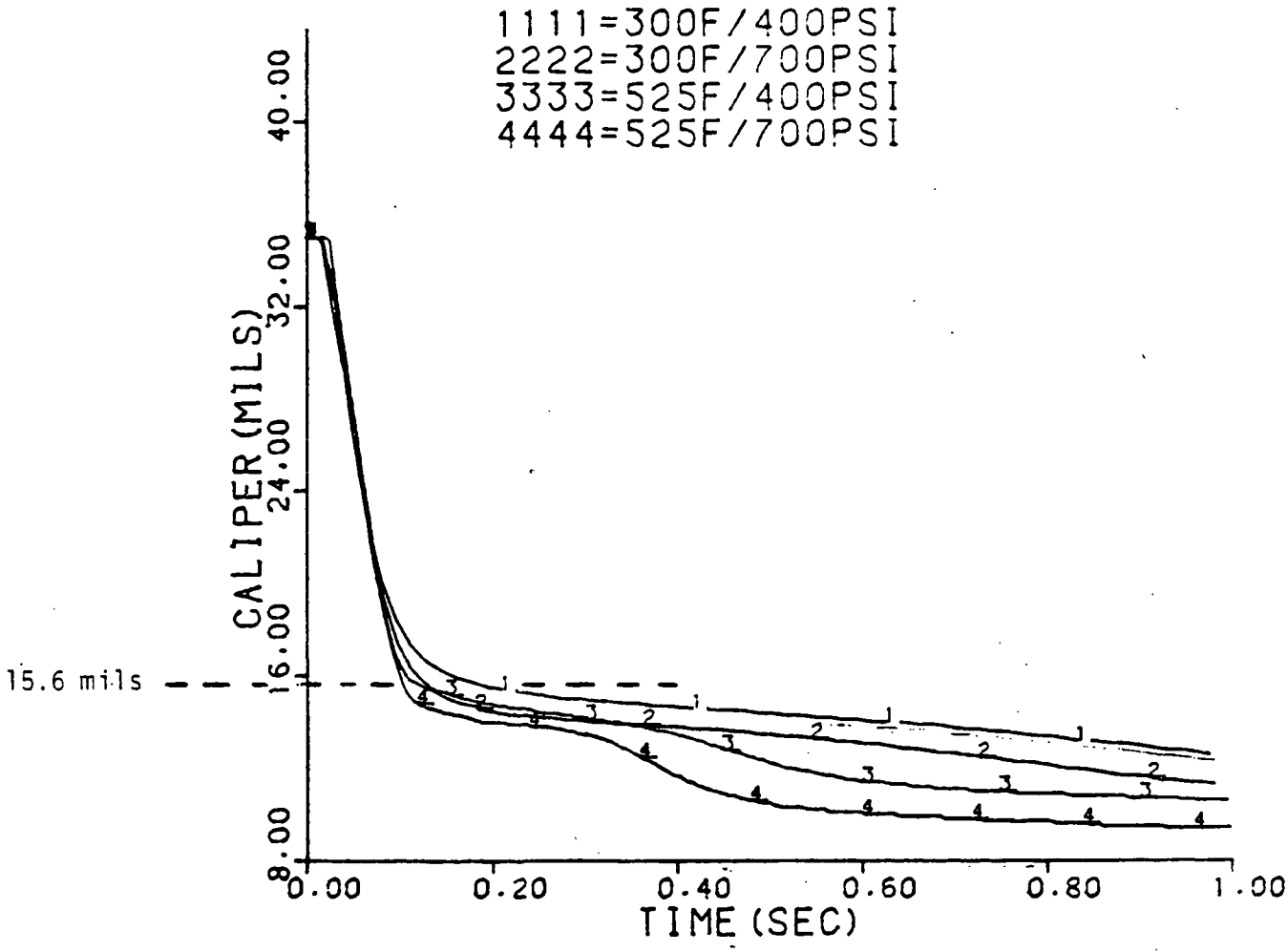

Figure 28. Caliper data showing that 525°F cases reach saturation caliper (15.6 mils) before the 300°F cases.

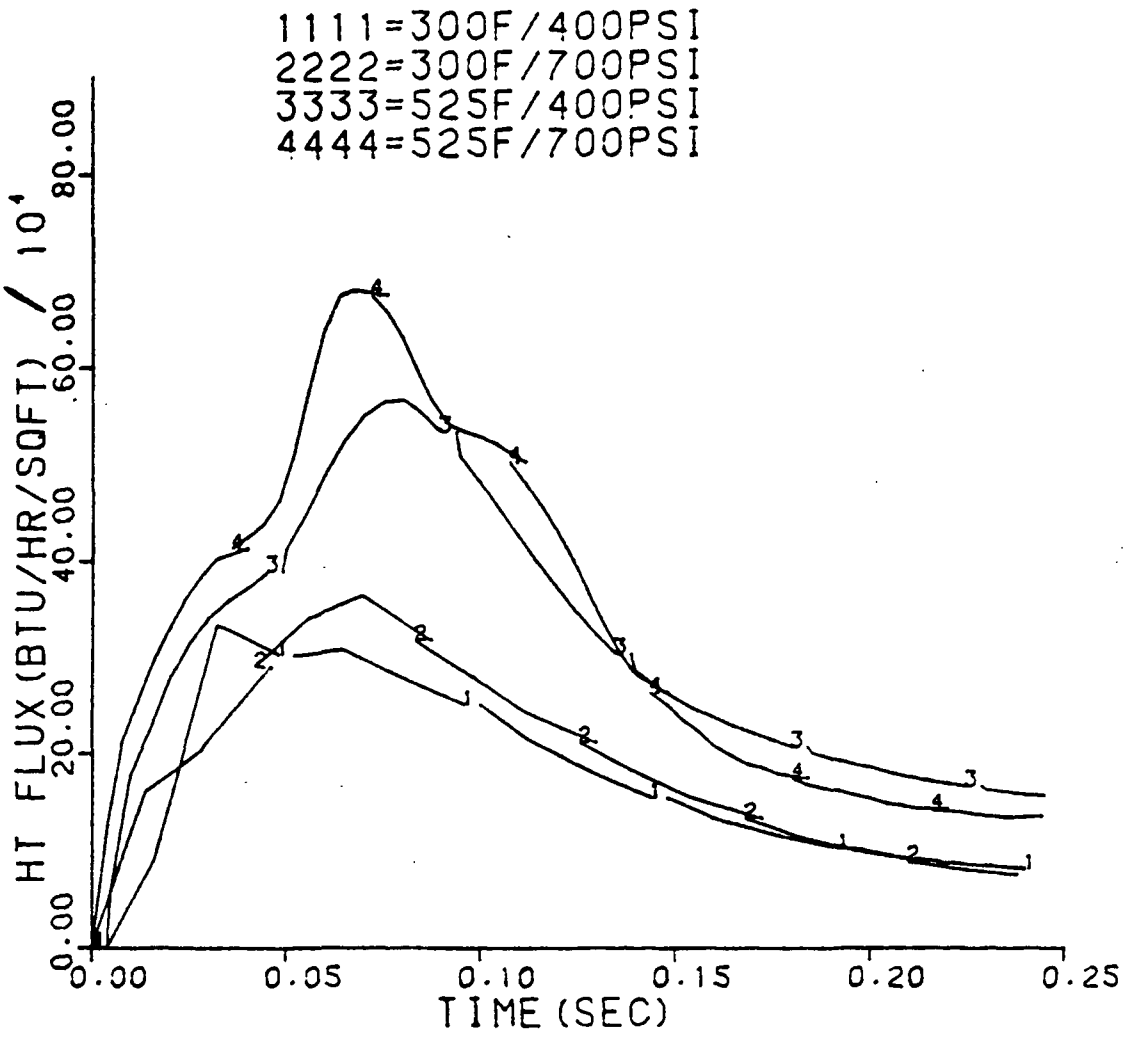

Figure 29. Heat flux data show no evidence of reinitiation of boiling at the hot surface after peak in data has been passed.

A volume reduction driven liquid dewatering mechanism is similar to what occurs in wet-pressing. However, in high-intensity drying, sheet temperatures are much higher from a considerable amount of energy storage and no significant means, as yet, to release this energy. This has important ramifications and is discussed in the next section.

Lastly, all of the mechanisms discussed in this section appear to occur in each of the drying conditions employed in this investigation. The 525°F cases

have higher sheet temperatures and slightly faster compression rates than the 300°F cases, but no significant departures from the basic mechanisms discussed thus far are evident. This issue is also elaborated on in the next section.

SUMMARY

High-intensity drying begins when the applied pressure brings the hot surface and sheet into contact. The initial compression process may be described as one of mechanical compression of an unsaturated sheet. However, heat transfer to the sheet modifies the compression process.

The intense drying conditions cause a large amount of heat to be transferred in a short period of time which results in a rapid generation of vapor and convective vapor transport away from the hot surface. The vapor flow, acting in concert with the flow resistance of the sheet, pressurizes the areas where evaporation is occurring. This allows the temperature to exceed 212°F. As the evaporation process begins in areas away from the hot surface, the sheet can be considered to be divided into two zones: a vapor pressurized zone and an unsaturated zone.

In the VPZ, evaporation-convection-condensation and conduction are the main heat transfer mechanisms. Evaporation-convection-condensation also redistributes liquid away from the hot surface in the VPZ. In the unsaturated zone, conduction is the only heat transfer mechanism, and it appears that little liquid redistribution occurs.

Near the saturation point, no vapor or liquid has left the sheet, and the volume available for vapor is very small. It is likely that the sheet becomes saturated with liquid and a small amount of vapor as the sheet volume is reduced further. Lastly, all of the mechanisms identified in this period appear to occur in each of the drying conditions employed in this investigation.

LIQUID DEWATERING PERIOD

LIQUID DEWATERING RESULTS

Table 5 gives the percentages of water removed as liquid in high-intensity drying as determined by the lithium loss method and an independent method based on sheet energy balances using integrated heat flux data. Both methods show that approximately 29% of the initial moisture in the sheet is removed in liquid form. Furthermore, the total amount of water removed in liquid form is largely independent of the drying conditions and total drying time in this study.

Table 5. Liquid dewatering data from high-intensity drying.

Drying Condition, °F/psi	Average Liquid Dewatering Heat Transfer, %	Average Liquid Dewatering (Lithium Loss), %
300/400	25	28
300/700	30	34
525/400	25	30
525/700	31	27

Wet-Pressing Data

Pressing Condition, sec/psi	Average Liquid Dewatering, %
0.5/400	3
0.5/700	5
1.0/400	3
1.0/700	9

The data in Fig. 30 show that liquid dewatering is completed within 0.25 sec in the 525°F cases, and within 0.75 sec in the 300°F cases. In addition, the data in Table 5 show that wet pressing (unheated lower platen) at 400 psi removed only about 3% of the water in the sheet; at 700 psi, about 9% water

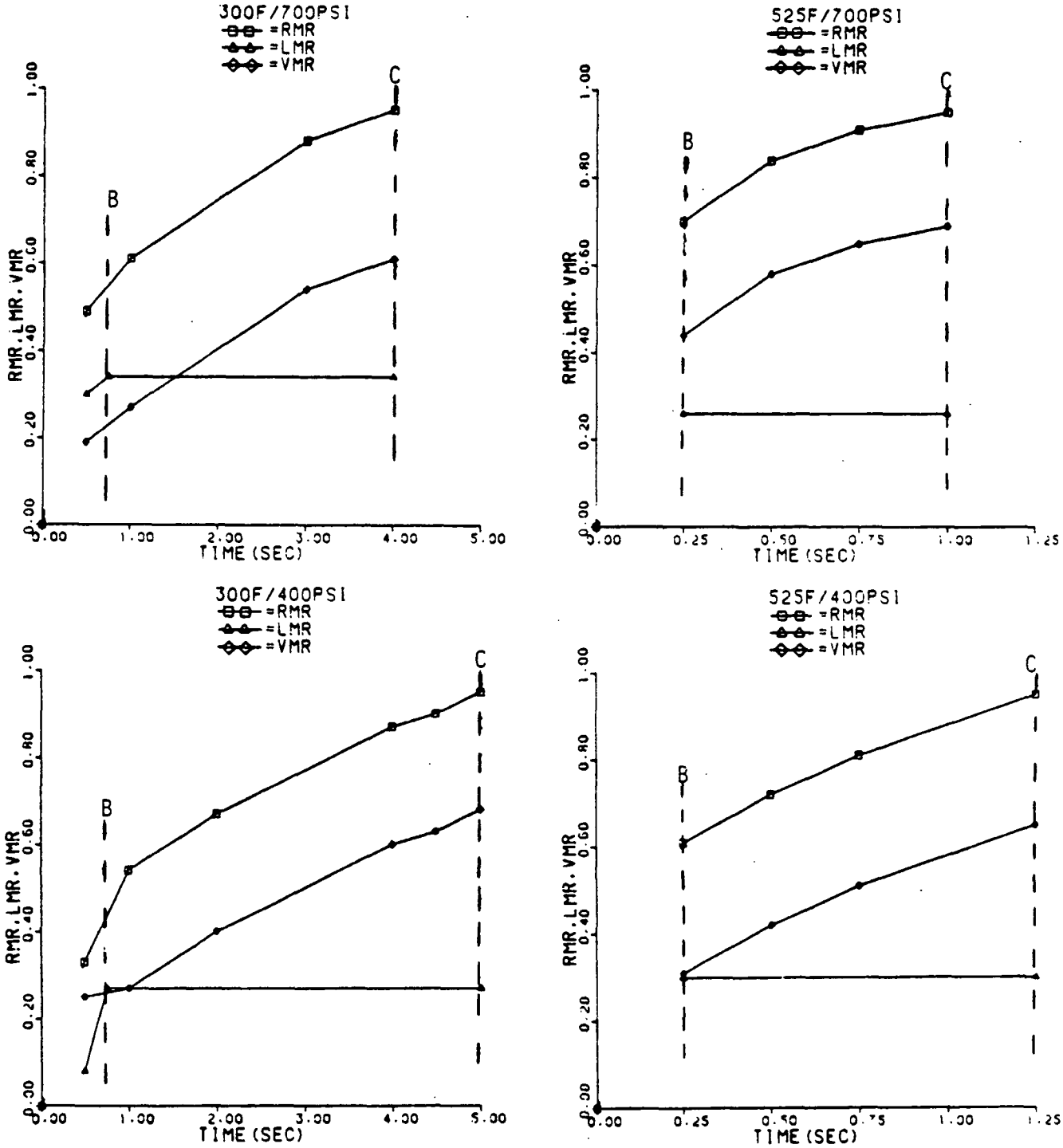

Figure 30. Moisture removal data showing that liquid dewatering is completed early in the drying run.

removal occurs. Thus, high-intensity drying produces a substantial liquid dewatering effect that is not available in conventional wet pressing or drying. This is one of the most important new features that high-intensity drying brings to water removal and sheet consolidation. The mechanism of this substantial liquid dewatering effect is discussed below.

EXPERIMENTAL EVIDENCE FOR DRYING PERIOD BOUNDARIES

It has already been shown that no significant amount of vapor or liquid has left the sheet up to the time when compression brings the sheet near the saturation caliper. Regardless of thermal effects, further compression will cause saturation and the development of fluid pressure through the entire sheet, which will initiate liquid dewatering. This liquid dewatering mechanism must be similar to that which occurs in wet pressing because it is the reduction in sheet volume which causes the development of the fluid pressure through the entire sheet. In the figures used herein, dashed line A denotes the beginning of liquid dewatering on the basis of the time when compression reduces the caliper to 0.0156 in. However, it is likely that not all of the sheets became saturated at exactly this caliper because of small variations in basis weight and initial moisture content from sheet to sheet. In addition, it is doubtful that a liquid filled sheet ever exists during drying, as discussed previously. The sheets probably became saturated with liquid and a small amount of vapor before the saturation caliper was reached. However, for purposes of analysis, a caliper of 0.0156 inch is taken as the saturation point. This should not produce any significant error in subsequent interpretations of the experimental data. Dashed line B denotes the approximate point in time when liquid dewatering has ended, as determined by the lithium loss method. Dashed line C denotes the 0.95 RMR point for the particular drying condition based on the data in Table 1.

VOLUME REDUCTION LIQUID DEWATERING

Liquid dewatering will continue via the volume reduction mechanism until the sheet volume can no longer be reduced by the applied pressure. This occurs when the sheet structural pressure approaches the applied pressure.[17] The wet pressing data in Table V show that this occurs after 3% liquid dewatering for the 400 psi case, and after 9% liquid dewatering for the 700 psi case. The amount of liquid dewatering from volume reduction alone in high-intensity drying could not be directly measured. The discussion below uses caliper data from wet pressing to estimate the amount of liquid dewatering from volume reduction.

Caliper data from wet pressing unsaturated sheets, taken from another investigation, are shown in Fig. 31.[17] For each run, the cause of the large change in slope of the data was attributed to the level of the structural pressure approaching that of the applied pressure. The break point in the data occurs at lower calipers when higher applied pressures are employed. However, the relationship between the applied pressure and final caliper is not linear, as the final caliper in the 15 psi case is nearly twice that of the 550 psi case. In addition, for every run, the much smaller change in slope after the break point was attributed to viscoelastic (creep) and fiber dewatering effects because the data are time dependent and independent of the applied pressure.

To the end of the Liquid Dewatering Period, the caliper data from this investigation, shown in Fig. 32, are similar to the wet-pressing caliper data cited above. The high-intensity drying caliper data exhibit a large change in slope shortly after the sheet is compressed below the saturation caliper. Significantly, the 700 psi cases have a large change in slope at lower calipers than the 400 psi cases, and the relationship between the applied pressure and

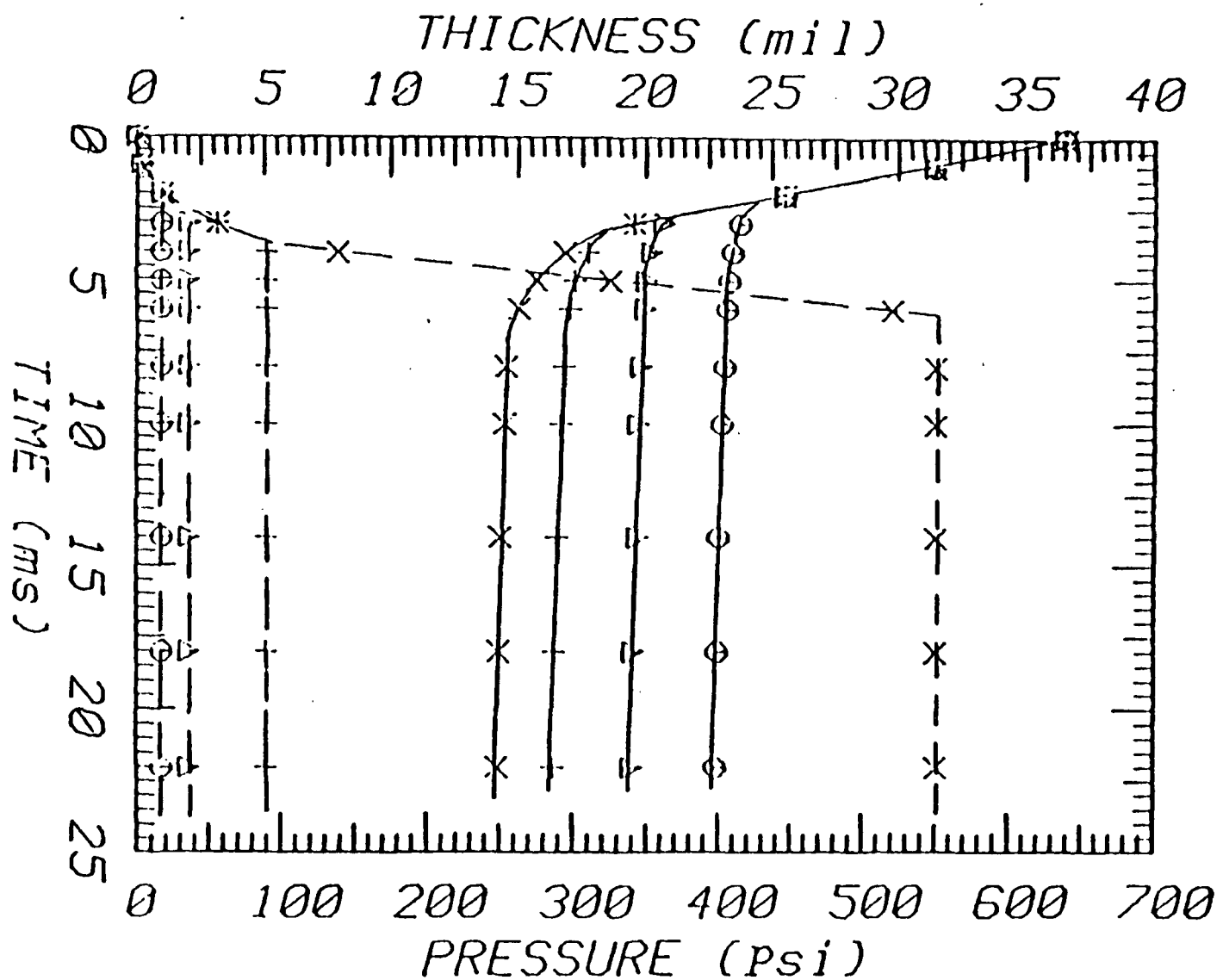

Figure 31. Corresponding caliper (solid lines) and applied pressure (dashed lines) for wet pressing of unsaturated sheets. The large change in slope of the caliper data was attributed to the sheet structural pressure approaching the applied pressure.[17]

final caliper is nonlinear. This nonlinear relationship is similar to the one shown by the wet-pressing caliper data in Fig. 31. The similarities in the wet pressing and high-intensity drying caliper data suggest that the high-intensity drying caliper data change slope for the same reason as the wet-pressing data, and at this time the end of volume reduction driven liquid dewatering in high-intensity drying is at hand.

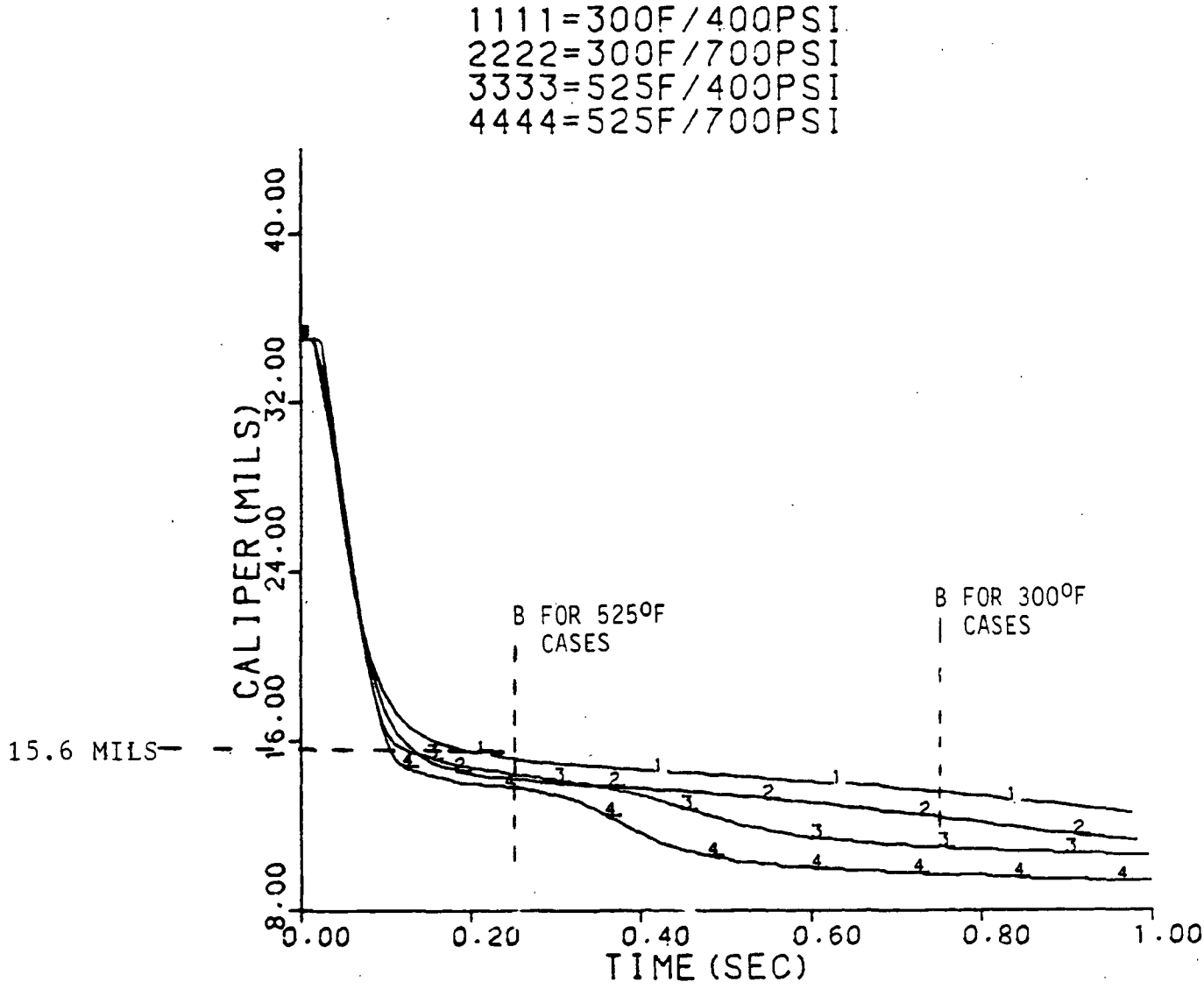

Figure 32. High-intensity drying caliper data are similar to wet pressing caliper data (shown in Fig. 31) through the Liquid Dewatering Period. This suggests that similar densification mechanisms are occurring in both processes through this period.

In addition, the slopes of the high-intensity drying caliper data after the break point behave similarly to those measured in the wet-pressing experiments. This again suggests that similar mechanisms (fiber dewatering and viscoelastic effects) are at work in wet pressing and in high-intensity drying at this point. These caliper data also indicate that the vapor phase pressure does not impede sheet densification to any significant degree in this period. If the vapor phase pressure were impeding sheet densification, the 525°F cases would show slower compression rates than the 300°F cases because of the greater vapor phase pressure in the 525°F cases. The caliper data in Fig. 32 do not indicate such an effect.

The many similarities between the wet pressing and high-intensity drying caliper data indicate that the amount of liquid dewatering in high-intensity drying via volume reduction is in the same range as that which occurs in wet pressing, for the same applied pressure. Volume reduction can only drive liquid out of the sheet until the structural pressure equals the applied pressure. The elevated sheet temperatures in high-intensity drying may cause some further liquid dewatering than what occurs in wet pressing by causing fiber softening and reducing the resistance to compression. However, the change in sheet compressibility is most likely not great enough to increase the amount of liquid dewatering to the levels found in high-intensity drying. Therefore, another mechanism must be operative in addition to the volume reduction mechanism. Identifying this new mechanism, or mechanisms, is the subject of the discussion below.

VAPOR DISPLACEMENT LIQUID DEWATERING

The small decrease in caliper after the large change in slope of the data, shown in Fig. 33, is probably attributable to the viscoelastic (creep) and fiber dewatering effects cited for wet pressing. These effects are most likely

enhanced by higher temperatures. Clearly, little volume reduction driven liquid dewatering can take place at this time. Any further liquid dewatering must be accomplished by a mechanism that can operate without a significant change in sheet volume.

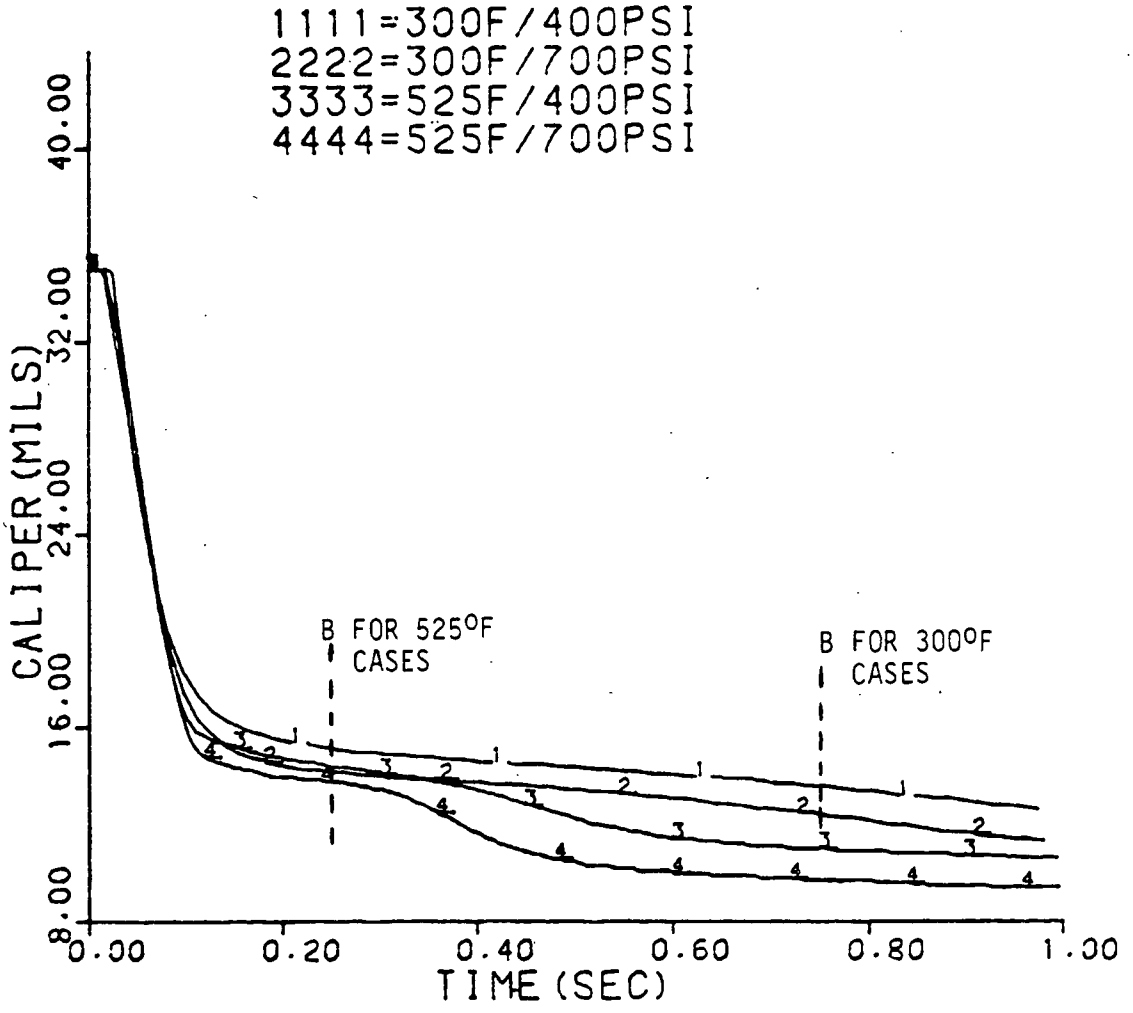

Figure 33. Caliper data showing slow sheet compression rate during liquid dewatering.

It has been previously shown that a vapor pressurized zone exists in the sheet before the saturation caliper is reached. However, it has been argued that only a small amount of vapor is actually present in the VPZ near the time the saturation caliper occurs because most of the pore volume is occupied by

liquid. This allows only a small amount of net evaporation to occur up to this point. The remainder of the heat being transferred into the sheet must be stored in the liquid and fibers, raising the sheet temperature and vapor phase pressure. If the vapor phase pressure is reduced, some of the liquid in the VPZ will flash evaporate. In fact, the data in Table 6 show that the cumulative amount of heat transferred to the sheet to the end of the Compression and Heat-Up Period is greater than the amount needed to raise enough vapor at 212°F to fill the entire sheet volume. In the process, this vapor could displace all of the remaining liquid, if not for other constraints. The data also show that only a very small fraction of the initial sheet moisture need be vaporized to displace the liquid because of the change in volume upon evaporation. This will hold true even if the evaporation temperature is somewhat higher than 212°F.

Table 6. Heat transfer and theoretical vapor generation data.

Drying Condition, °F/psi	Cumulative Heat Transfer,[a] Btu	Sensible Heat,[b] Btu	Heat Available for Evaporation, Btu	Mass of Vapor Produced from Available Heat,[c,d] lb	Volume of Vapor Produced,[e] ft^3	Volume of Sheet at Saturation Caliper,[f] ft^3
300/400	1.74	1.48	0.26	2.68×10^{-4}	7.18×10^{-3}	2.14×10^{-4}
300/700	1.55		0.07	7.21×10^{-5}	1.93×10^{-3}	
525/400	2.25		0.77	7.94×10^{-4}	2.13×10^{-2}	
525/700	2.44		0.96	9.89×10^{-4}	2.65×10^{-2}	

[a]To end of compression and heat-up period, data from Table 4.
[b]Sensible enthalpy change of fiber and vapor from 80 to 212°F, data from Table 4.
[c]Latent enthalpy change at 212°F = 970.3 Btu/lb.
[d]Mass of initial liquid in sheet = 8.86×10^{-3}/lb.
[e]Vapor specific volume at 212°F = 26.799 ft^3/lb.
[f]Caliper = 0.0156 inch, sheet diameter = 5.5 inch.

In wet pressing, the hydraulic pressure from volume reduction drives liquid out of the sheet. Eventually, the hydraulic pressure approaches zero as the structural pressure approaches the applied pressure. However, the sheet is still saturated at this point.[17] In high-intensity drying, the fluid pressure from volume reduction will suppress evaporation in the VPZ, in addition to driving liquid out of the sheet. Eventually, however, the fluid pressure will decline and allow some of the liquid in the VPZ to superheat slightly and flash into vapor. The data in Fig. 34 show that a substantial part of the sheet, depending on the drying condition, is occupied by the VPZ when the saturation caliper is reached. This indicates that a considerable amount of liquid has the potential to flash at this time. When the fluid pressure begins to decline, liquid flashing probably commences at the hot surface because the temperature is greatest there. The vapor from flashing will then start to displace liquid in the saturated network pores in an attempt to exit the sheet. This displacement process can cause liquid dewatering without any significant reduction in sheet volume, making it consistent with the caliper data. Vapor displacement of liquid is the most likely mechanism that continues the liquid dewatering process when liquid dewatering caused by volume reduction begins to wane. This mechanism causes the increase in liquid dewatering in high-intensity drying over what is achievable by wet pressing alone.

There is no clear point of reference when liquid dewatering via volume reduction ends and liquid dewatering via vapor displacement begins. Chances are that liquid dewatering via volume reduction is augmented by vapor displacement before vapor displacement becomes solely responsible for liquid dewatering. However, it is convenient to think of the liquid dewatering process as being initiated by volume reduction and continued to completion by vapor displacement. The

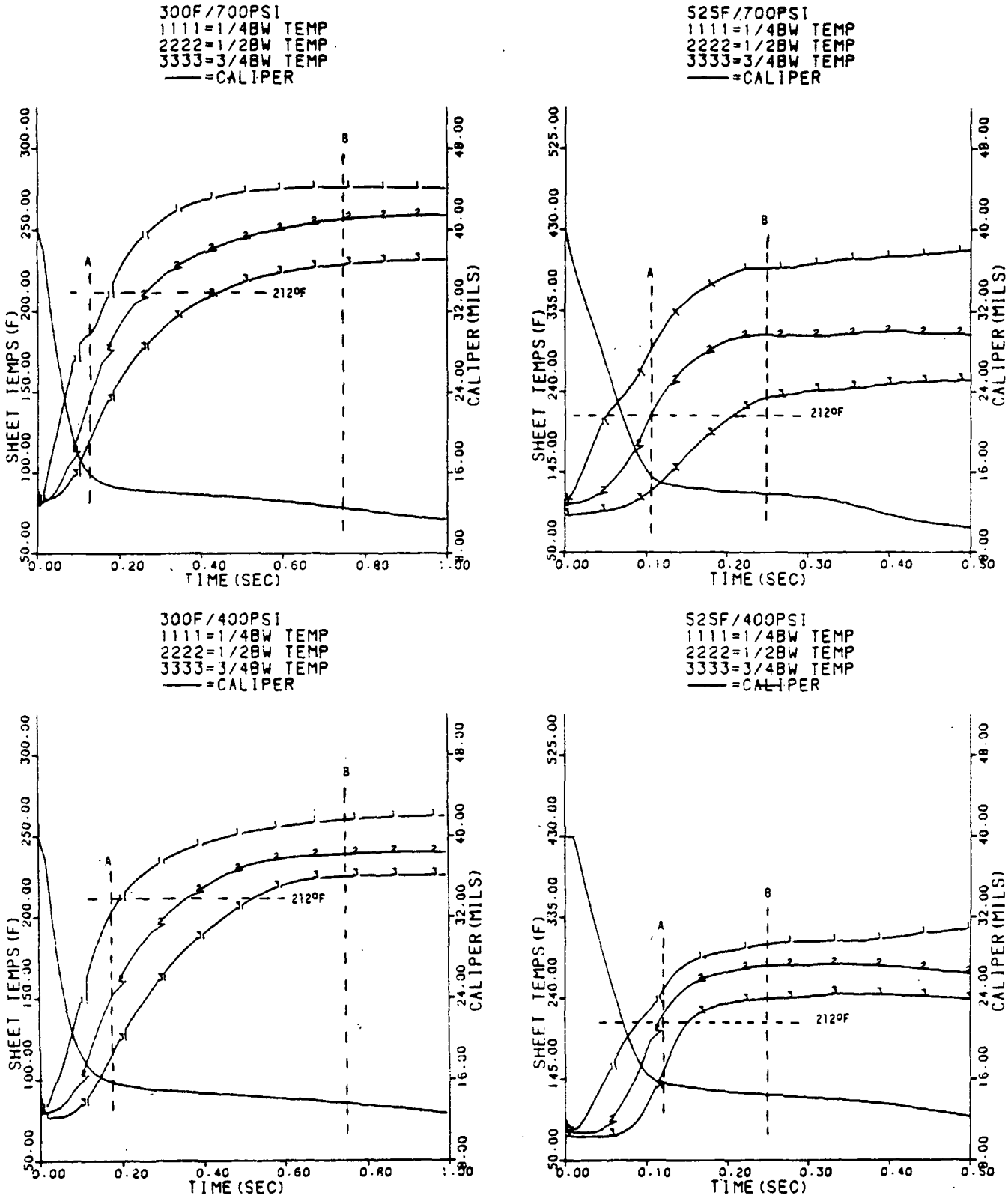

Figure 34. Sheet temperature and caliper data showing that the temperature near the hot surface exceeds 212°F when the saturation caliper (15.6 mils) is reached.

discussion below attempts to justify the existence of the vapor displacement mechanism by showing that it is consistent with the experimental data.

SUPPORTING EXPERIMENTAL EVIDENCE FOR VAPOR DISPLACEMENT LIQUID DEWATERING

The sheet must remain pressurized for vapor to displace liquid and continue the liquid dewatering process. Under these circumstances, pressurization can only be maintained at maximum levels if liquid saturation of the pores ahead of the vapor flow prevails. Otherwise, some of the vapor will channel into network pores which are open to the atmosphere and liquid dewatering by this mechanism will be reduced.

The temperature data in Fig. 35 provide support for pressurization of the sheet and vapor displacement in the following ways. In all of the drying conditions, the 3/4 basis weight temperature is below 150°F at the beginning of this period. Vapor will not be permitted to flow through this area until the temperature is at least 212°F, and channeling cannot occur. Eventually, the temperature does reach 212°F, and beyond, but only toward the end of the Liquid Dewatering Period. In addition, the continued rise in sheet temperatures throughout most of this period provides support for pressurization and vapor displacement. If the sheet were not pressurized, the temperatures would level off near 212°F. Also, any significant channeling would probably cause an anomaly in the temperature data. This does not appear to be the case, as the temperatures rise fairly uniformly with no sharp jumps or discontinuities. Further support for vapor displacement and against channeling comes from considering the liquid dewatering data in Table 5 with the temperature data. The 525°F cases have higher internal temperatures than the 300°F cases, and therefore, have higher vapor phase pressures in the sheet. These higher vapor phase pressures create a greater

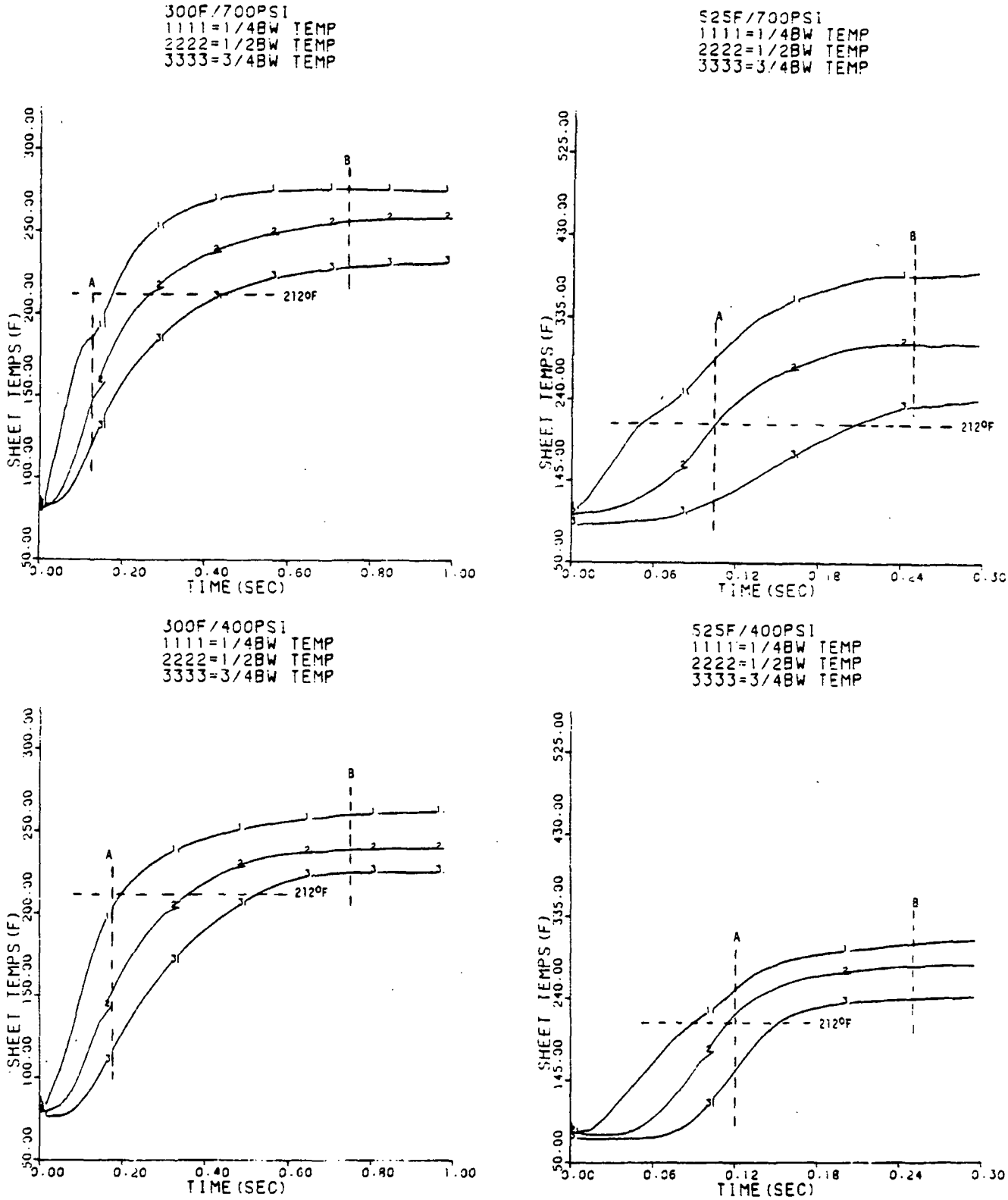

Figure 35. The sheet temperature data provide support for vapor displacement and against vapor channeling in the sheet.

tendency toward channeling. If channeling were to occur, the vapor would have a direct path out of the sheet and the amount of liquid dewatering would be less in the 525°F cases than the 300°F cases. This cannot be the case as the amount of liquid dewatering is approximately the same for all drying conditions. Thus, vapor displacement liquid dewatering is consistent with the temperature and liquid dewatering data.

IN-SHEET MECHANISMS DURING VAPOR DISPLACEMENT LIQUID DEWATERING

As in the Compression and Heat-Up Period, the temperature data in this period indicate that the sheet can be considered as being divided into two zones in the thickness direction. In this case, the sheet is divided into a vapor pressurized zone and a liquid pressurized zone (LPZ), since channeling has been largely ruled out. The interface between the zones will move toward the cold surface as the VPZ expands, and more liquid is displaced. This movement must occur somewhat uniformly through the sheet thickness in the absence of channeling. In addition, the temperature at the interface must exceed 212°F because the entire sheet is pressurized during liquid dewatering.

Heat continues to be transferred into the sheet as vapor displacement is occurring, as shown by the heat flux data in Fig. 36. However, the heat transfer rate is still declining, albeit at a decreasing rate, in this period. The continued decline is probably being caused by the same factors that precipitated the original decline, namely, rising sheet temperatures and an insulating layer of vapor and fiber at the hot surface.

Even though there is sufficient heat available, there can only be a small amount of net evaporation in the VPZ because the vapor phase pressure will impede evaporation. The pressure will not allow any more evaporation than is necessary

to fill the volume formerly occupied by liquid before displacement. The amount of net evaporation will be limited by the pressure as long as the LPZ is saturated and seals the VPZ from the atmosphere. This pressure effect on evaporation is compounded by the slowly decreasing caliper and the large specific volume of the vapor.

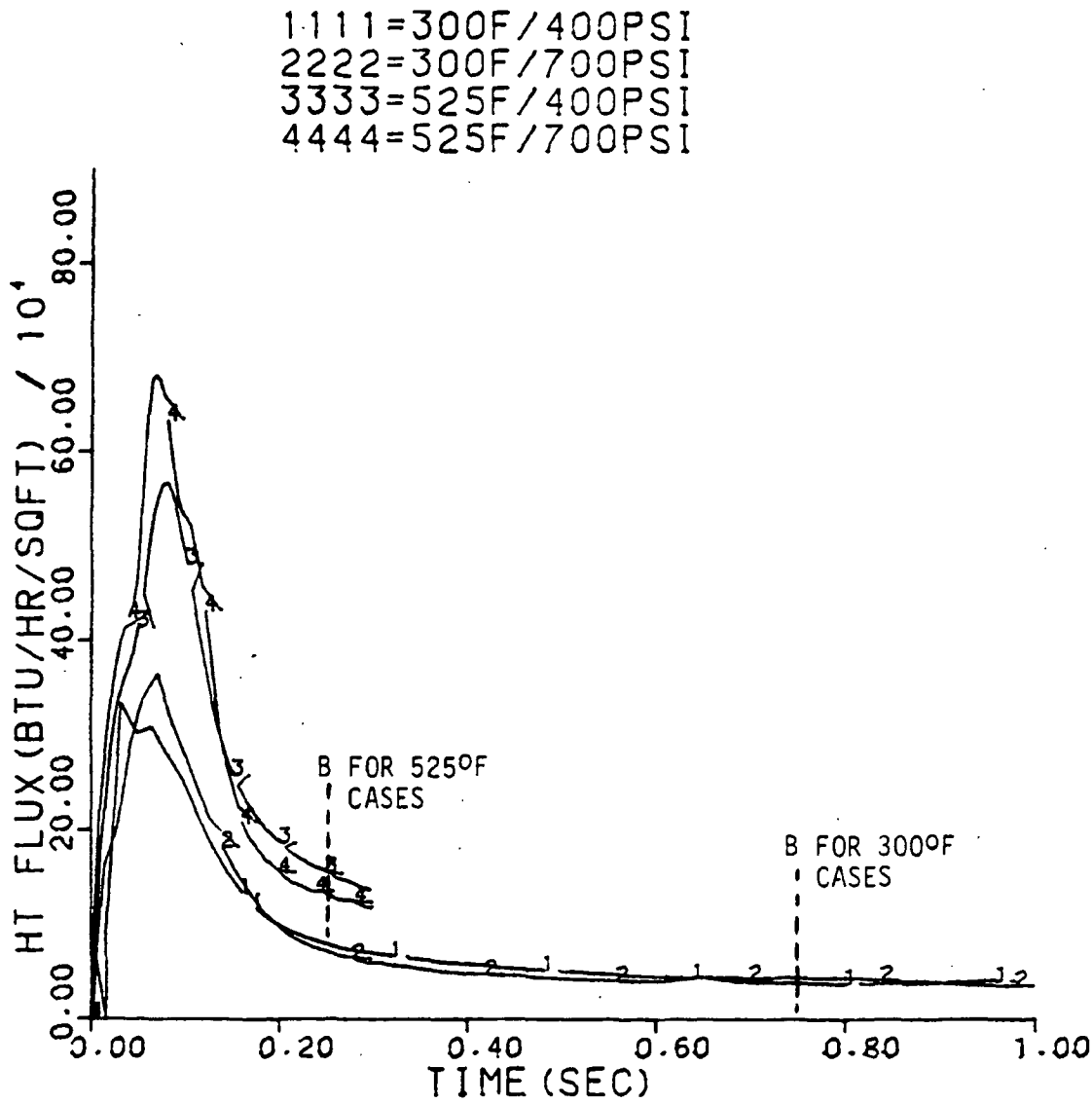

Figure 36. The heat flux data continue to decline during liquid dewatering.

As previously noted, the small amount of net evaporation will cause most of the heat transferred into the sheet to be stored in the liquid and fibers, keeping the temperatures rising. Correspondingly, the pressure will rise in the VPZ. A higher vapor phase pressure will not only displace liquid more quickly, but also increase the heat transfer rate through the VPZ by the E-C-C mechanism. Evaporation/condensation cycles will occur continuously throughout the VPZ because liquid is in contact with vapor, and the amount of net evaporation is small. Thus, the E-C-C mechanism will become more important as the VPZ moves progressively through the sheet thickness. This is in addition to conduction which will transfer heat throughout the sheet because of the temperature gradient inferred by the data in Fig. 37. The E-C-C mechanism, plus conduction, will transfer heat to the VPZ-LPZ interface to heat up the area so liquid can be displaced by vapor. Lastly, a small amount of heat will be transferred by convection in the LPZ because of warmer liquid being displaced by vapor into cooler areas.

The division of the sheet into a VPZ and LPZ has two other important consequences. First, while a considerable amount of heat has been transferred to the sheet, only a small fraction of this heat is transported out of the sheet as sensible heat with the liquid dewatering. The major part of the energy remains stored in the sheet. This large amount of stored energy has a major effect on the events in the next period.

The second consequence of sheet division is not as evident as the first, but is just as important. The data in Table V show that the amount of liquid dewatering is approximately 29%, regardless of drying condition. The majority of this liquid dewatering occurs by vapor displacement and the remainder from volume reduction. The amount of liquid dewatering from volume reduction is probably small. Assuming this to be the case, the lack of dependence of the amount

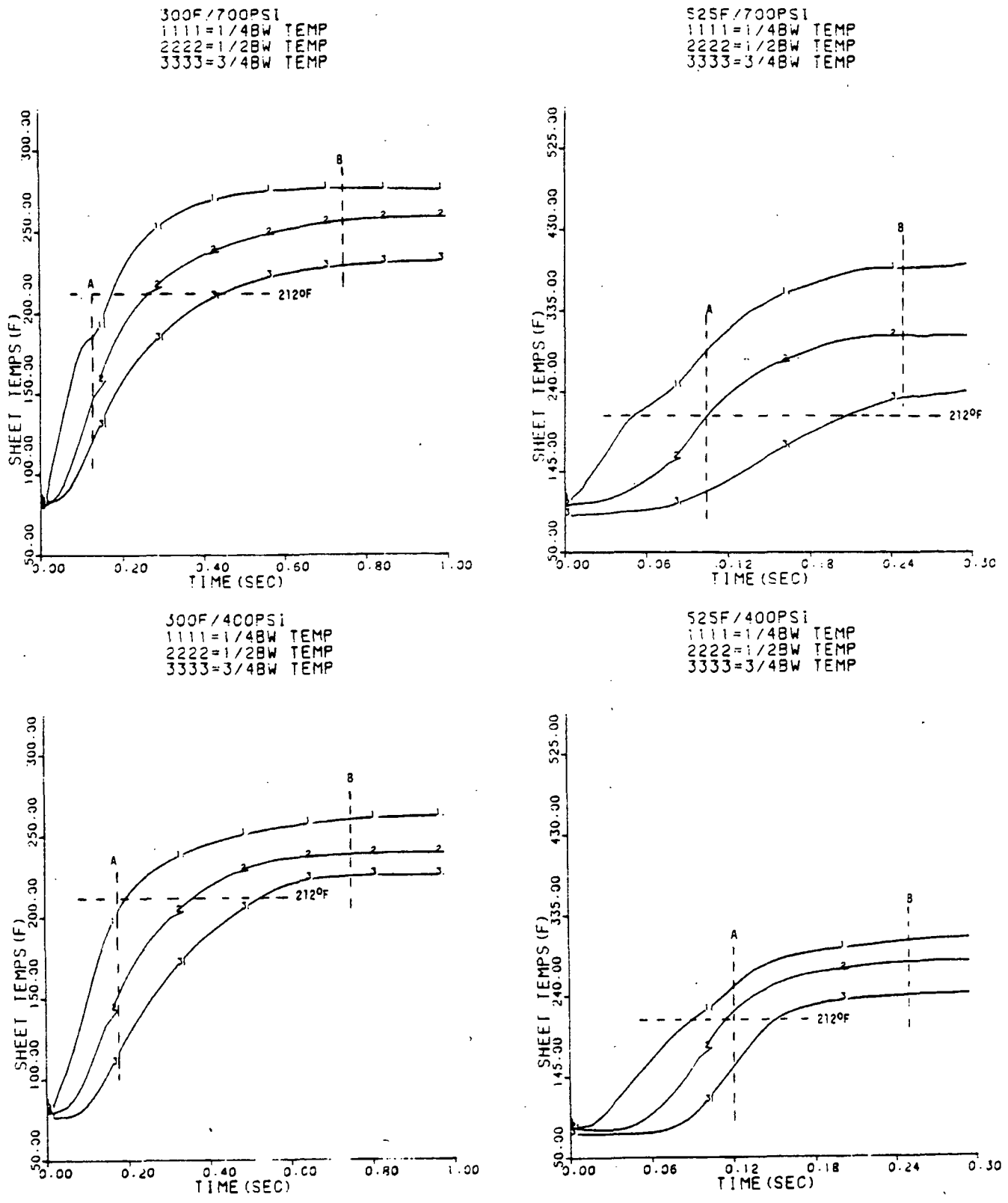

Figure 37. Sheet temperature data showing temperature drop through the sheet early in the drying run.

of liquid dewatering on drying conditions suggests that the amount of liquid dewatering is determined by conditions in the sheet. Considering that the sheet is divided into zones, and that the VPZ must expand somewhat uniformly toward the cold surface in the absence of channeling, it follows that the amount of liquid dewatering must be determined by the amount of liquid available for displacement by vapor. In any case, the division of the sheet into zones makes possible the significant amount of liquid dewatering found in high-intensity drying.

Lastly, similar to the Compression and Heat-Up Period, all of the mechanisms described to this time appear to occur in every drying condition. This is illustrated by the caliper data in Fig. 38 which reflect many of the mechanisms which are occurring. Regardless of drying condition, the shapes of the curves remain similar, only the rate of change is different. Significantly, the rate of change is fastest for the most intense drying condition, and slowest for the least intense condition. The data in Fig. 39 show that the rate of heat transfer to the sheet becomes greater as the drying conditions become more intense. Thus, it appears that, so far, regardless of the drying condition, the drying mechanisms remain the same; only the rates at which these mechanisms occur are changed, primarily by the rate of heat transfer to the sheet.

SUMMARY

High-intensity drying produces a substantial liquid dewatering effect that is not available in either wet pressing or conventional drying. In this investigation, approximately 29% of the initial moisture left the sheet in liquid form. Liquid dewatering occurs by two mechanisms, namely, volume reduction and vapor displacement.

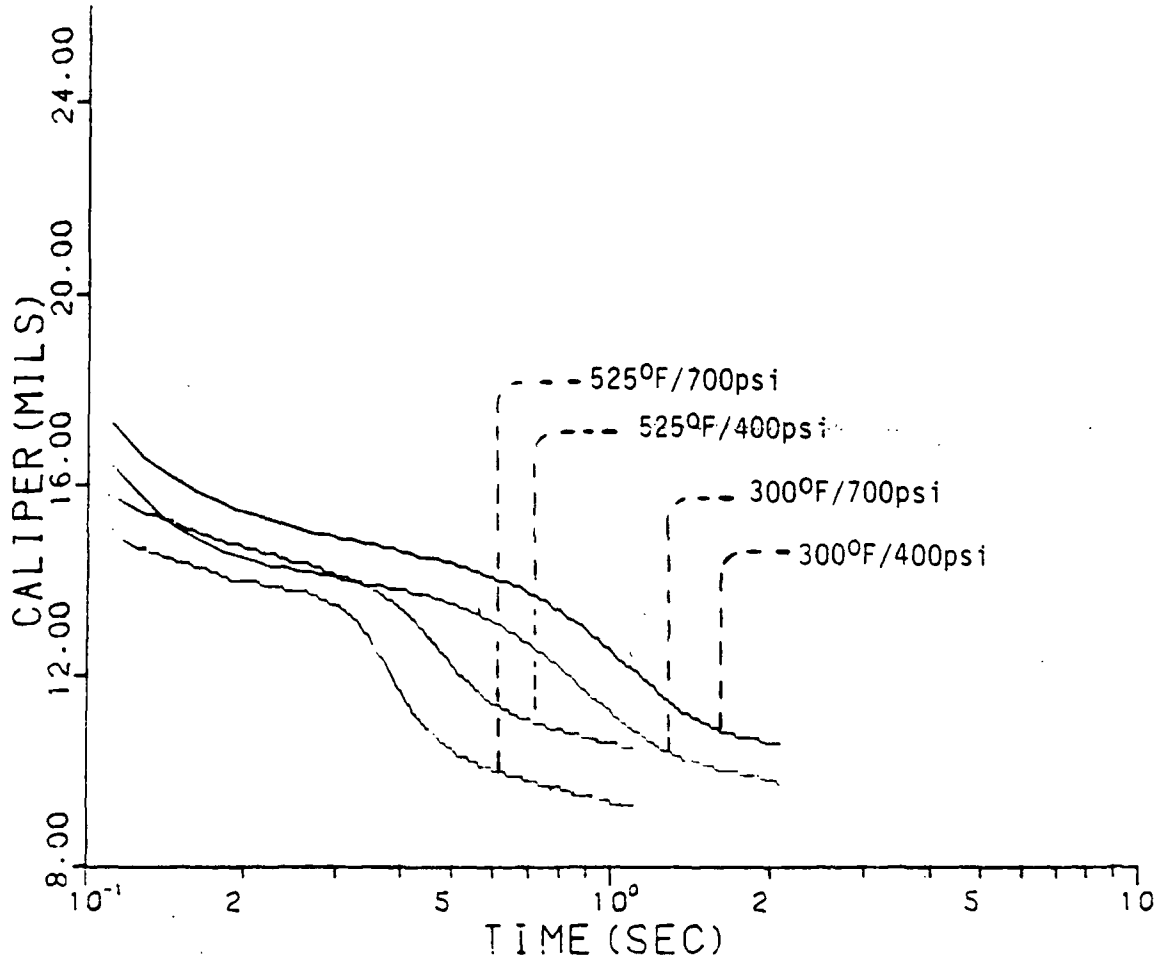

Figure 38. The caliper data are similar in shape regardless of drying condition; only the rate of change of the data is different.

The volume reduction mechanism is similar to what occurs in wet pressing, and only produces a small amount of liquid dewatering. Vapor displacement of liquid in the network pores is the mechanism that causes the large increase in liquid dewatering in high-intensity drying over what can be achieved by wet pressing. Vapor displacement begins when the pressure drop in the sheet after saturation allows liquid near the hot surface to superheat and a small amount flashes into vapor. The vapor begins to displace liquid in the network pores as it attempts to exit the sheet. As the vapor makes its way toward the cold surface, the sheet becomes divided into a vapor pressurized zone and a liquid

pressurized zone. The large amount of liquid dewatering from this mechanism is both caused by, and made possible by, the liquid in the network pores in the liquid pressurized zone which seals the sheet from the atmosphere. As in the first drying period, evaporation-convection-condensation and conduction are the main heat transfer mechanisms in the vapor pressurized zone. These mechanisms maintain the energy flow to the interface between the zones to keep vapor displacement liquid dewatering viable. Conduction and liquid convection are the main heat transfer mechanisms in the liquid pressurized zone.

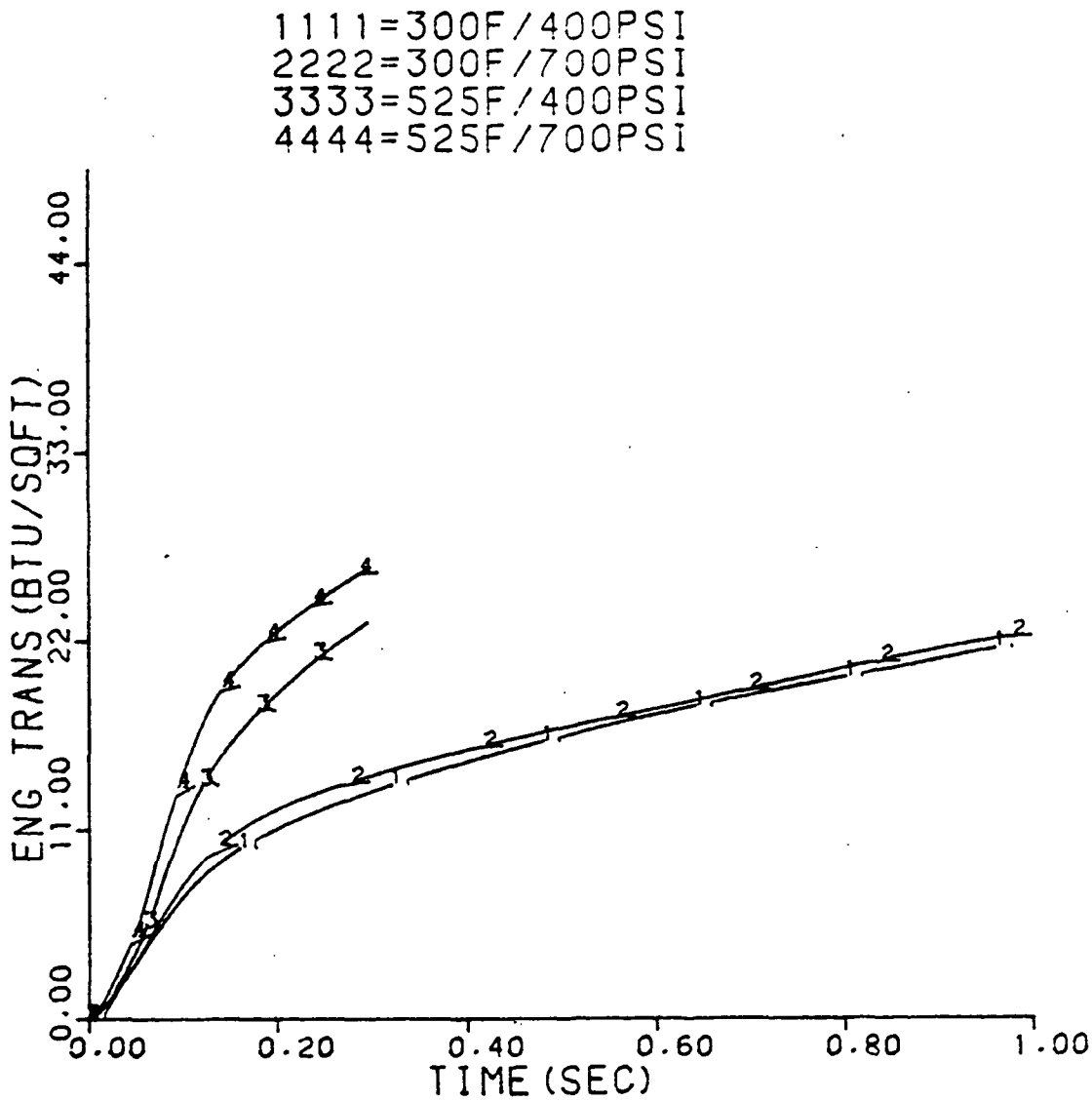

Figure 39. Cumulative heat transfer data showing that the heat transfer rate to the sheet is higher for the more intense drying conditions.

An important result of vapor displacement is that while a considerable amount of heat has been transferred to the sheet up to the end of liquid dewatering, only a small fraction of this heat is transported out of the sheet with the liquid; the rest remains stored in the sheet. Lastly, similar to the first drying period, the mechanisms discussed in this period appear to occur in every drying condition. Only the rates at which these mechanisms occur are changed, primarily by the rate of heat transfer to the sheet.

EVAPORATION PERIOD

DRYING RATE RESULTS

Table 1, repeated here, lists the average overall drying rates for the drying conditions employed during this investigation.

Table 1. Drying rate data.

Drying Condition, °F/psi	Average Overall Drying Rate,[a] lb/hr/ft^2	Average Overall Drying Time,[a] seconds
300/400	37	5.0
300/700	46	4.0
525/400	147	1.25
525/700	184	1.0

[a]To 0.95 RMR.

As expected, the more intense conditions produce higher drying rates. For the 300°F cases, the drying rates are approximately 7 to 10 times higher than those for conventional drying.[1] The increase in drying rates for these conditions is largely caused by the much higher applied pressure because a hot surface temperature of 300°F is not uncommon in conventional drying. The drying rates for the 525°F cases are over an order of magnitude higher than those found in conventional drying. For these cases, the much higher hot surface temperature has a dramatic effect on drying rate, in addition to the effect of the applied pressure.

The overall drying rates are based on the time required for the sheet to reach the 0.95 RMR point, regardless of whether moisture exits the sheet as liquid or vapor. It has already been shown that no significant amount of vapor

leaves the sheet before or during liquid dewatering, and that approximately 29% of the initial moisture leaves the sheet in liquid form. The remaining moisture must leave the sheet as vapor. This evaporation process is the subject of the discussion below.

ENERGY STORAGE IN THE SHEET AT THE END OF LIQUID DEWATERING

The data in Table 7 show that approximately 50% of the total heat transfer to the sheet during drying has occurred by the end of the Liquid Dewatering Period. These data were taken from the integrated heat fluxes shown in Fig. 40.

Table 7. Heat transfer data at the end of the liquid dewatering period.

Drying Condition, °F/psi	Cumulative Heat Transfer To End of Liquid Dewatering,[a] Btu	Total Heat Transfer To 0.95 RMR,[a] Btu	% of Total Heat Transfer At End of Liquid Dewatering	Maximum Sensible Heat with Liquid Dewatering,[b] Btu	Minimum Energy Stored in Sheet at End of Liquid Dewatering, Btu
300/400	3.21 (t=0.75 sec)	7.35 (t=5.00 sec)	43.7	0.33	2.88
300/700	3.28 (t=0.75 sec)	6.46 (t=4.00 sec)	50.8	0.40	2.88
525/400	3.53 (t=0.25 sec)	6.99 (t=1.25 sec)	50.5	0.35	3.18
525/700	4.05 (t=0.25 sec)	6.99 (t=1.00 sec)	57.9	0.32	3.73

[a]From Fig. 40 (x 0.165 ft^2) at times listed.
[b]Enthalpy change from 80°F to 212°F for liquid dewatering percentages listed in Table 2, mass of initial liquid in sheet = 8.86×10^{-3} lb.

The data also show that only a small amount of sensible heat could have left the sheet with the liquid dewatering. These data represent the maximum amount of energy that could have left the sheet during liquid dewatering because it was assumed that the liquid exit temperature was 212°F. The net energy remaining in the sheet at the end of the Liquid Dewatering Period is also listed in the Table. These data show that considerable energy is stored in the sheet by the end of the Liquid Dewatering Period.

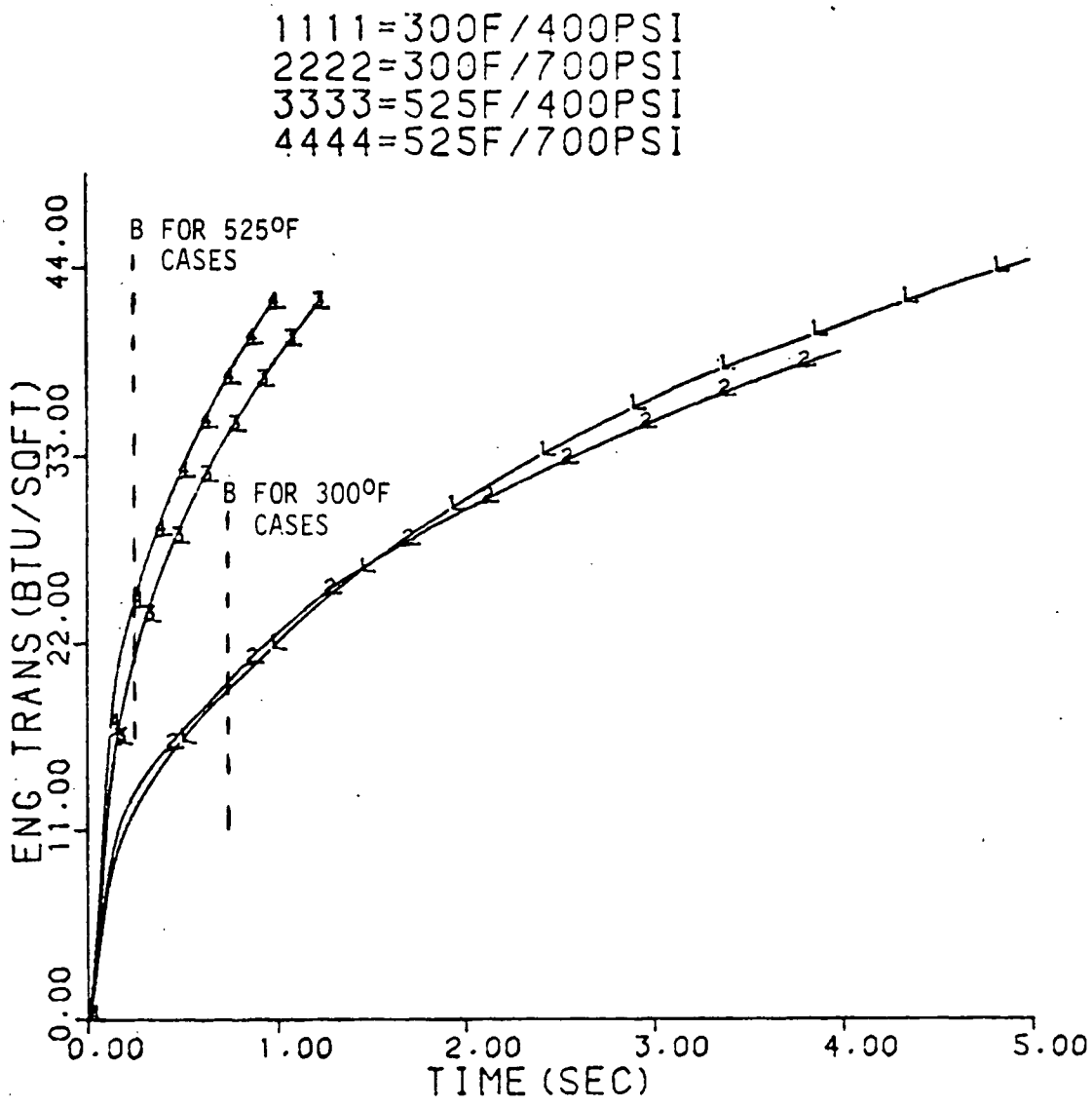

Figure 40. Cumulative heat transfer data showing that approximately 50% of the total heat transfer has occurred by the end of liquid dewatering.

PRESSURIZED FLASH DRYING

The temperature data in Fig. 41 begin to level off as liquid dewatering is ending. Given the situation in the sheet described above, it is likely that the temperature data level off because the stored energy and heat transferred from the hot surface are now being used for evaporation rather than for sensible

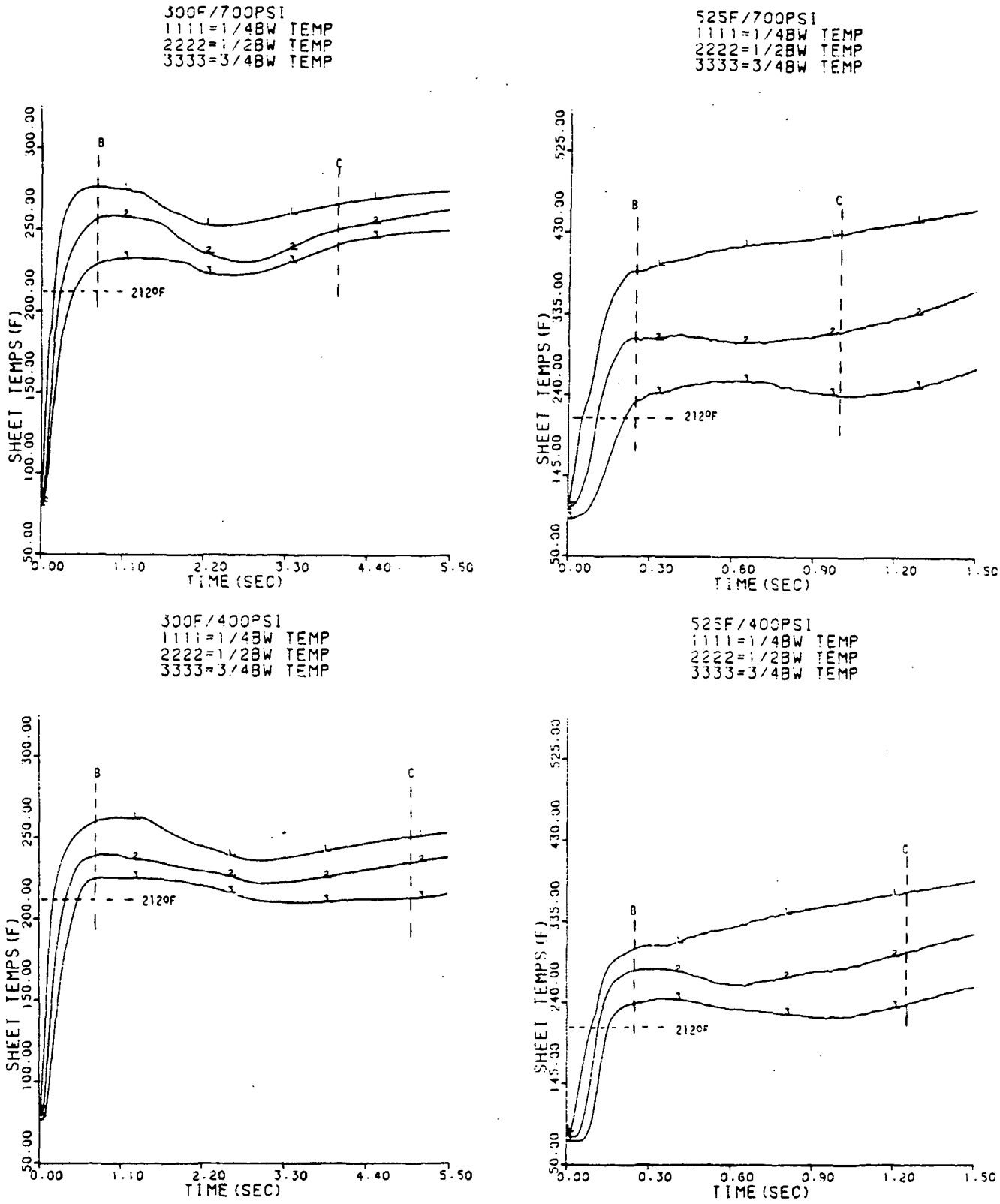

Figure 41. Sheet temperature data showing that the temperatures begin to level off near the time when liquid dewatering has ended.

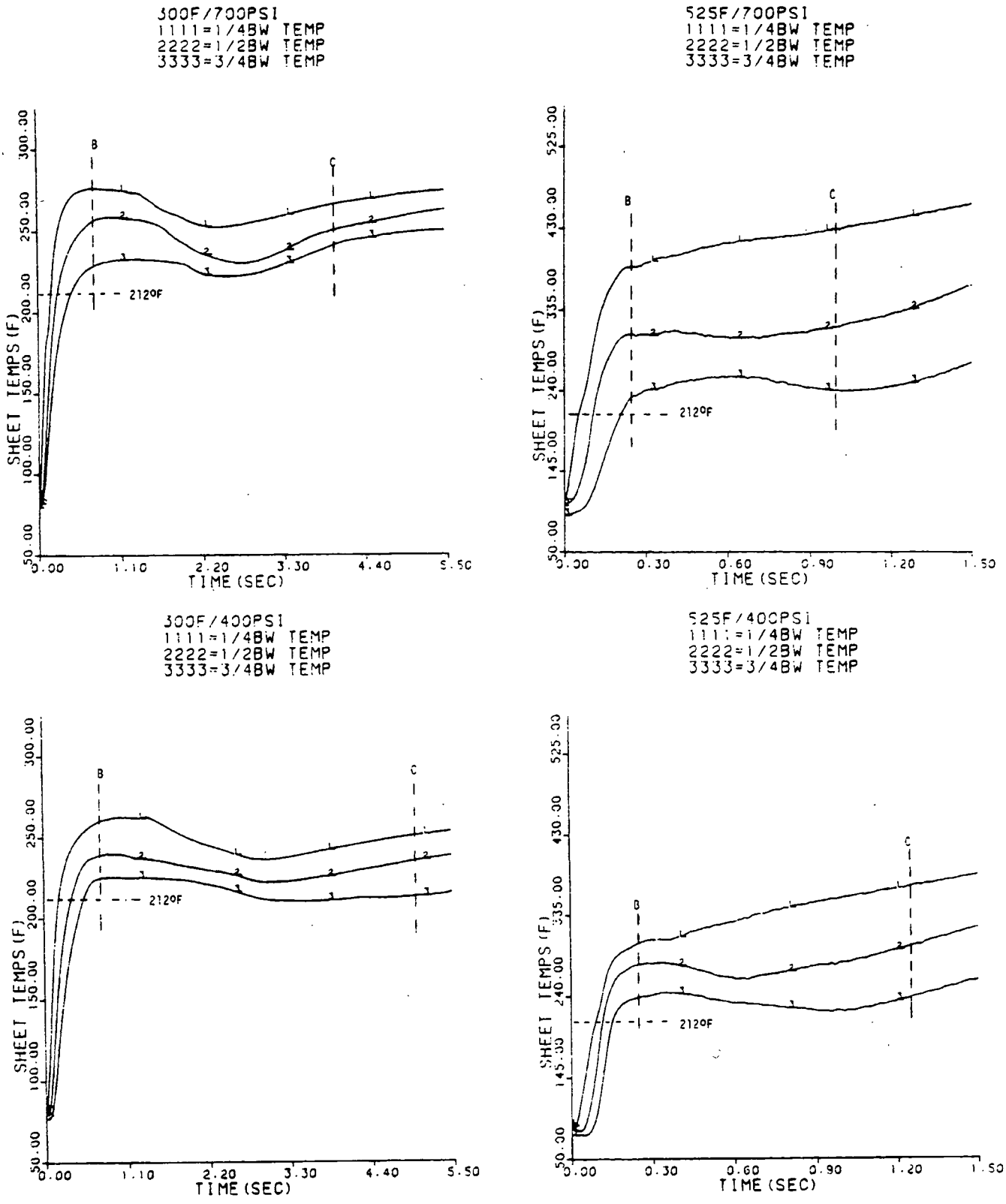

Figure 42. Sheet temperature data showing that the entire sheet is above 212°F by the time liquid dewatering has ended.

heating. However, this does not fully describe the mechanisms which are occurring at this time in high-intensity drying.

As a consequence of the VPZ reaching the cold surface, the entire sheet is now at a temperature of 212°F or greater, as shown by the data in Fig. 42. The flow resistance in the network pores must also be significantly reduced because the pores are now connected to the atmosphere, and the flow resistance corresponds to vapor rather than liquid flow. This will allow vapor to begin to rapidly exit the sheet. As vapor begins to exit the sheet, the vapor phase pressure will begin to decline. This decline in vapor phase pressure must be small because the temperature data in Fig. 42 do not show a sharp decline at this time. The small drop in pressure will allow the liquid in the sheet to become slightly superheated and begin to flash into vapor. This is similar to what occurs to initiate vapor displacement liquid dewatering. However, in this instance, there is no subcooled liquid region to condense the vapor, or liquid blocking the network pores and impeding vapor from leaving the sheet. The absence of these conditions permits a vigorous flash evaporation process to begin, using the stored energy and heat transferred into the sheet from the hot surface. This flashing process will seek to maintain the vapor phase pressure. Very quickly, a quasi-steady-state will be reached in which the vapor phase pressure effects a balance between the evaporation rate and the vapor flow rate out of the sheet. Thus, even though the liquid is at a temperature above 212°F and has the potential to flash instantaneously, the vapor phase pressure, which is well above atmospheric pressure, will control the evaporation rate. Hence, the name coined for this process is pressurized flash drying. The vapor phase pressure will remain relatively constant as long as there is sufficient energy and liquid available for evaporation. The constant vapor phase pressure will, in turn, keep the temperature constant.

An estimation of the amount of flash drying which would occur at 212°F is given in Table 8. These data only provide a rough estimate of the amount of flash drying because temperatures in the sheet are above 212°F. However, the estimate is based on the amount of heat transferred to the sheet up to the end of the Liquid Dewatering Period. Heat transfer to the sheet during pressurized flash drying will increase the amount of evaporation and partially offset the assumption of a 212°F evaporation temperature.

Table 8. Estimation of the amount of flash drying.

Drying Condition, °F/psi	Minimum Energy Stored in Sheet at End of Liquid Dewatering,[a] Btu	Sensible Heat in Sheet at End of Liquid Dewatering,[b] Btu	Net Heat Available for Evaporation, Btu	Amount of Flash Drying at 212°F,[c] lb	Sheet RMR After Liquid Dewatering and Flash Drying
300/400	2.88	1.15	1.73	1.78×10^{-3}	0.48
300/700	2.88	1.08	1.80	1.86×10^{-3}	0.55
525/400	3.18	1.13	2.05	2.11×10^{-3}	0.54
525/700	3.73	1.16	2.57	2.65×10^{-3}	0.57

[a]From Table 7.
[b]Sensible enthalpy change from 80 to 212°F for liquid and fiber left in sheet after liquid dewatering.
[c]Latent enthalpy change at 212°F = 970.3 Btu/lb.

Table 9 also lists the sheet RMR values for the drying conditions after combining the estimated amount of flash drying and the known amount of liquid dewatering. The RMR values indicate that a considerable amount of moisture removal occurs by flash drying and liquid dewatering in high-intensity drying. It is also interesting to note that the RMR values are not widely scattered, and only a small applied pressure effect is evident in the data. This is another indication that similar mechanisms are occurring in every drying condition, and

only the rates of change of the mechanisms vary, primarily with the intensity of the drying condition. The data also show that pressurized flash drying does not cause enough evaporation to bring the sheet to the 0.95 RMR point. Additional heat transfer to the sheet is needed to bring the sheet to the 0.95 RMR point. This is elaborated on in a later section.

The heat transfer mechanisms during pressurized flash drying are conduction and evaporation-convection-condensation. Conduction will transfer heat through the entire sheet because of the temperature gradient inferred by the data in Fig. 43. E-C-C will also transfer heat through the entire sheet now that the VPZ has reached the cold surface and a vigorous evaporation process has begun. In addition, the heat transfer rate to the sheet continues to decline in this period, as shown by the data in Fig. 44. This relatively low rate of heat transfer, caused by conditions at the hot surface and the elevated sheet temperature, has important consequences later in this period. The effect of pressurized flash drying on sheet structure is explored below.

SHEET DENSIFICATION DURING PRESSURIZED FLASH DRYING

The scanning electron photomicrographs of a freeze-dried sheet and a high-intensity dried sheet are shown in Fig. 45. Some of the fibers in the freeze-dried sheet still have open lumens, and individual fibers are readily evident. In the high-intensity dried sheet, there are no open lumens and few distinct fibers. The lumens are collapsed, and the sheet appears highly compacted. The compacted nature of the high-intensity dried sheet is reflected in the apparent density values listed in Table 9 for each drying condition at the 0.95 RMR point. The caliper data used in calculating the sheet densities were taken from Fig. 46.

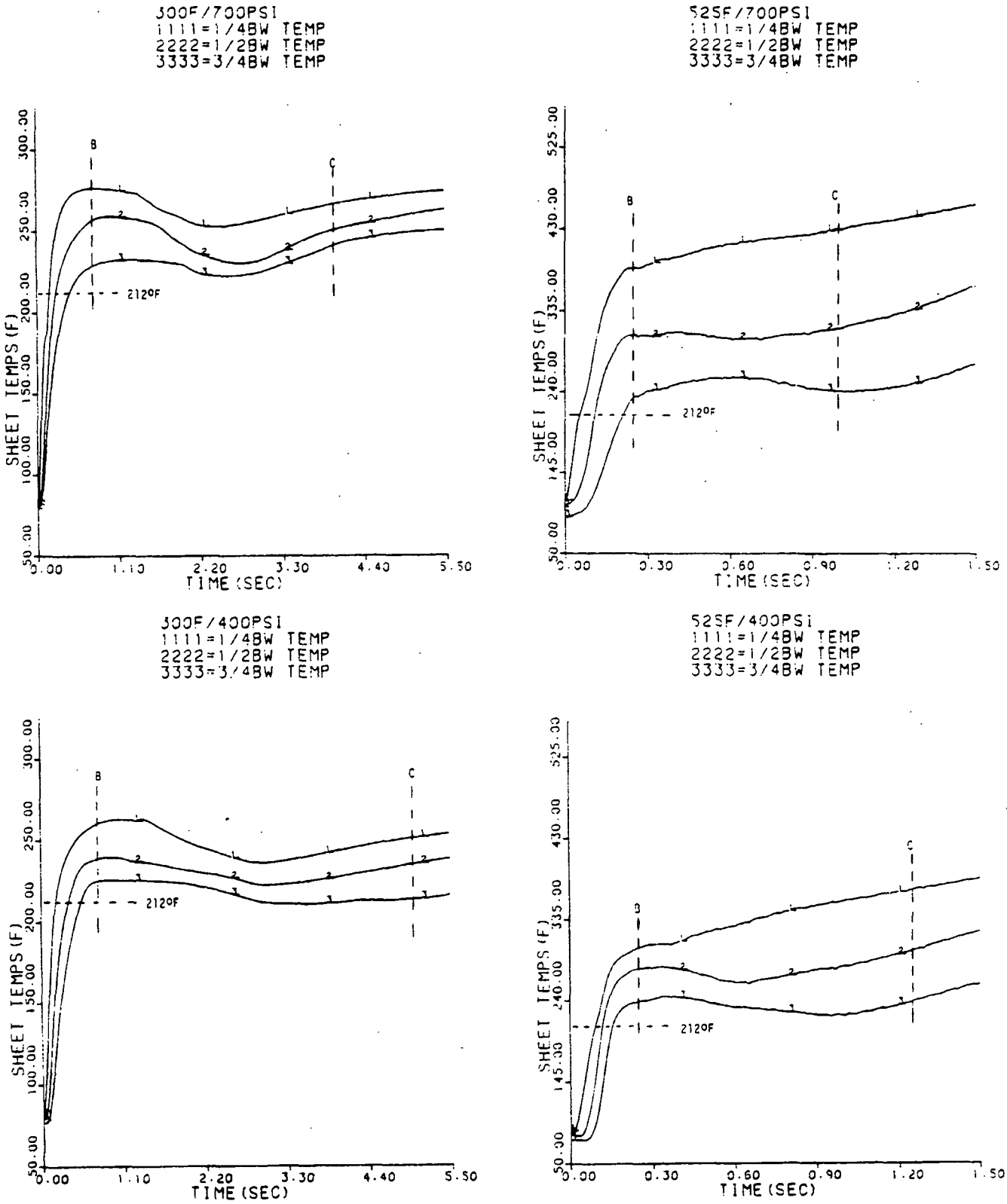

Figure 43. Sheet temperature data showing the temperature drop through the sheet during the drying run.

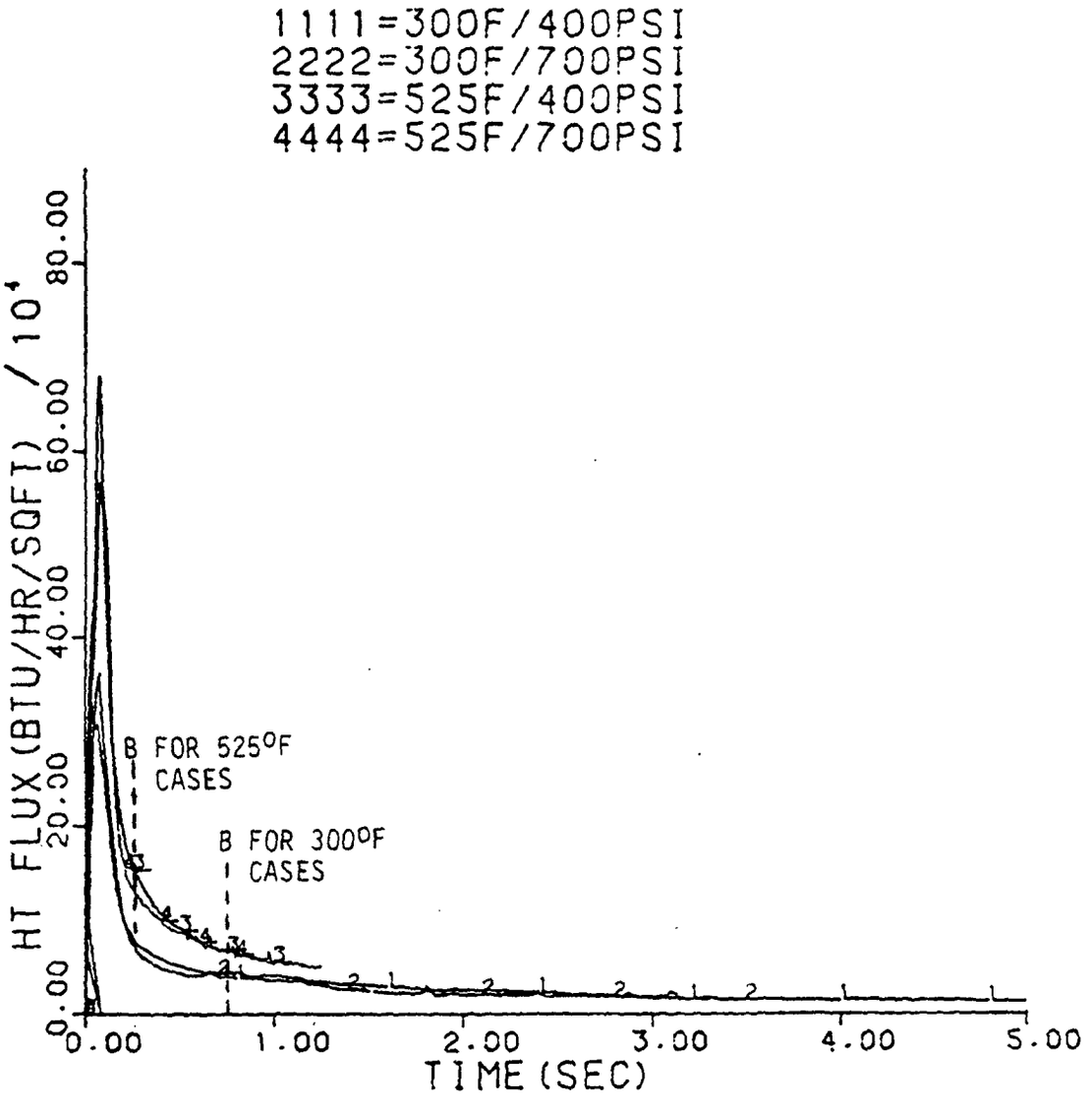

Figure 44. Heat flux data showing relatively low rate of heat transfer to the sheet later in drying.

The high-intensity dried sheet densities are not widely scattered, and only show a small dependence on applied pressure. This again indicates that similar mechanisms are at work in every drying condition. The densities are also considerably higher than the density shown for the conventionally dried sheet. The data also show what apparent density value the high-intensity dried sheets would assume if the sheets were dried to 0.95 RMR and no further caliper decrease

Freeze-Dried Sheet

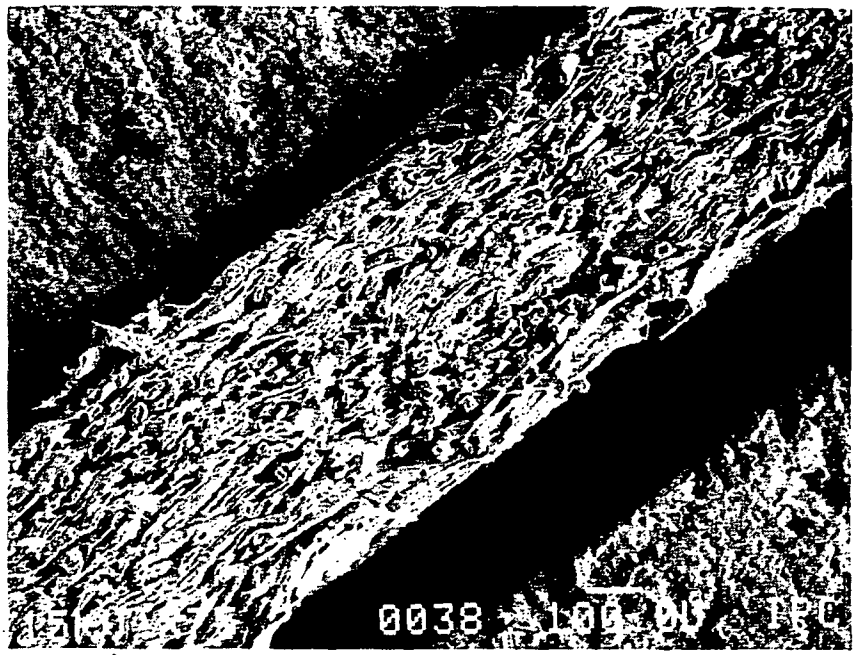

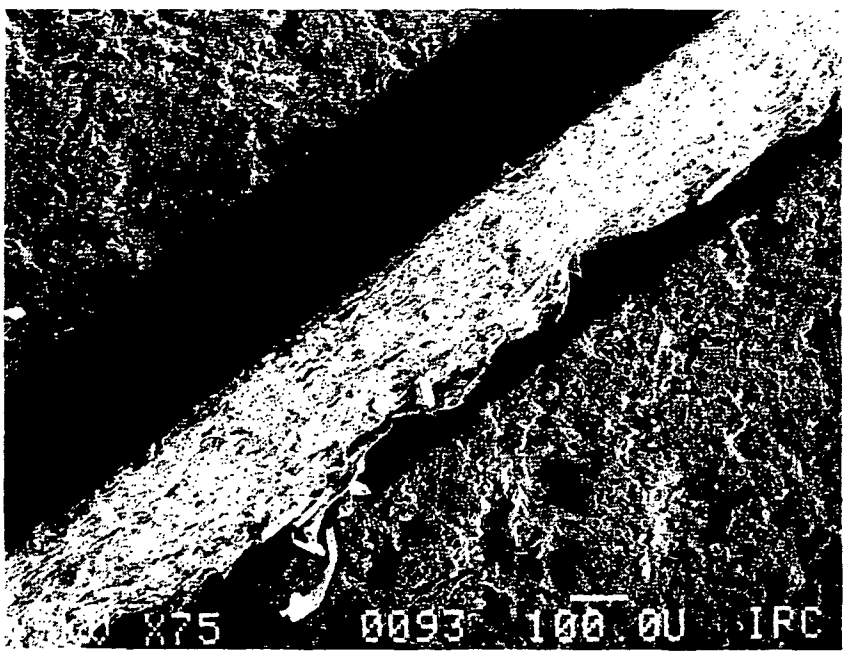

High-Intensity Dried Sheet

Figure 45. Scanning electron photomicrographs of freeze-dried and high-intensity dried sheets.

occurred after the end of the Liquid Dewatering Period. These apparent density values and the value for conventional drying are similar. This indicates that a significant sheet densification mechanism must be active during the Evaporation Period in high-intensity drying.

Table 9. Apparent sheet density data.

Drying Condition, °F/psi	Apparent Sheet Density at 0.95 RMR,[a] g/cm^3	Typical Apparent Sheet Density From Conventional Drying,[b] g/cm^3	Apparent Sheet Density From Caliper at End of Liquid Dewatering and 0.95 RMR Basis Weight,[a] g/cm^3
300/400	0.82 (t=5.00 sec)	0.68	0.62 (t=0.75 sec)
300/700	0.92 (t=4.00 sec)		0.67 (t=0.75 sec)
525/400	0.82 (t=1.25 sec)		0.59 (t=0.25 sec)
525/700	0.89 (t=1.00 sec)		0.61 (t=0.25 sec)

[a]Average basis weight at 0.95 RMR = 2.14 x 10^{-2} g/cm^2, caliper taken from Fig. 46 at times listed.
[b]From Ref. 22, commercially available, machine-made linerboard, 2.07 x 10^{-2} g/cm^2 basis weight, 7.8% MC.

The initial large decline in sheet caliper early in this period, shown by the data in Fig. 46, indicates when densification occurs. Significantly, sheet densification begins when temperatures are at peak values, that is, during pressurized flash drying. The elevated temperatures and the presence of moisture inside the fibers allows the fiber structure to begin to soften in the later stages of the Compression and Heat-Up Period, as shown by the caliper data in Fig. 28. However, the softened fibers cannot collapse under the applied load until the liquid inside the fibers begins to evaporate because even at elevated temperatures liquid water is a relatively incompressible fluid.[23] As pressurized flash drying begins to evaporate liquid inside the softened fibers, the fiber structure gradually collapses under the applied load. The densification mechanism is not available in wet-pressing or conventional drying, and is one of the most important new features of high-intensity drying. In addition, it has

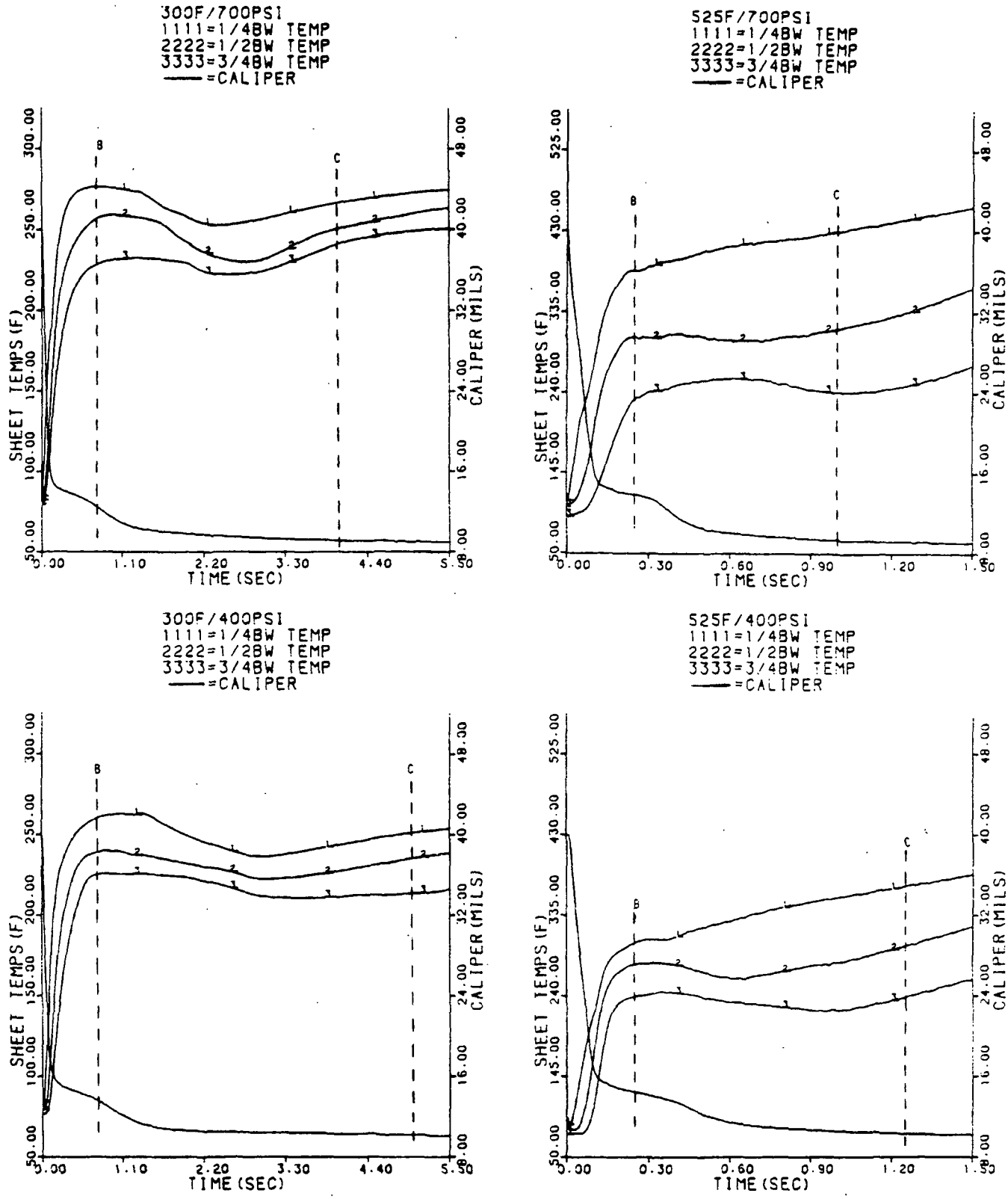

Figure 46. Sheet temperature and caliper data showing that a significant densification of the sheet occurs during pressurized flash drying.

already been mentioned that sheet densification occurs concurrently with the temperatures at peak values during the drying run. Correspondingly, the vapor phase pressures must also be at peak values. This indicates, once again, that the vapor phase pressure does not significantly impede sheet densification during high-intensity drying, even though the temperatures indicate that the vapor phase pressure can be over 100 psi in the 525°F/700 psi case.

END OF PRESSURIZED FLASH DRYING

Sheet temperatures begin to decline in this period, as shown by the data in Fig. 47. It has already been shown that the temperatures were kept relatively constant by the vapor phase pressure which seeks to balance the evaporation rate and the vapor flow rate out of the sheet. However, the magnitude of the vapor phase pressure is ultimately dependent on the supply of energy and liquid available for evaporation. It is likely then, that the availability of energy and liquid must play some role in causing the vapor phase pressure and, therefore, the temperature, to decline. The RMR data in Fig. 48 show that the sheet has not dried out to the 0.95 RMR point at the time the temperatures begin to decline. This indicates that there is an adequate amount of liquid available for evaporation, and it is the lack of availability of energy which is causing the evaporation rate and hence the vapor phase pressure and temperature, to decline. Most likely, the stored energy has been depleted by pressurized flash drying, and the heat transfer rate to and through the sheet is not great enough to offset this evaporative cooling effect. Thus, the drying rate becomes heat transfer limited. This is supported by the data in Fig. 49 which show that the heat flux is at a very low value at this time compared to the peak value earlier in drying. The decline in sheet temperatures signals the end of pressurized flash drying and the beginning of an evaporation process which dries out the sheet. This evaporation process is discussed below.

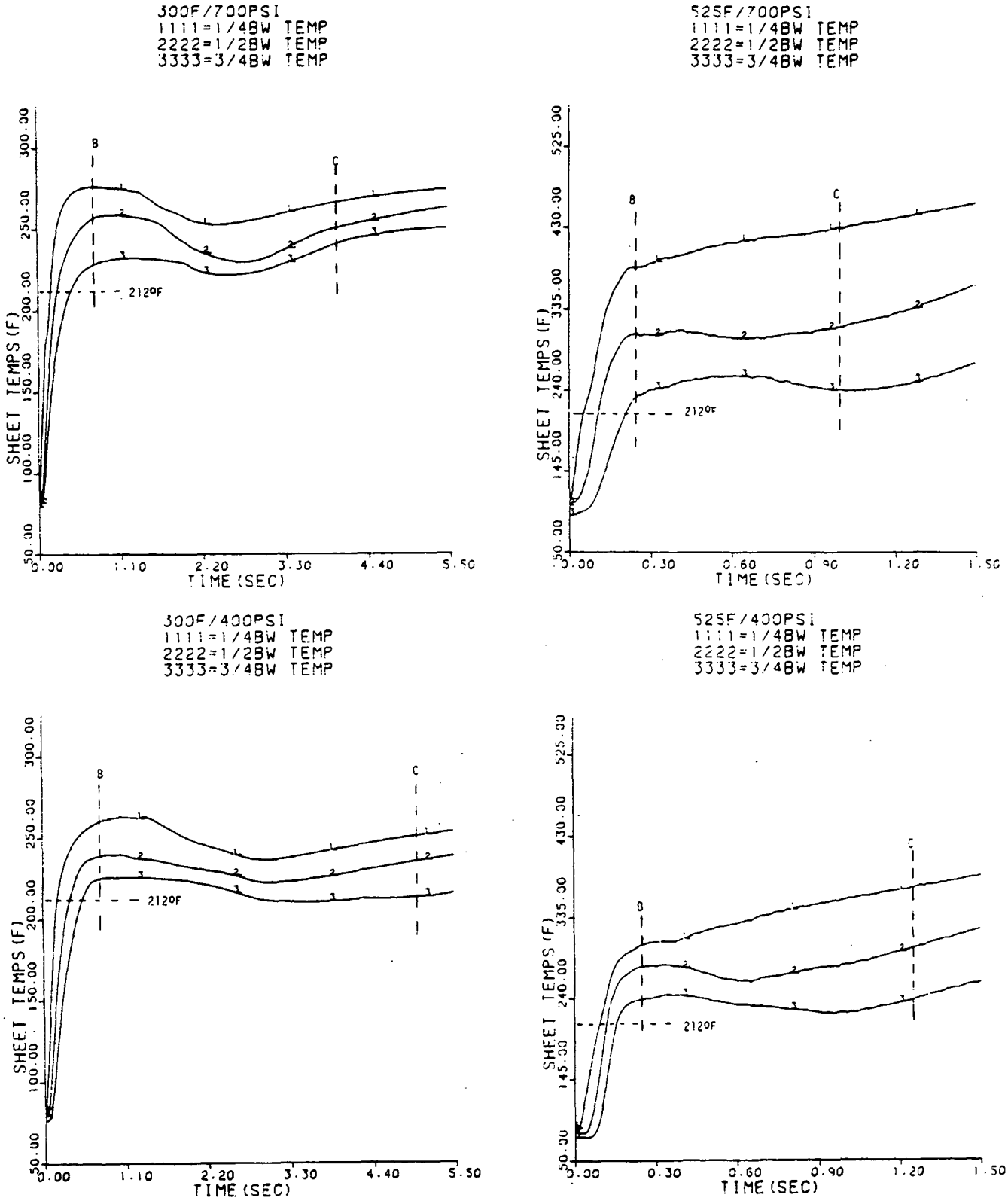

Figure 47. Sheet temperature data showing that the temperatures decline during the evaporation period.

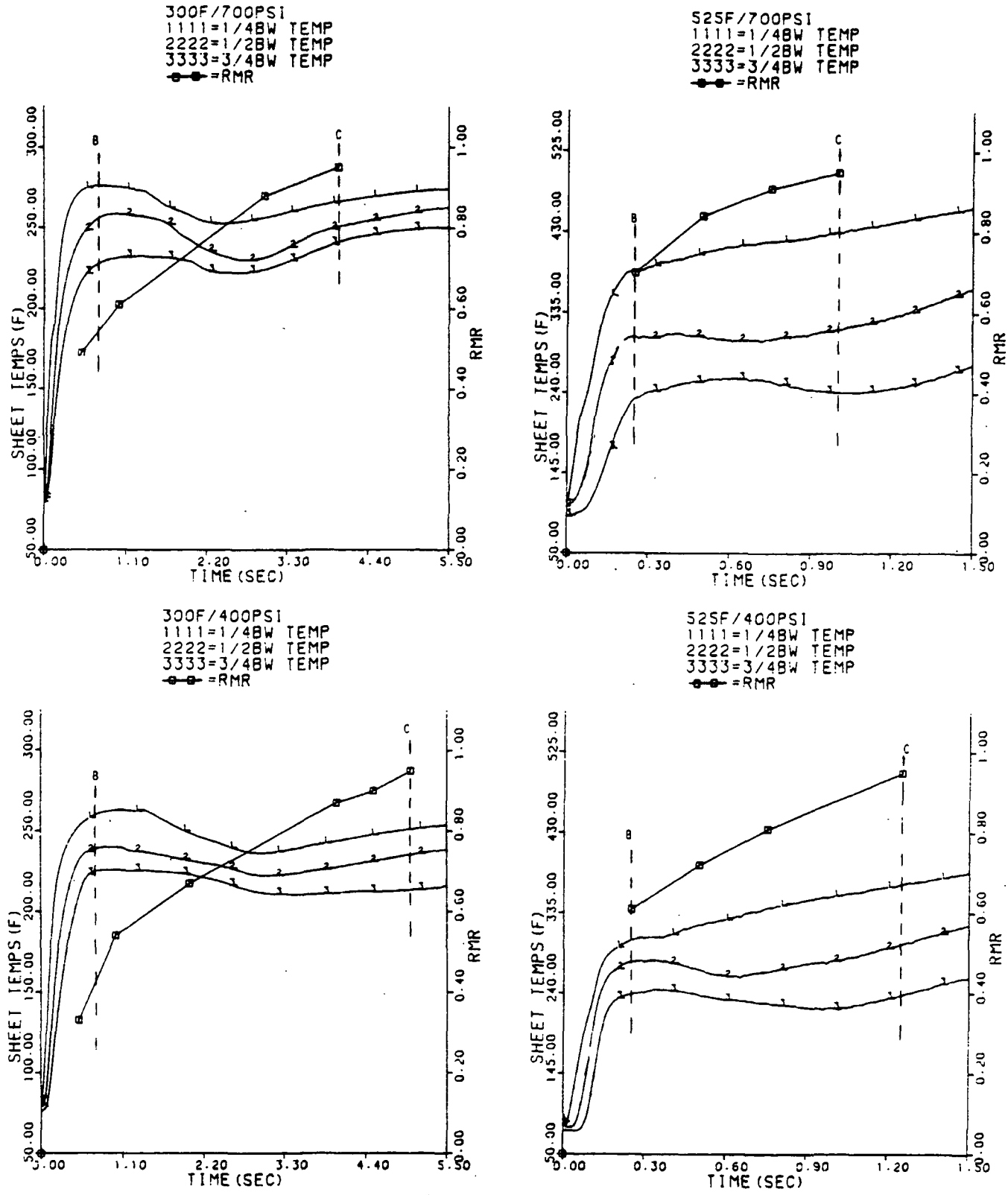

Figure 48. Sheet temperature and RMR data showing that the sheet has not dried out to the 0.95 RMR point when the temperatures begin to decline.

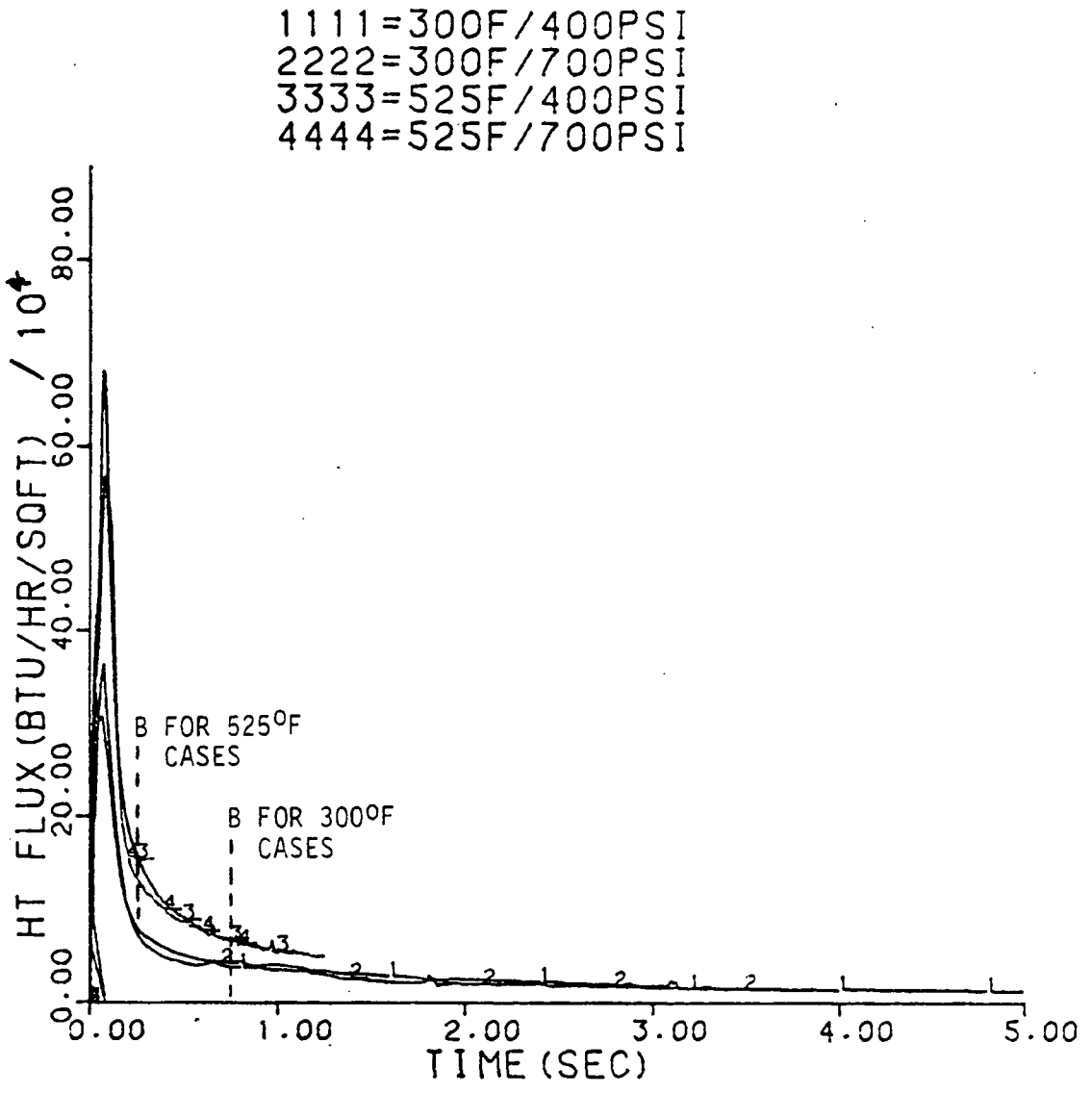

Figure 49. Heat flux data showing relatively low rate of heat transfer to the sheet later in drying.

PROGRESSIVE DRYING OUT OF THE SHEET

For the most part, the temperature data in Fig. 50 decline progressively from the hot surface to the cold surface of the sheet. After a minimum point, the temperatures begin to rise progressively through the sheet. This temperature rise can only be caused by the fibers storing energy because the RMR values in Fig. 51 indicate that drying is almost over at this time. The progressive rise

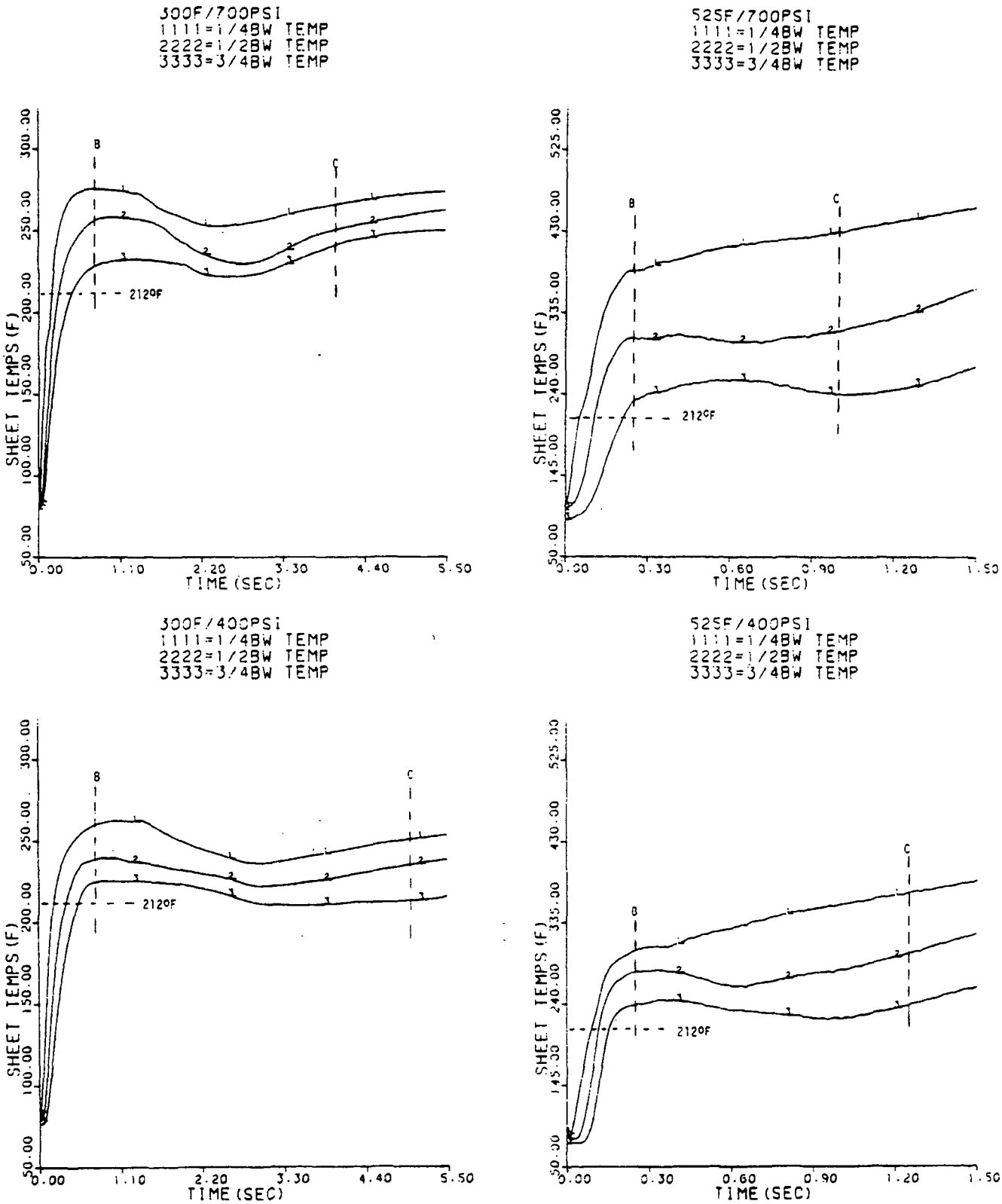

Figure 50. Sheet temperature data showing the progressive decline of temperatures from the hot surface to the cold surface of the sheet later in drying.

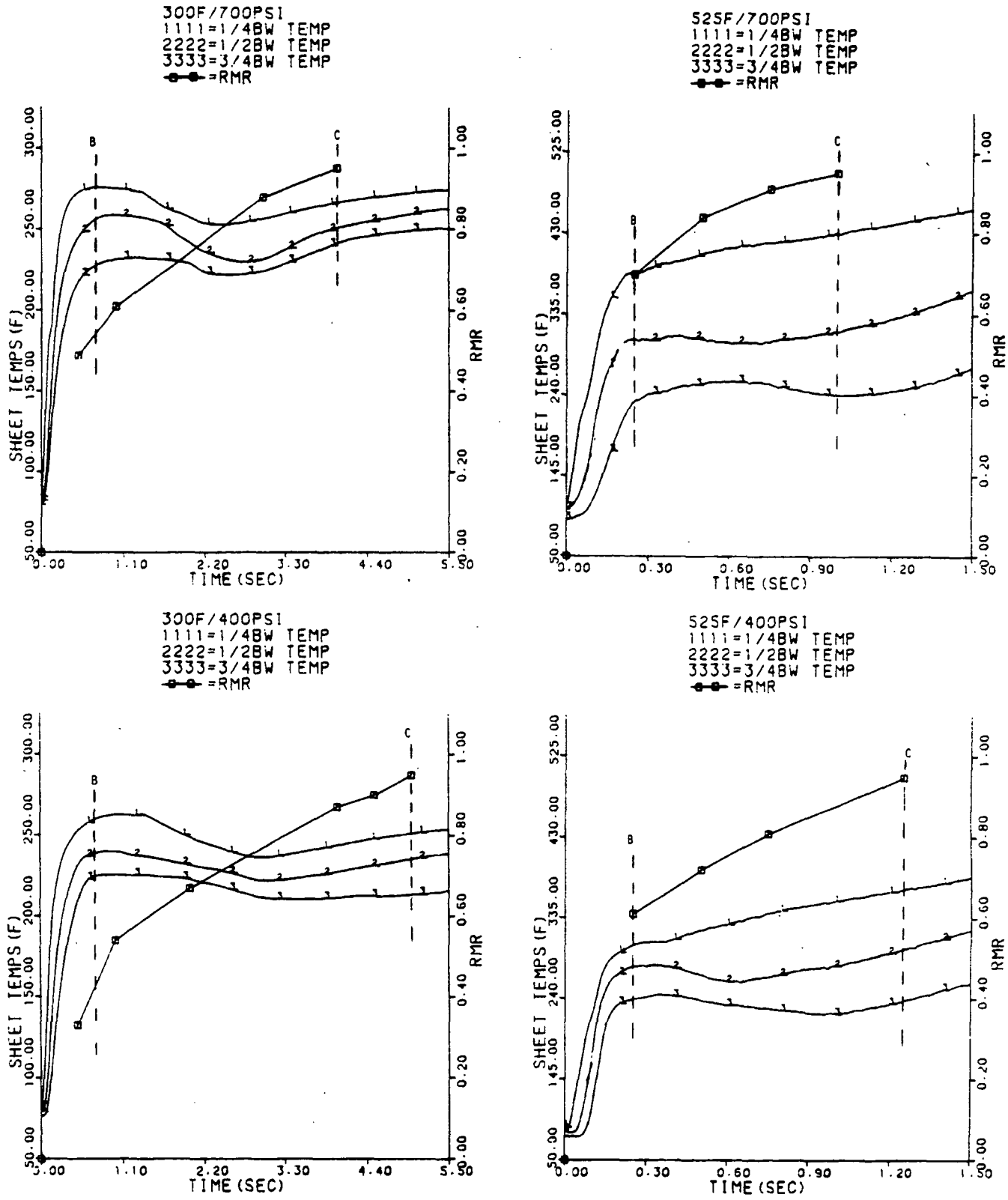

Figure 51. Sheet temperature and RMR data showing the temperature rise near the end of drying.

in sheet temperatures indicates that energy is no longer being used primarily for evaporation, and that the sheet is drying out progressively, starting near the hot surface and continuing through the sheet thickness to the cold surface. Thus, the sheet can again be considered as being divided into zones. In this case, the zones are a zone of dry fibers and vapor, and an evaporation zone. In the evaporation zone, the evaporation rate will become solely dependent on the heat transfer rate to the sheet. This differs from pressurized flash drying where significant amounts of stored energy are used for evaporation. Liquid will evaporate at a pressure just high enough to overcome the flow resistance and exit the sheet. In essence, this is a high temperature conventional drying process, but occurs more quickly because the heat transfer and mass flow processes are driven by convection rather than by diffusion. The dry zone will further decrease the heat transfer rate through the sheet because E-C-C heat transfer will be limited to the evaporation zone, and heat must be conducted to the evaporation zone through an increasingly thicker layer of insulating fibers and vapor. However, the heat transfer rate will still be higher than what occurs in conventional drying because of the intense drying conditions. The vapor in the dry zone will no longer have a pressure corresponding to the local temperature because of the absence of evaporation. This vapor will have a pressure corresponding to the temperature of the interface between the dry and evaporation zones. Hence, the vapor in the dry zone will be superheated because the temperatures in the dry zone are higher than those at the interface between the zones.

Lastly, the data in Fig. 51 show that the 1/4 basis weight temperatures for the 525°F cases continue to increase after staying constant for a short time, rather than declining and then rising as do all of the other temperature data.

In this instance, the stored energy and heat transfer during evaporation are sufficient to evaporate all of the liquid in the area, so the local drying process does not become heat transfer limited. This is a direct result of the more intense drying conditions. However, on the whole, the mechanisms discussed in this period appear to occur in every drying condition; only the rate of change of the mechanisms differs between the drying conditions. Thus, it appears from the results of this investigation that the overall drying mechanism does not change significantly with the drying conditions employed. However, the rate of change of the individual mechanisms and the overall drying rate can be greatly increased by increasing the intensity of the drying conditions.

SUMMARY

High-intensity drying can produce drying rates which are over an order of magnitude higher than those achievable by conventional drying. Liquid dewatering is partially responsible for the high drying rates, but the majority of the initial moisture still leaves the sheet as vapor. Considering the high drying rates, a rapid evaporation process must also occur in high-intensity drying. This evaporation process can be divided into two parts, namely, pressurized flash drying, followed by progressive drying out of the sheet.

Pressurized flash drying begins when liquid dewatering ends. At the end of liquid dewatering, a large amount of stored energy resides in the sheet, and heat is still being transferred into the sheet from the hot surface. In addition, the flow resistance in the network pores has been reduced from being opened to the atmosphere. As vapor rapidly exits the sheet, the vapor phase pressure begins to decline, allowing liquid to superheat and flash evaporate using significant quantities of stored energy. Very quickly, a quasi-steady-state is

established in which the vapor phase pressure effects a balance between the evaporation rate and the vapor flow rate out of the sheet. It is the vapor phase pressure, which is well above atmospheric pressure, which controls the evaporation rate, even though the liquid is at temperatures greater than 212°F and can flash into vapor instantaneously. Rough estimates show that the combination of liquid dewatering and pressurized flash drying removes over half of the initial moisture in the sheet. The heat transfer mechanisms during pressurized flash drying are evaporation-convection-condensation and conduction.

High-intensity drying produces sheet densities which are considerably higher than those achieved by conventional drying. The additional densification achieved in high-intensity drying occurs during pressurized flash drying. The additional sheet densification is a result of the applied load and is considerably augmented by thermal softening.

Later in the period, the drying rate becomes heat transfer limited as the stored energy is depleted, and the sheet begins to dry out progressively from the hot surface to the cold surface. The sheet again can be considered to be divided into zones. In this case, there exists a zone of fibers and vapor, and an evaporation zone. This progressive drying out of the sheet is essentially a high temperature conventional drying process, but occurs more quickly because of convection driven heat transfer and mass flow processes. At this time, the evaporation rate depends on the heat transfer rate, and evaporation occurs at a pressure just high enough for the vapor to overcome the flow resistance and exit the sheet. The evaporation process is hindered by the relatively slow rate of heat transfer through the dry zone to the evaporation zone which must occur by conduction alone.

Lastly, it can be concluded from the results of this investigation that, with few exceptions, the overall high-intensity drying mechanism does not change significantly with the drying conditions employed. Only the rates of change of the individual mechanisms, and hence the overall drying rate, are increased by employing increasingly intense drying conditions.

CONCLUSIONS

For handsheets made of unbleached kraft pulp with basis weights and initial moisture contents of approximately 42 lb/1000 ft^2 and 57%, respectively, and dried under applied pressures ranging from 400 psi to 700 psi, and hot surface temperatures ranging from 300°F to 525°F, the following conclusions can be drawn.

1. High-intensity drying can produce drying rates which are over an order of magnitude higher than those found in conventional drying.
2. The higher drying rates are a result of the intense drying conditions which cause convective heat transfer and mass (liquid and vapor) flow processes in the sheet.
3. Approximately 29% of the initial moisture leaves the sheet in liquid form. This value remains relatively constant regardless of the drying condition employed. The amount of liquid dewatering is also several times higher than what can be achieved by room temperature wet pressing alone.
4. The liquid dewatering process is initiated by a sheet volume reduction mechanism that is essentially the same mechanism that is active in wet pressing. However, the major part of the liquid dewatering occurs via a vapor displacement mechanism.
5. High-intensity drying produces sheet densities that are significantly higher than those normally produced by conventional drying.
6. Sheet densification is caused by the applied load and is considerably augmented by thermal softening. Thermal softening

is enhanced because the fibrous structure is pressurized by vapor, allowing moisture and the fiber wall material to reach elevated temperatures.

7. The overall high-intensity drying mechanism does not change significantly with the drying conditions employed. Only the rates of change of the individual mechanisms, and hence the overall drying rate, are increased by employing increasingly intense drying conditions.

RECOMMENDATIONS FOR FUTURE WORK

Future efforts in high-intensity drying should be made in the following areas.

A method to measure the internal sheet moisture content during drying, plus the internal sheet temperature data, would aid in calculating more precise mass and energy balances. Measurement of the vapor phase pressure at the hot surface would also aid in understanding more about the ongoing transport processes, in particular during liquid dewatering.

The sheet conditions (basis weight, initial moisture content, pulp freeness, etc.) were kept constant during this investigation. A more complete study should be performed to determine how these conditions affect the overall drying mechanism. This study should be performed in conjunction with the development of a mathematical model for predicting drying behavior under various drying and sheet conditions.

Lastly, hot pressing and heated dry sheet compression experiments should be performed in an attempt to separate the contributions of volume reduction and vapor displacement to the liquid dewatering process.

ACKNOWLEDGMENTS

I gratefully acknowledge the support of The Institute of Paper Chemistry and member companies in the conduct of this work and for affording me the opportunity for a first rate graduate school education.

I would also like to thank the following members of my Thesis Advisory Committee: Dr. Frederick W. Ahrens - Major Advisor, Dr. Clyde H. Sprague - Advisor in Residence, and Drs. Harry T. Cullinan, Jr., Peter E. Parker, and Douglas Wahren.

In addition, I would like to thank the other faculty members, staff, and students who have helped me in this work. Special thanks go to my typist, Kathy L. Gossens, for her diligent efforts in reading my handwriting.

Lastly, I thank my parents and family for their support throughout my college years.

LITERATURE CITED

1. Ahrens, F. W.; Kartsounes, G. T.; Ruff, D. L. A laboratory study of hot-surface drying at high temperature and mechanical loading. Proceedings of the CPPA Technical Section Annual Meeting, Vol. B, Montreal 1982:93-7.

2. Ruff, D. L. Experimental evaluation of paper drying using higher than normal temperatures and pressures. A-291 Report, Appleton, WI, The Institute of Paper Chemistry, 1981.

3. Holm, R. A.; Holderby, J. M.; Perry, J. F. Machine operating conditions and their influence on drying rate, Report Three, Project 2693. Appleton, WI, The Institute of Paper Chemistry, 1970. 65 p.

4. Arenander, S.; Wahren, D. Impulse drying adds new dimension to water removal. Tappi 66(9):123-6 (1983).

5. Ahrens, F. W. Fundamentals of drying, Status Report to the Engineering Project Advisory Committee, Project 3470. Appleton, WI, The Institute of Paper Chemistry, 1984. 21 p.

6. Burton, S. W. An investigation of dynamic densification under impulse drying conditions, Progress Report Six. Appleton, WI, The Institute of Paper Chemistry, 1985. 30 p.

7. Pounder, J. R. A mathematical model of high-intensity paper drying. Doctoral Dissertation. Appleton, WI, The Institute of Paper Chemistry, 1986. 180 p.

8. Ahrens, F. W. Fundamentals of drying, Status Report to the Engineering Project Advisory Committee, Project 3470. Appleton, WI, The Institute of Paper Chemistry, 1983. 20 p.

9. Fang, Y. P. An investigation of the drying mechanism in the press-drying process, Progress Report Two. Appleton, WI, The Institute of Paper Chemistry, 1981. 11 p.

10. Kirk, L. A.; Jones, G. T. Hot surface drying of paper. Paper Technology 11(5):347-52, 397-403 (1970).

11. Back, E. L.; Bucko, J.; Jansson, M. B. Determination of vaporized water during press-drying of hardboard. Svensk Papperstid. 81(5):153-5(1978).

12. Baughman, G. D. SEM/EDX analysis of filled papers: image processing software for the generation of a relative z-direction elemental distribution profile. A-291 Report, Appleton, WI, The Institute of Paper Chemistry, 1984.

13. Parham, R. A. X-ray/SEM analysis of materials: principles and applications to paper. Paperi Puu 55(12):959-72(1973).

14. Finck, J. L. Mechanism of heat flow in fibrous materials. Bureau of Standards Journal of Research, Research Paper No. 243, 5(5):973-84 (1930).

15. Russell, H. W. Principles of heat flow in porous insulators. J. American Ceramic Society 18:1-5(1935).

16. Schotte, W. Thermal conductivity of packed beds. AIChE Journal 6(1):63-7 (1960).

17. Ceckler, W. H.; Thompson, E. V. The University of Maine at Orono Wet Pressing Project, Final Report. Washington, DC, U.S. Department of Energy, 1982. 335 p.

18. Lienhard, J. H. A heat transfer textbook. Englewood Cliffs, NJ, Prentice-Hall, Inc., 1981:388.

19. Byrd, V. L. Flow and adhesion of hemicellulose and lignin. Tappi 62(7): 81-4(1979).

20. Horn, R. A. Bonding in press-dried sheets from high-yield pulps. Tappi 62(7):77-80(1979).

21. Back, E. L.; Swenson, R. The present state of press-drying of paper. Proceedings of the Seventh International Water Removal Symposium, Cambridge 1981.

22. Continuous base-line study (modified), mill linerboard data for July, August, September 1983, Report Eighty Nine, Progress Report to Fourdrinier Kraft Board Group of the American Paper Institute, Project 2694-1. Appleton, WI, The Institute of Paper Chemistry, December 1983, 5 p.

23. Lienhard, J. H. A heat transfer textbook. Englewood Cliffs, NJ, Prentice-Hall, Inc., 1981:499.

24. Ahrens, F. W. Heat transfer aspects of hot-surface drying at high temperature and mechanical loading. Proceedings of the 1982 International Water Removal Symposium, Vancouver 1982:113-7.

25. Arnson, T. R. The adsorption of complex aluminum species by cellulosic fibers from dilute solutions of aluminum chloride and aluminum sulfate. Doctoral Dissertation. Appleton, WI, The Institute of Paper Chemistry, 1980. 122 p.

APPENDIX I

EXPERIMENTAL PROCEDURES

DRYING RATE STUDY

Handsheets were made on the constant rate filtration apparatus using tap water. The target basis weight and initial moisture content of each sheet was 42 lb/1000 ft^2 and 57%, respectively. All handsheets formed for use in this investigation had these basis weight and initial moisture content targets. The initial moisture content was achieved by pressing a sheet between pulp blotters for 3.5 minutes at 250 psi. Unless otherwise noted, all sheets were brought to the initial moisture content in this manner. The drying rate data were obtained gravimetrically by interrupting the drying process. Prior to a run, the hot surface temperature was raised to 5°F above the target temperature before the heaters were turned off. A piece of insulation was then used to cover the hot surface in order to provide a gradual cooling and near uniform block temperature. When the surface cooled to the target temperature, the insulation was removed and a run was made. This was the procedure for all drying runs in this investigation.

LIQUID DEWATERING STUDY

Handsheets were made from a slurry that contained 935 ppm lithium chloride. Appendix II discusses sheetmaking with lithium chloride in more detail.

Liquid dewatering measurements were obtained by interrupting the drying process and comparing the amount of lithium in a high-intensity dried sheet with that of an air-dried (control) sheet. One minus the ratio of these lithium contents is the fraction of liquid water that was pushed out of the sheet,

rather than evaporated, during drying.[11] It was assumed that any dilution of the lithium caused by vapor condensation was negligible. The lithium content of a sheet was determined by Flame Emission Spectroscopy after ashing the sheet.

Handsheets used for wet-pressing were prepared similarly to those in the Drying Rate Study. The moisture loss measurements were made gravimetrically.

LIQUID MOVEMENT STUDY

Handsheets were made similarly to the Liquid Dewatering Study except that the stock slurry contained 7600 ppm lithium chloride.

Qualitative evidence for the redistribution of liquid water in the sheet during drying was determined by x-ray mapping the chlorine distribution through a portion of the thickness of a high-intensity dried sheet and comparing it with that of a freeze-dried sheet. The chlorine distribution in a sheet dried to dryness is indicative of the local cumulative evaporation in the sheet because the chlorine only moves with the liquid and is deposited onto the fibers when the liquid evaporates. The x-ray mapping technique, using Scanning Electron Microscope/Energy Dispersive Spectroscopy, has been discussed in detail elsewhere.[12,13]

HEAT FLUX STUDY

Handsheets were made similarly to those in the Drying Rate Study. The sheets were weighed before and after drying, and their oven-dried weights were also obtained for further calculations.

The heat flux, from the hot surface to the sheet, was computed from the surface temperature history of the heater block by modeling the block as a finite slab. More information on this model is given by Ahrens.[24]

INTERNAL SHEET TEMPERATURE STUDY

The sheets for this study had similar basis weights and initial moisture contents as the previous studies. However, these sheets were made of four plies of equal basis weight. The plies were made on the constant-rate filtration former using tap water. After formation each ply was pressed at 10 psi for 30 seconds to give the plies enough inherent strength to be handled. The plies were then stacked together with a 0.002 inch Type T thermocouple placed between the plies. The composite sheet was then pressed at 100 psi for two minutes to achieve the desired initial moisture content.

CALIPER STUDY

Handsheets were made similarly to those in the drying rate study.

As previously noted, pulp blotters were not used in this study to capture vapor and liquid escaping the nip. Calibration problems would have developed had blotters been used. Instead, the support plate of the drying apparatus was heated to 215°F to allow vapor and liquid to escape the nip without condensing or rewetting the sheet, respectively. As far as could be determined this arrangement had no effect on the drying rate.

APPENDIX II

SHEETMAKING WITH LITHIUM CHLORIDE

Adding lithium chloride to the sheetmaking stock slurry served two purposes. The chlorine was used to aid in determining the movement of liquid in the web. The lithium was used to calculate the amount of liquid dewatering. For the dewatering experiments the stock slurry was prepared in the following way.

The pulp for sheetmaking was taken from the cold room and 120 g (40 g O.D.) weighed out, mixed with 1.5 L of distilled water, and disintegrated for five minutes. The fibers were then added to 325 L of distilled water (0.012% consistency) in the stock tank of the constant-rate filtration apparatus and mixed for two hours to ensure adequate dispersion. Following Back, et al.[11] aluminum, as aluminum nitrate, was added to the slurry to satisfy the anionic demand of the fibers before the lithium chloride was added. Otherwise, the lithium could adsorb onto the fibers and bias the liquid dewatering results downward. The amount of aluminum nitrate added was 195 g or enough to give the stock slurry a concentration of 1.5×10^{-3} M aluminum, typical of mill concentrations. The pH of the slurry was dropped to 4.0 with nitric acid to release the aluminum in its trivalent form. This was judged to be the most efficient way to satisfy the anionic demand of the fibers.[25] The slurry was then mixed overnight. Lastly, 305 g (935 ppm) of lithium chloride was added, and the slurry was mixed for two hours before sheetmaking.

For the liquid movement experiments the stock slurry was prepared similarly, except that 2500 g (7600 ppm) of lithium chloride were added to the slurry.

APPENDIX III

SHEET WEIGHT DATA FOR DRYING RATE AND RMR CALCULATIONS

The following tables present the raw sheet weight data that were used to calculate the drying rates and RMR values for the four drying conditions.

DRYING CONDITION: 300°F/400 psi

Sheet	Drying Time, sec	Wet Sheet Weight, g	Dried Sheet Weight, g	O.D. Sheet Weight, g	RMR	Av. RMR
98	0.25	7.23	6.52	3.16	0.17	0.18
72	0.25	7.28	6.50	3.16	0.19	
87	0.50	7.05	5.80	3.07	0.31	0.33
94	0.50	6.93	5.61	3.05	0.34	
118	1.0	6.96	4.85	3.01	0.53	0.54
88	1.0	7.15	4.98	3.14	0.54	
95	2.0	7.04	4.50	3.14	0.65	0.67
37	2.0	6.88	4.23	3.00	0.68	
115	4.0	6.90	3.47	3.01	0.88	0.87
105	4.0	7.27	3.74	3.14	0.85	
45	4.5	7.23	3.59	3.19	0.90	0.90
28	4.5	7.09	3.51	3.10	0.90	
117	5.0	6.90	3.34	3.13	0.95	0.95

DRYING CONDITION: 300°F/700 psi

Sheet	Drying Time, sec	Wet Sheet Weight, g	Dried Sheet Weight, g	O.D. Sheet Weight, g	RMR	Av. RMR
48	0.25	7.05	5.78	3.05	0.32	0.32
106	0.50	6.98	5.03	3.01	0.49	
61	0.50	7.20	5.29	3.11	0.47	0.49
101	0.50	7.22	5.14	3.05	0.50	
71	1.0	7.14	4.65	3.05	0.61	
110	1.0	7.25	4.69	3.06	0.61	0.61
53	1.0	7.17	4.67	3.05	0.61	
75	3.0	7.23	3.61	3.10	0.88	0.88
64	4.0	6.90	3.17	2.94	0.94	0.94
19	4.0	7.12	3.29	3.02	0.93	

DRYING CONDITION: 525°F/400 psi

Sheet	Drying Time, sec	Wet Sheet Weight, g	Dried Sheet Weight, g	O.D. Sheet Weight, g	RMR	Av. RMR
120	0.25	7.22	4.86	3.14	0.58	
25	0.25	7.22	4.67	3.12	0.62	0.61
4	0.25	7.33	4.69	3.16	0.63	
57	0.50	7.21	4.29	3.10	0.71	0.72
15	0.50	7.28	4.28	3.12	0.72	
50	0.75	7.17	3.94	3.10	0.79	
22	0.75	7.09	3.82	3.09	0.82	0.81
101	0.75	7.55	4.08	3.22	0.81	
1	1.25	7.43	3.54	3.20	0.93	
113	1.25	7.20	3.49	3.22	0.93	0.93
61	1.25	7.30	3.41	3.17	0.94	

DRYING CONDITION: 525°F/700 psi

Sheet	Drying Time, sec	Wet Sheet Weight, g	Dried Sheet Weight, g	O.D. Sheet Weight, g	RMR	Av. RMR
58	0.25	7.21	4.23	3.05	0.72	
43	0.25	7.02	4.14	3.01	0.72	0.70
56	0.25	7.41	4.68	3.19	0.65	
79	0.50	7.10	3.78	3.10	0.83	
54	0.50	7.21	3.80	3.08	0.83	0.84
78	0.50	7.04	3.66	3.05	0.85	
19	0.75	6.97	3.30	3.00	0.92	
104	0.75	6.93	3.39	3.01	0.90	0.91
20	0.75	7.28	3.53	3.12	0.90	
13	1.0	6.96	3.39	3.23	0.96	0.96

APPENDIX IV

LIQUID DEWATERING CALCULATIONS FROM LITHIUM LOSS MEASUREMENTS AND WET-PRESSING RESULTS

The following tables present the amounts of lithium found in the handsheets used in the Liquid Dewatering Study. Calculations of the amount of liquid dewatering at various times during drying are also given for the four drying conditions. In addition the raw sheet weight data used in calculating the amount of liquid dewatering from wet-pressing are listed.

LITHIUM LOSS RESULTS

DRYING CONDITION: 300°F/400 psi

Sheet	Drying Time, sec	Lithium Content, µg	Average Lithium Content, µg	Standard Deviation Lithium Content, µg
105	air-dried	690		
66	air-dried	670	683	12
42	air-dried	690		
74	0.50	650		
114	0.50	610	630	28
118	0.75	510		
28	0.75	500		
59	1.0	470	495	17
37	1.0	500		

Assume liquid dewatering was over at 0.75 second.

Average percent liquid dewatering (0.75 sec) =

$$= 1 - \frac{\frac{510 + 500 + 470 + 500}{4}}{\frac{690 + 670 + 690}{3}} \times 100 = 1 - \frac{495}{685} \times 100 = 28\%$$

DRYING CONDITION: 300°F/700 psi

Sheet	Drying Time, sec	Lithium Content, µg	Average Lithium Content, µg	Standard Deviation Lithium Content, µg
12	air-dried	670		
40	air-dried	670	670	0
82	0.50	480		
86	0.50	460	470	14
111	0.75	430		
47	0.75	450	440	14

Assume liquid dewatering was over at 0.75 sec.

Average percent liquid dewatering (0.75 sec) =

$$= 1 - \frac{\frac{430 + 450}{2}}{\frac{670 + 670}{2}} \times 100 = 1 - \frac{440}{670} \times 100 = 34\%$$

Average percent liquid dewatering (0.50 sec) =

$$= 1 - \frac{\frac{480 + 460}{2}}{\frac{670 + 670}{2}} \times 100 = 1 - \frac{470}{670} \times 100 = 30\%$$

DRYING CONDITION: 525°F/400 psi

Sheet	Drying Time, sec	Lithium Content, µg	Average Lithium Content, µg	Standard Deviation Lithium Content, µg
49	air-dried	700		
2	air-dried	690	695	7
96	0.25	500		
31	0.25	480		
67	1.5	470	483	13
89	1.5	480		

Assume liquid dewatering was over at 0.25 second.

Average percent liquid dewatering (0.25 sec) =

$$= 1 - \frac{\frac{500 + 480 + 470 + 480}{4}}{\frac{700 + 690}{2}} \times 100 = 1 - \frac{485}{695} \times 100 = 30\%$$

DRYING CONDITION; 525°F/700 psi

Sheet	Drying Time, sec	Lithium Content, µg	Average Lithium Content, µg	Standard Deviation Lithium Content, µg
22	air-dried	605		
51	air-dried	635		
34	air-dried	605	609	19
18	air-dried	590		
58	0.25	430		
43	0.25	465		
8	0.50	440		
79	0.50	430	445	15
19	0.75	460		
04	0.75	445		

Assume liquid dewatering was over at 0.25 second.

Average percent liquid dewatering (0.25 sec) =

$$= 1 - \frac{\frac{430 + 465 + 440 + 430 + 460 + 445}{6}}{\frac{605 + 635 + 605 + 590}{4}} = 1 - \frac{445}{610} \times 100 = 27\%$$

ROOM TEMPERATURE WET PRESSING RESULTS

Sheet	Pressing Condition, sec/psi	Wet Sheet Weight, g	After Pressing Weight, g	O.D. Weight, g	RMR	Av. RMR
21	1.0/400	7.06	6.95	3.10	0.03	
66	1.0/400	7.38	7.26	3.22	0.03	0.03
89	1.0/400	7.44	7.32	3.23	0.03	
100	0.5/400	6.90	6.80	3.05	0.03	
42	0.5/400	7.18	7.07	3.10	0.03	0.03
9	0.5/400	6.86	6.76	3.01	0.03	
102	1.0/700	6.82	6.56	3.01	0.07	
52	1.0/700	7.16	6.74	3.10	0.10	0.09
81	1.0/700	7.08	6.74	3.11	0.09	
37	0.5/700	7.05	6.82	3.04	0.06	0.05
74	0.5/700	6.90	6.75	3.06	0.04	

APPENDIX V

LIQUID DEWATERING CALCULATIONS FROM HEAT TRANSFER MEASUREMENTS

Energy balances from sheet weight and temperature data, and heat transfer measurements from surface temperature data were used to calculate the amounts of liquid dewatering found in Table III. The energy balances assumed that the water in the sheets was evaporated under atmospheric pressure at 212°F and no liquid dewatering occurred. The energy balances were calculated on the basis of 95% moisture removal from the sheets. The heat transfer measurements were taken from time integrations of the heat fluxes like those shown in Fig. 52. The cumulative energy transfer values at the 0.95 RMR point were compared with the energy balance values that assumed no liquid dewatering to determine the amounts of liquid dewatering. Given below are the sheet weight and temperature data, heat transfer data, and a sample liquid dewatering calculation.

DRYING CONDITION: 300°F/400 psi

LIQUID DEWATERING CALCULATION DATA

Sheet	Wet Sheet Weight, g	O.D. Sheet Weight, g	Initial Sheet Moisture Weight, g	Total Enthalpy Change,[a] Btu	Heat Transfer Measured,[a] Btu	Liquid Dewatering, %
70	7.19	3.11	4.08	9.80	7.75	20.9
17	7.34	3.17	4.17	10.00	7.35	26.5
77	7.40	3.21	4.19	10.06	7.47	25.7
71	7.24	3.14	4.10	9.84	7.19	26.9

[a]To 0.95 RMR.

Average percent liquid dewatering = 25%

Standard Deviation of average percent liquid dewatering = 3%

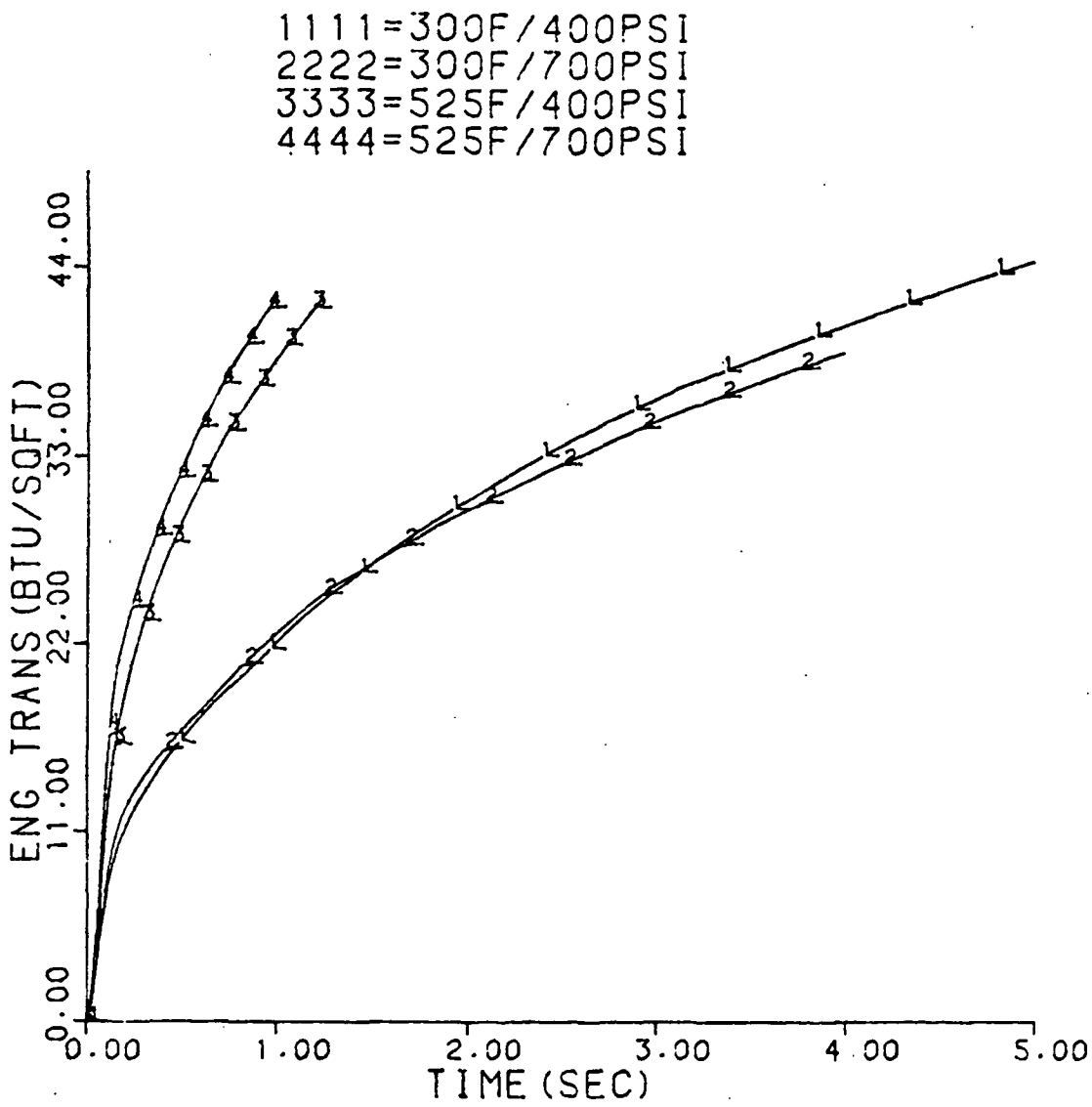

Figure 52. Cumulative energy transfer data.

SAMPLE CALCULATION FOR SHEET 17

Calculation constants

Heat capacity of dry fibers = 0.35 Btu/lb/°F
Heat capacity of liquid water = 1.0 Btu/lb/°F
Cross-sectional area of sheet = 0.165 ft^2
Latent enthalpy of water at 212°F = 970.3 Btu/lb

Laboratory measured heat transfer to sheet

From Fig. 52, heat transfer measured
taken at 5 seconds (0.95 RMR) = 44.5 Btu/ft^2 x 0.165 ft^2
= 7.35 Btu

Sheet weight data

O.D. sheet weight = 3.17g
Initial sheet moisture weight = wet sheet weight - O.D. sheet weight
= 7.34g - 3.17g = 4.17g
Weight of water evaporated = initial sheet moisture weight x 0.95
= 4.17g x 0.95 = 3.96g

Temperature data

Initial sheet temperature = 80°F

Total enthalpy change of sheet during drying with no liquid dewatering

Sensible enthalpy change of fibers

$$\frac{3.17\text{g}}{} \left| \frac{1\text{ lb}}{453.6\text{g}} \right| \frac{0.35\text{ Btu}}{\text{lb} \cdot {}^\circ\text{F}} \left| \frac{212^\circ\text{F} - 80^\circ\text{F}}{} \right. = 0.32\text{ Btu}$$

Sensible enthalpy change of liquid

$$\frac{4.17\text{g}}{} \left| \frac{1\text{ lb}}{453.6\text{g}} \right| \frac{1.0\text{ Btu}}{\text{lb} \cdot {}^\circ\text{F}} \left| \frac{212^\circ\text{F} - 80^\circ\text{F}}{} \right. = 1.21\text{ Btu}$$

Latent enthalpy change of water

$$\frac{3.96\text{ g}}{} \left| \frac{1\text{ lb}}{453.6\text{g}} \right| \frac{970.3\text{ Btu}}{\text{lb}} = 8.47\text{ Btu}$$

Total enthalpy change = 10.00 Btu

$$\text{Liquid Dewatering (\%)} = 1 - \frac{\text{heat transfer measured}}{\text{total enthalpy change}} \times 100$$

$$= 1 - \frac{7.35 \text{ Btu}}{10.00 \text{ Btu}} \times 100 = 26.5\%$$

All other calculations were done similarly with the data provided.

DRYING CONDITION: 300°F/700 psi

LIQUID DEWATERING CALCULATION DATA

Sheet	Wet Sheet Weight, g	O.D. Sheet Weight, g	Initial Sheet Moisture Weight, g	Total Enthalpy Change,[a] Btu	Heat Transfer Measured,[a] Btu	Liquid Dewatering, %
112	7.29	3.17	4.12	9.89	7.10	28.2
36	7.28	3.13	4.15	9.96	6.46	35.1
113	7.26	3.17	4.09	9.82	6.90	29.7
116	7.00	3.07	3.93	9.44	6.92	26.7
29	7.15	3.10	4.05	9.72	6.60	32.1

[a]To 0.95 RMR.

Average percent liquid dewatering = 30%

Standard deviation of average percent liquid dewatering = 3%

ADDITIONAL DATA NEEDED FOR CALCULATIONS

Initial sheet temperature = 80°F

Heat transfer measured taken at 4 seconds (0.95 RMR)

DRYING CONDITION: 525°F/400 psi

LIQUID DEWATERING CALCULATION DATA

Sheet	Wet Sheet Weight, g	O.D. Sheet Weight, g	Initial Sheet Moisture Weight, g	Total Enthalpy Change,[a] Btu	Heat Transfer Measured,[a] Btu	Liquid Dewatering, %
59	6.99	3.12	3.87	9.20	7.41	19.5
91	7.25	3.15	4.10	9.73	6.99	28.2
97	7.36	3.18	4.18	9.92	7.23	27.1
92	7.23	3.16	4.07	9.66	7.25	24.9

[a]To 0.95 RMR.

Average percent liquid dewatering = 25%

Standard deviation of average percent liquid dewatering = 4%

ADDITIONAL DATA NEEDED FOR CALCULATIONS

Initial sheet temperature = 90°F
Heat transfer measured taken at 1.25 seconds (0.95 RMR)

DRYING CONDITION: 525°F/700 psi

LIQUID DEWATERING CALCULATION DATA

Sheet	Wet Sheet Weight, g	O.D. Sheet Weight, g	Initial Sheet Moisture Weight, g	Total Enthalpy Change,[a] Btu	Heat Transfer Measured,[a] Btu	Liquid Dewatering, %
88	6.95	2.96	3.99	9.46	6.00	36.6
87	7.13	3.04	4.09	9.70	7.05	27.3
98	7.24	3.10	4.14	9.82	6.98	28.9

[a]To 0.95 RMR.

Average percent liquid dewatering = 31%

Standard deviation of average percent liquid dewatering = 5%

ADDITIONAL DATA NEEDED FOR CALCULATIONS

Initial sheet temperature = 90°F
Heat transfer measured taken at 1 second (0.95 RMR)

APPENDIX VI

HEAT LOSSES DURING DRYING

Figure 10 shows that the values of the heat fluxes did not go to zero at the end of drying. This suggests that heat losses to the surroundings were occurring during drying. To determine whether the heat losses were a significant fraction of the total heat transfer to the 0.95 RMR point, the following experiment was performed.

It was assumed that the majority of the heat losses during drying were occurring from the cold side of the sheet to the support plate. Because the cold side of the sheet was exposed to atmospheric pressure, its temperature during drying must have been 212°F. Thus, the driving force for heat loss was a temperature drop of 212°F-80°F (80°F = room temperature). To prevent this heat loss the support plate of the drying apparatus was heated to 215°F. A heat flux run was then made at 300°F/700 psi. This was judged to be the condition that would have the highest heat losses for two reasons. First, the higher pressure would provide better contact between the sheet and support plate. Second, since it was assumed that the heat losses were occurring at a steady rate, longer drying times would have higher heat losses.

Figure 53 shows the time integrals of the heat fluxes from the runs where the support plate was heated and unheated. The curve for the heated support plate levels off signifying the end of heat transfer and thus, no heat losses. The two curves begin to deviate toward the end of drying. At the 0.95 RMR point (4 seconds) the difference in the total amount of heat transferred between the two runs is only 5%. Therefore, heat losses to the 0.95 RMR point can be ignored for all four drying conditions.

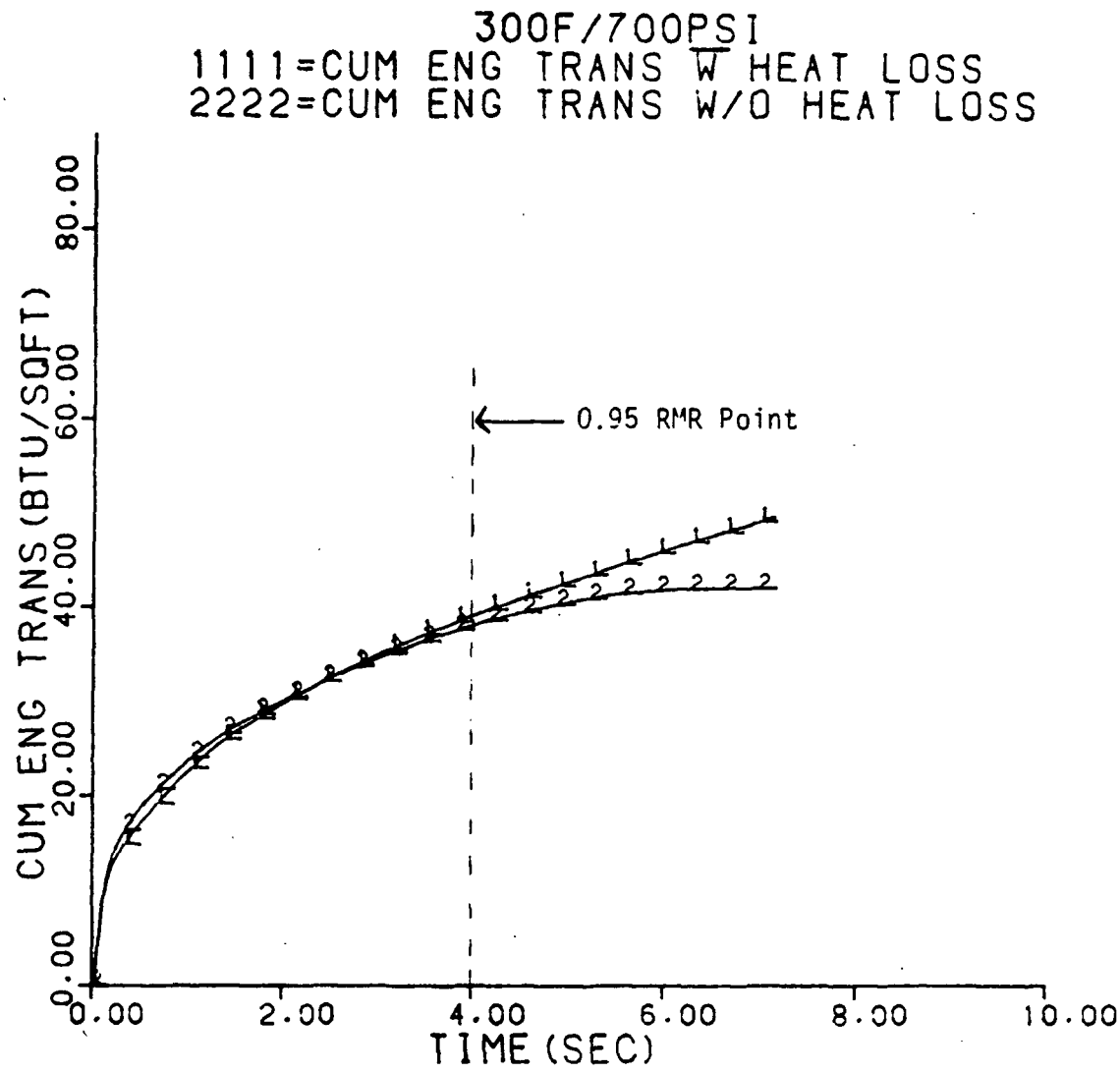

Figure 53. Plots of cumulative energy transfer to the sheet during drying with and without heat losses to the surroundings.

APPENDIX VII

CALCULATION OF SHEET TEMPERATURE INCREASE FROM RADIATION HEAT TRANSFER FROM HOT SURFACE TO SHEET

Drying Condition: 525°F/700 psi

Assume: The hot surface and sheet are black bodies.

Radiation Heat Transfer Equation: $Q = \sigma A t(T_s^4 - \overline{T}_p^4)$

Where: Q = radiation heat transfer to sheet, Btu

σ = Stefan-Boltman constant = 4.761×10^{-13} Btu/ft^2 · sec · °R^4

A = cross-sectional area of sheet (5.5 inch diameter) = 0.16 ft^2

t = drying time = 1 sec (Table 1)

T_s = hot surface temperature = 525°F = 985°R

$\overline{T}_p$ = average sheet temperature = 300°F = 760°R (Fig. 11)

Calculation of Radiation Heat Transfer

$$Q = \frac{4.761 \times 10^{-13} \text{ Btu}}{\text{ft}^2 \cdot \text{sec} \cdot {}^\circ\text{R}^4} \left| \frac{0.16 \text{ ft}^2}{} \right| \frac{1 \text{ sec}}{} \left| \frac{((985)^4 - (760)^4)\,{}^\circ\text{R}^4}{} \right| = 0.05 \text{ Btu}$$

Calculation of temperature increase from radiation heat transfer

Assume: Only the water is being heated.

Temperature increase equation: $T_F = T_i + \frac{Q}{MC_p}$

Where: T_F = final sheet temperature, °F
T_i = initial sheet temperature = 80°F
Q = 0.05 Btu
M = initial mass of water in sheet = 0.0089 lb (Appendix III)
C_p = specific heat of water = 1.0 But/lb °F

$$T_F = 80^\circ\text{F} + \frac{0.05 \text{ Btu}}{(0.0089 \text{ lb})(1.0 \text{ Btu/lb } {}^\circ\text{F})} = 86^\circ\text{F}$$

APPENDIX VIII

DATA STORAGE FILE NAMES

The surface and internal sheet temperatures, caliper, heat flux, and integrated heat flux data are stored in the Institute's Burroughs computer for the different drying conditions under the following names.

Drying Condition, °F/psi	File Name
300/400	CD/D/300/400
300/700	CD/D/300/700
525/400	CD/D/525/400
525/700	CD/D/525/700

The applied pressure data are stored under the following names.

Drying Condition, °F/psi	File Name
300/400	CD/P/300/400
300/700	CD/P/300/700
525/400	CD/P/525/400
525/700	CD/P/525/700

All other experimental data can be found in Research Notebooks numbers 3546 and 3627.